

Technische Universität München

Lehrstuhl für biomolekulare NMR-Spektroskopie

Department Chemie

Structural and functional studies of the farnesylated peroxisomal membrane protein receptor PEX19

Ulrike Eva Schütz

Vollständiger Abdruck der von der Fakultät für Chemie der Technischen Universität München zur Erlangung des akademischen Grades eines Doktors der Naturwissenschaften genehmigten Dissertation.

Vorsitzender: Univ. - Prof. Dr. Aymelt Itzen

Prüfer der Dissertation: 1. Univ. - Prof. Dr. Michael Sattler

2. Hon. - Prof. Dr Elena Conti, PhD

Ludwig-Maximilian-Universität München

Die Dissertation wurde am 07.05.2012 bei der Technischen Universität München eingereicht und durch die Fakultät für Chemie am 06.07.2012 angenommen.

Technische Universität München

Lehrstuhl für biomolekulare NMR-Spektroskopie

Department Chemie

*Structural and functional studies of the farnesylated
peroxisomal membrane protein receptor PEX19*

Ulrike Eva Schütz

München 2012

Wir müssen uns daran erinnern, dass das, was wir
beobachten, nicht die Natur selbst ist, sondern Natur,
die unserer Art der Fragestellung ausgesetzt ist.

Werner Karl Heisenberg

I. Summary

Peroxisomes accommodate various important reactions in lipid metabolism including fatty acid degradation and the decomposition of the toxic byproduct hydrogen peroxide. All peroxisomal proteins (peroxins) are directed to the organelle posttranslationally via distinct transport systems for matrix and membrane proteins. Recognition and delivery of the peroxins to the peroxisome is mediated by targeting signals and involves a complex and dynamic interplay of cargo and receptor proteins in the cell. This work presents structural and functional investigations of important factors of the peroxisomal protein transport system. The main focus is on the central component of peroxisomal membrane protein transport, PEX19 which is posttranslationally modified by farnesylation. Additionally, Pex4p and Pex22p from the matrix protein pathway were investigated. Structural analysis by NMR methods combined with functional analysis in biochemical and cell-based experiments provided novel insight about the underlying molecular mechanisms.

Chapter 1.1 introduces the peroxisomal system together with a description of the known protein lipidation variations as the biological context of the topic. Chapter 1.2 presents theoretical and practical aspects of protein NMR techniques used in this study. In Chapter 2, the experimental details of the biochemical and NMR methods used are documented.

Chapter 3.1 contains NMR and biochemical data that characterize the structural and molecular effects of PEX19 farnesylation. NMR spectra of full-length and different C-terminal constructs of PEX19 were used to select the PEX19 C-terminal domain (PEX19 CTD residues 161-299), which includes the folded, cargo-binding region and the farnesylation site, for structural investigations. Biochemical and NMR data confirm the complete farnesylation of PEX19 *in vitro*. ^{15}N NMR relaxation and solvent PRE data demonstrate that the flexible C-terminal region in non-farnesylated PEX19 CTD becomes rigid and solvent protected upon farnesylation. Using a combination of specific labeling schemes full resonance assignments were obtained for farnesylated PEX19 CTD. The NMR solution structure was calculated using state-of-the-art methods and shows that the farnesyl is bound in a cavity of the PEX19 CTD structure. Chapter 3.2 contains the studies on PEX19-cargo interactions using peptides from various peroxisomal membrane proteins (PMPs) for NMR titrations, flotation assays and affinity measurements by microscale thermophoresis (MST) assays. Chapter 3.3 describes

the results of biochemical and cell-based experiments investigating the effect of structure-based mutations of the farnesyl recognition site. Chapter 3.4 addresses the interplay of two components of the peroxisomal ubiquitination machinery, Pex4p and Pex22p, which are part of the peroxisomal matrix protein transport. Chapter 3.5 describes a collaborative project where solvent PRE measurements have been used to investigate intramolecular interactions within the peptidyl-prolyl isomerase FKBP38. Chapter 4 reviews the results of the study and discusses implications for the role of farnesylation in peroxisomal membrane protein transport.

This thesis presents a structural and functional characterization of PEX19 highlighting the impact of PEX19 farnesylation, which has not been studied on atomic level before. Specific labeling schemes were adapted to obtain complete resonance assignments not only for the protein but also for the unlabeled farnesyl group. Solution state NMR techniques and structure determination provide detailed information about the structure and dynamics of farnesylated PEX19. MST experiments were successfully applied to quantify PEX19 CTD-PMP cargo interactions, which were challenging to study using other techniques because of the hydrophobicity of the complex. Structure-based mutations of residues that mediate farnesyl recognition *in vitro* severely affect PEX19 function in cell-based studies performed in collaboration with Dr. R. Rucktäschel and Dr. Wolfgang Schliebs at the Ruhr-Universität Bochum. In addition, the interaction between Pex4p and Pex22p linked to the peroxisomal ubiquitination machinery and dynamics of FKBP38 were investigated by NMR.

Structural analysis of PEX19 reveals that the farnesyl group is buried within a hydrophobic cavity inside the protein. This mode of farnesyl recognition has not been observed previously. Additionally, the data indicate that the farnesyl moiety arranges the putative PMP-binding site and stabilizes a distinct conformation of PEX19, suggesting a molecular mechanism how farnesylation can enhance the PMP interaction. *In vitro* and *in vivo* analysis demonstrates that mutations in the farnesyl recognition site strongly interfere with peroxisomal protein transport with the most severe defects probably caused by a mislocalization of the farnesyl group outside the binding cavity. The results thus outline a novel structure-based model for the role of farnesylation in PMP transport in which a change of the farnesyl position upon PMP binding could mediate membrane targeting of the complex.

II. Table of Contents

I. Summary	I
II. Table of Contents	III
1. Introduction.....	1
1.1 Biological background.....	1
1.1.1 Peroxisome discovery and function.....	1
1.1.2 Diseases associated with malfunctions in peroxisomal proteins	3
1.1.3 Transport of peroxisomal matrix proteins	3
1.1.4 The peroxisomal ubiquitination factors Pex4p and Pex22p.....	7
1.1.5 Transport of peroxisomal membrane proteins	8
1.1.6 The peroxisomal membrane protein receptor Pex19p.....	9
1.1.7 Posttranslational lipid modifications	12
1.1.7.1 Cholesterol modifications.....	12
1.1.7.2 Myristoylation.....	13
1.1.7.3 Palmitoylation.....	14
1.1.7.4 Isoprenylation.....	14
1.1.8 Pex19p farnesylation.....	15
1.2 Nuclear magnetic resonance spectroscopy (NMR)	17
1.2.1 Basic principles of NMR.....	17
1.2.2 Relaxation	19
1.2.3 NMR of proteins	20
1.2.4 Ligand binding.....	22
1.2.5 Paramagnetic effects.....	23
1.2.6 Structure calculation.....	24
1.3 Scope of the Thesis.....	26
2. Materials and Methods	28
2.1 Materials.....	28
2.1.1 Bacterial strains and vectors.....	28
2.1.2 Media and buffers.....	29
2.1.2.1 Media and solutions for protein expression.....	29
2.1.2.2 Buffers for protein purification.....	30
2.2 Biochemical methods.....	33
2.2.1 Cloning	33
2.2.2 Protein expression and isotope labeling.....	34
2.2.3 Protein purification	35
2.2.4 <i>In vitro</i> farnesylation.....	36
2.2.5 Microscale thermophoresis assays.....	37
2.2.6 Spin labeling	37
2.2.7 Hydrophobic interaction chromatography	38
2.2.8 Peroxisomal protein import assay in fibroblasts	38

2.3 NMR techniques	40
2.3.1 Resonance assignments.....	40
2.3.2 Secondary chemical shift analysis and chemical shift perturbations	41
2.3.3 Peptide titrations.....	41
2.3.4 Relaxation analysis	42
2.3.5 Residual dipolar couplings.....	43
2.3.6 Structure calculation.....	43
2.3.7 Solvent PREs.....	43
3. Results	45
3.1 Structural analysis of PEX19 farnesylation	45
3.1.1 Comparison of PEX19 constructs.....	45
3.1.2 Farnesylation of PEX19	47
3.1.3 NMR analysis of secondary structure and relaxation properties of PEX19 CTD with and without farnesylation.....	49
3.1.4 Spin labeling	51
3.1.5 Solvent paramagnetic relaxation enhancement	53
3.1.6 Farnesyl spectra and assignments.....	54
3.1.7 Specific labeling strategies	56
3.1.8 NMR solution structure of farnesylated PEX19 CTD	60
3.1.9 Discussion: Farnesyl recognition in PEX19	63
3.2 PEX19-PMP interactions	65
3.2.1 PEX19-PMP NMR titrations	65
3.2.2 Fusion construct of PEX19 CTD and a PMP peptide	68
3.2.3 Flotation assays.....	69
3.2.4 Microscale thermophoresis assays.....	70
3.2.5 Discussion: The influence of farnesylation on PMP interactions and PEX19 membrane association.....	71
3.3 <i>In vitro</i> and <i>in vivo</i> analysis of mutations in the farnesyl recognition site	75
3.3.1 Design and NMR analysis of structure-based mutations.....	75
3.3.2 Hydrophobic interaction chromatography.....	78
3.3.3 PMP binding of the mutated PEX19 CTD variants	80
3.3.4 Functional studies of PEX19 wildtype and mutants in a cell-based assay	83
3.3.5 Discussion: Effects of mutations in the farnesyl recognition site	85
3.4 NMR studies of the ubiquitin-conjugating enzyme Pex4p and its co-activator Pex22p (Collaboration with Dr. C. Williams and Dr. M. Wilmanns, EMBL Hamburg)	87
3.5 Solvent paramagnetic relaxation enhancement studies of FKBP38 (Collaboration with Dr. Ye Hong and Prof. Dr. Ho Sup Yoon, School of Biological Sciences, Nanyang Technological University, Singapore)	89
4. Discussion	92
4.1 A model for the role of farnesylation in peroxisomal membrane protein transport	92
4.2 Conclusions and outlook	94
5. References	95

6. List of Figures	104
III. Appendix	VI
III.I Primers for site-directed mutagenesis.....	VI
III.II Resonance assignments of PEX19 CTD	VII
III.III RDCs included in structure calculation	XVII
Abbreviations	XXII
Acknowledgements.....	XXIII
Curriculum Vitae	XXIV

1. Introduction

1.1 Biological background

1.1.1 Peroxisome discovery and function

The complex metabolism of a cell integrates a multitude of enzymatic reactions which have to be tightly coordinated and regulated in time and space. The sub-organization of eukaryotic cells into organelles as separated compartments allows for the specific localization of macromolecules and thus for a spatial sectioning of metabolic processes. To perform the corresponding reactions each of the cellular compartments has to be equipped with a specific subset of proteins.

In 1954, J. Rhodin identified a new class of cellular organelles which he named microbodies. Their biological function remained unclear until several years later C. de Duve detected hydrogen peroxide producing and decomposing enzymes in a subclass of these microbodies and renamed them as peroxisomes (de Duve, 1969). Together with the discovery of lysosomes these findings earned him the Nobel Prize in Physiology or Medicine in 1974. Subsequent studies led to further subclassifications of microbodies into peroxisomes, glyoxysomes (Tolbert and Essner, 1981), glycosomes (Opperdoes and Borst, 1977) and Woronin bodies (Jedd and Chua, 2000), all of which share a common composition of a granular matrix surrounded by a single membrane. The number of peroxisomes per cell can vary in adaptation to different growth conditions as illustrated in Fig. 1.1: *Hansenula polymorpha* cells only contain a few small peroxisomes when grown on glucose. After switching to methanol as sole carbon source peroxisomes can expand to up to 80% of the cell volume (Erdmann and Schliebs, 2005).

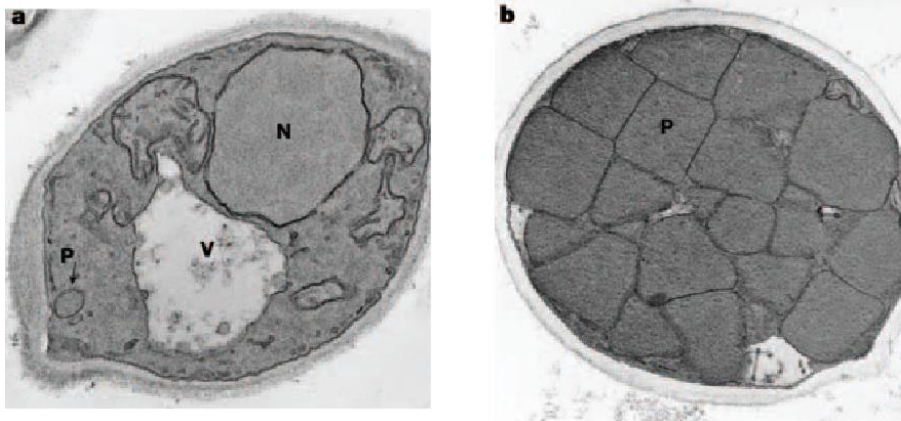


Figure 1.1 Peroxisome proliferation in *H. polymorpha* (Erdmann and Schliebs, 2005). The number and size of peroxisomes increases when the growth conditions are changed. (A) A small number of peroxisomes is sufficient when grown on glucose. (B) Switching to methanol as sole carbon source induces a strong increase in the number and size of peroxisomes.

Peroxisomes have been found ubiquitously in eukaryotic cells from virtually every part of the evolutionary tree of life. Peroxisomal enzymes perform a variety of reactions from lipid metabolism including both anabolic and catabolic pathways. As for the anabolic part, peroxisomes harbor enzymes from ether phospholipid biogenesis, e. g. protein dihydroxyacetone phosphate acyltransferase (DHAPAT) which catalyzes the esterification of dihydroxyacetone phosphate (DHAP) with long chain acyl CoA and thus the first step in plasmalogen synthesis (Gootjes et al., 2002). Catabolism includes several pathways, first to name is beta-oxidation of fatty acids as also found in mitochondria. However, this metabolic path is not redundant in both organelles but specialized for different substrates. While mitochondria degrade mainly fatty acids taken up with food the peroxisomal system targets very-long-chain fatty acids (VLCFAs), pristanic acid, di- and trihydroxycholestanoic acid, tetracosahexanoic acid and long-chain dicarboxylic acids (Kemp and Wanders, 2007). Second, fatty acids methylated at position three are not degradable by beta-oxidation and are therefore alpha-oxidized, a metabolic pathway that is exclusively found in peroxisomes. Third, peroxisomal alanine glyoxylate aminotransferase catalyzes the conversion of glyoxylate to glycine (Wanders and Waterham, 2006). Lipid decomposition also yields hydrogen peroxide, a highly reactive oxygen species, as a toxic byproduct. But as peroxisomes also contain catalase hydrogen peroxide is immediately converted to water and thus detoxified for the cell (Sies, 1974).

1.1.2 Diseases associated with malfunctions in peroxisomal proteins

Studies on peroxisomal disorders (PDs) have contributed to a better understanding of the metabolic functions of the peroxisome. PDs can be further classified into peroxisomal biogenesis diseases (PBDs) and single peroxisomal enzyme deficiencies (PEDs). Depending on the affected enzyme or transporter protein PEDs can vary from mild phenotypes like in PH1 (primary hyperoxaluria type 1) to death within two years after birth as found for DBP (D-bifunctional protein) deficiency patients (Wanders and Waterham, 2006). PBDs, however, which include the spectrum of the Zellweger syndrome and rhizomelic chondrodysplasia punctata (RCDP) with mutations in *pex7*, are characterized by a total absence of peroxisomal structures. Due to the ubiquitous occurrence and essential function of peroxisomes PBDs cause a multiplicity of clinical features, most of which lead to death in early childhood for the affected patients (Steinberg et al., 2006). The association of malfunctions in peroxisomal biogenesis and protein transport with the causative mutated gene constituted the family of PEX genes with the gene products referred to as peroxins. To date, 32 peroxins have been identified (Schrader and Fahimi, 2008). Nomenclature distinguishes between PEX for mammalian and Pexp for yeast proteins. To introduce the peroxisomal system, yeast nomenclature will be used unless otherwise specified.

1.1.3 Transport of peroxisomal matrix proteins

In contrast to mitochondria and chloroplasts peroxisomes do not contain nucleic acids or their own translation machinery, therefore, peroxisomal proteins are synthesized on free ribosomes in the cytosol and directed to the organelle posttranslationally. Interestingly, peroxisomal enzymes are not translocated as a nascent or otherwise unfolded polypeptide chain but cross the peroxisomal membrane in an already folded and sometimes even oligomeric state. Walton et al. (Walton et al., 1995) demonstrated that gold particles with a diameter of up to 9 nM covered with the PTS1 (peroxisomal targeting signal)-sequence were delivered into the peroxisomal matrix. As gold particles cannot be distorted this experiment elegantly proved the hypothesis that the peroxisomal matrix protein import system allows the passage of cargo with the size of a protein in its final three-dimensional shape (Fig. 1.2.A).

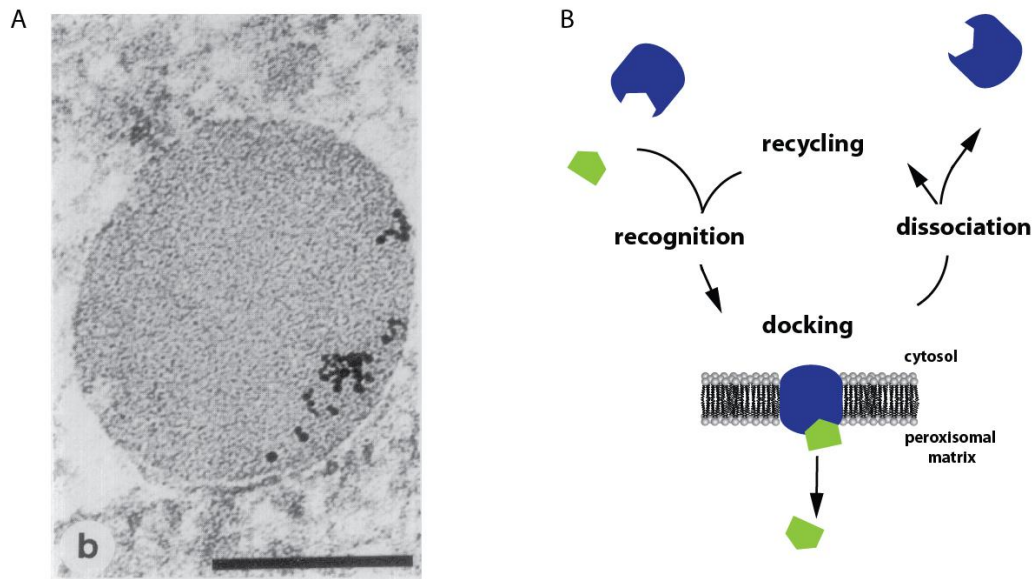


Figure 1.2 Concepts in peroxisomal protein transport. (A) Gold particles with a diameter between four and nine nm coated with human serum albumin modified with a C-terminal peroxisomal targeting sequence are imported into the peroxisomal matrix (adapted from Walton et al molbiolcell1995). (B) Schematic representation of peroxisomal transport: Cargo proteins are directed to the organelle via a receptor which associates with docking proteins and is released back to the cytosol after cargo delivery (Walton et al., 1995).

Peroxisomal protein transport can be schematically pictured as follows: A cargo protein destined for transfer to the peroxisome contains a signal sequence which is recognized by a receptor and delivered to the organelle where the complex associates with one or more docking proteins. After release of the cargo to the peroxisomal matrix or membrane the receptor returns to the cytosol and is available for another round of cargo shuttling (Fig. 1.2.B). Distinct and specific machineries exist for the transport of peroxisomal matrix and membrane proteins respectively. Although both systems include different sets of proteins they share the same principle described above.

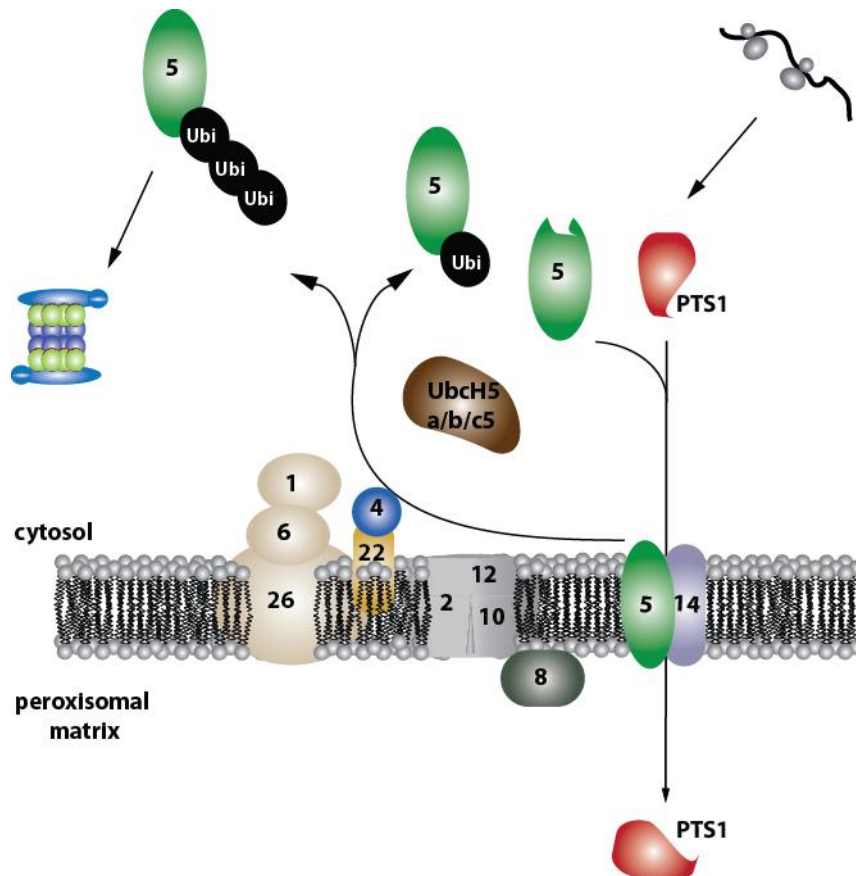


Figure 1.3 Model for peroxisomal matrix protein import. Pex5p recognizes PTS1-cargo in the cytosol. The receptor-cargo complex associates with Pex14p at the peroxisome and inserts into the membrane. After cargo release Pex8p links Pex5p to the RING complex consisting of the ubiquitin ligases Pex2p, Pex10p and Pex12p. The ubiquitin-conjugating enzyme Pex4p assisted by its activator Pex22p mediate monoubiquitination of Pex5p which is then released from the organelle by the AAA proteins Pex1p and Pex6p. Alternatively, polyubiquitination marks Pex5p for proteasomal degradation.

Peroxisomal matrix proteins follow one of two import pathways depending on their sorting sequence. First, proteins containing a C-terminal consensus sequence SKL termed PTS1 (Keller et al., 1991) are sequestered by Pex5p which comprises seven TPR (tetratricopeptide repeats) domains where the targeting signal is bound (Stanley et al., 2006). Second, a subset of peroxisomal matrix proteins travels via the PTS 2-pathway where the signal sequence is located at the N-terminus and consists of a nonapeptide with a consensus sequence of R-(L/V/I/Q)-xx--(L/V/I/H)-(L/S/G/A)-x-(H/Q)-(L/A) (Swinkels et al., 1991). In contrast to Pex5p in PTS1-dependent transport receptor function is shared between several proteins which vary depending on the organism. PTS2 recognition is always mediated by the six WD (tryptophane-aspartic acid) repeats in Pex7p but shuttling also requires the co-receptors Pex18p and Pex21p (for *S. cerevisiae*), Pex20p (in *Y. lipolytica*, *P. pastoris*, *H. polymorpha* and *N. crassa*) or, in plants and mammals, a splice variant of Pex5p. The longer isoform, Pex5L, is

involved in PTS2 transport and differs by 37 amino acids from Pex5S (Girzalsky et al., 2010). This comparably short stretch is essential for PTS2 transport and therefore replaces Pex18p and Pex21p functions (Stanley et al., 2006). This second pathway is only used by a minority of peroxisomal matrix proteins with only a few known PTS2-proteins in mammals and two – 3-ketoacyl thiolase and the NAD⁺-dependent glycerol 3-phosphate dehydrogenase (Gdp1) – in *S. cerevisia* but for a significantly higher number of peroxisomal proteins in plants (Reumann et al., 2009). A third class of peroxisomal matrix proteins without any targeting signal reaches its destination by binding to a PTS-containing protein (McNew and Goodman, 1994).

In spite of the large size of a system which allows for the import of folded proteins such a protein structure has not been observed in the peroxisomal membrane by electron microscopy. As a permanent channel of these dimensions would also permit uncontrolled traffic of organellar and cytoplasmic enzymes and solutes the temporary formation of a pore structure has been suggested.

The cycling receptor Pex5p combines the required properties for the predominant component in this transient pore model. It is found both soluble in the cytosol and as an integral membrane protein. After recognition of the PTS1 cargo the Pex5p-PTS1 complex associates with the docking proteins Pex13p and Pex14p, integral peroxisomal membrane proteins. Pex5p enters the membrane and together with Pex14p forms a pore which can vary in diameter and conductivity (Meinecke et al., 2010). The mechanism for release of the cargo proteins into the peroxisomal matrix is still unknown and might involve Pex8p in yeast on the intraperoxisomal side of the membrane. Neither cargo binding, release nor translocation requires ATP. Pex8p also links the pore components to a complex of RING (really interesting new gene)-finger complex of Pex2p, Pex10p and Pex12p which have ubiquitin ligase function for Pex5p (Wolf et al., 2010). The nature of ubiquitylation decides about the fate of the receptor molecule. Either one ubiquitin molecule is attached to a cysteine in Pex5p and the monoubiquitylated protein is released from the membrane back to the cytosol by the AAA-peroxins Pex6p and Pex1p where it is available for further cargo shuttling. In case of defects in the Pex5p pathway, Pex5p can also undergo classical polyubiquitination where several ubiquitin units are attached via a lysine residue and thus Pex5p is marked as a substrate for proteasomal degradation. The export of the receptor is the only ATP-consuming step in this transport pathway (Platta et al., 2005)

1.1.4 The peroxisomal ubiquitination factors Pex4p and Pex22p

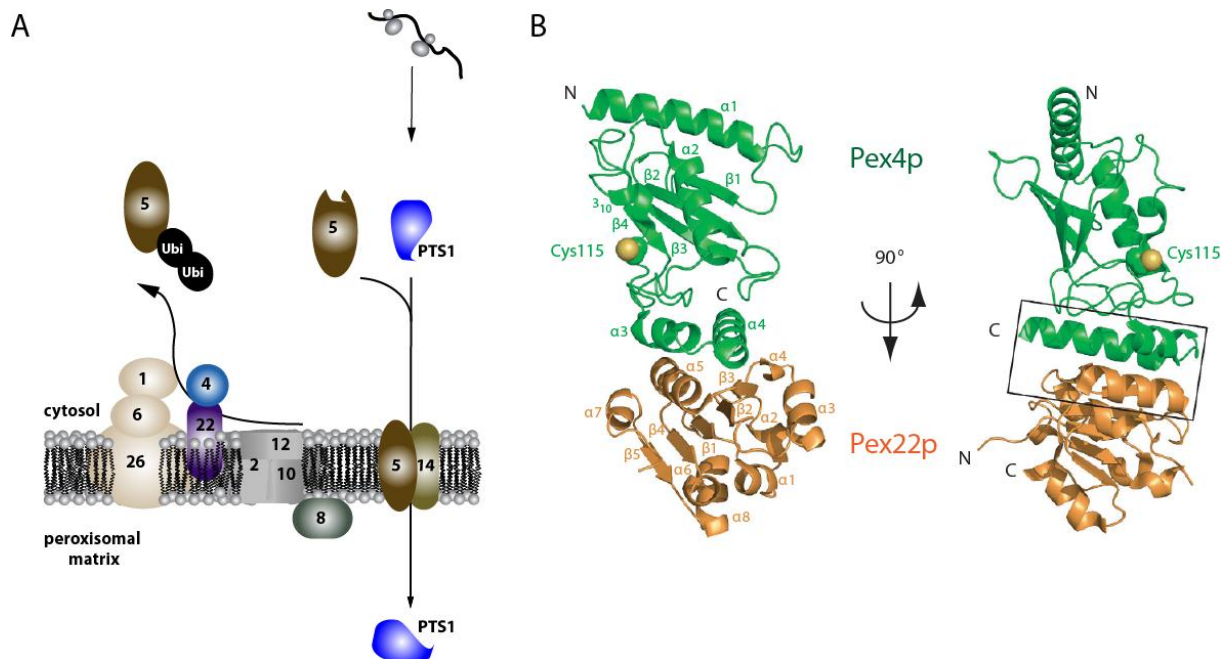


Figure 1.4 The ubiquitin-conjugating enzyme Pex4p and its activator Pex22p. (A) Model for Pex4p/Pex22p function in peroxisomal matrix protein transport: After transporting PTS1 cargo to the peroxisomal lumen two ubiquitin molecules are attached to Pex5p which leads to receptor recycling. This monoubiquitination is mediated by Pex4p and Pex22p. (B) Crystal structure of the complex of Pex4p (green) and Pex22p (orange) with the active site cysteine in Pex4p highlighted as yellow sphere.

In peroxisomal matrix protein import, the shuttling receptor Pex5p delivers proteins with a peroxisomal targeting signal type-1 (PTS1) to the lumen of the organelle. Release of the receptor to the cytosol depends on its ubiquitination. Generally, ubiquitination requires three different enzymes as there are a ubiquitin-activating enzyme E1, a ubiquitin-conjugating enzyme E2 and a ubiquitin ligase E3 (Weissman et al., 2011). Whereas the classic ubiquitination cascade results in polyubiquitination via a lysine in the target protein Pex5p is modified with two ubiquitin molecules at a cysteine residue which involves Pex4p as the peroxisome-specific E2 enzyme (Williams et al., 2007). A recent study shows the crystal structure of Pex22p in complex with Pex4p and demonstrates that Pex22p, an integral peroxisomal membrane protein, functions as a co-activator to stimulate ubiquitin-conjugating activity of Pex4p (Williams et al., 2012).

1.1.5 Transport of peroxisomal membrane proteins

Compared to peroxisomal matrix proteins the understanding of processes from the pathway for peroxisomal membrane proteins (PMPs) is still limited. In mutants characterized by a total absence of peroxisomal structures the organelles were restored by complementation with *pex3*, *pex16* and *pex19* which were thus identified as the key components of peroxisomal biogenesis and membrane protein transport. Although indispensable no explicit function has been assigned to Pex16p. The protein from yeast has a totally different topology from human Pex16p and also controls different activities: the *S. cerevisiae* Pex16p is found at the inside of the peroxisomal membrane and seems to suppress peroxisomal fission while the mammalian counterpart contributes to early steps of peroxisomal biogenesis (Honscho et al., 2002).

Pex19p combines the functions of a chaperone for newly synthesized PMPs and also as a shuttling receptor and will be discussed in detail below. Subdivision into class I and II PMPs is based on their dependency on Pex19p for transfer to the peroxisomal membrane. The majority of PMPs belongs to class I, is transported by Pex19p and contains a peroxisomal membrane targeting signal (mPTS) (Heiland and Erdmann, 2005). The mPTS includes the Pex19 binding site together with a segment for membrane association. This membrane anchor can be provided by a transmembrane domain in the same protein or, if absent, a protein-protein-interaction site for another PMP (Rottensteiner et al., 2004). In contrast to the PTS1 and 2 signals for matrix proteins the mPTS has no well-defined consensus sequence. Binding to Pex19p is thought to require a minimal recognition sequence of 11 amino acids with a high percentage of hydrophobic and positively charged amino acids in a presumably α -helical conformation (Halbach et al., 2005). The complex of Pex19p and its PMP cargo has an enhanced affinity for the docking protein Pex3p compared to free Pex19p (Pinto et al., 2006) which mediates targeting to the peroxisomal membrane. The mechanism of PMP insertion is currently not known, and controversial data exist about the ATP requirement of this step. After cargo insertion Pex19p is - probably ATP-independently - released to the cytosol and can start a new cycle of PMP transport.

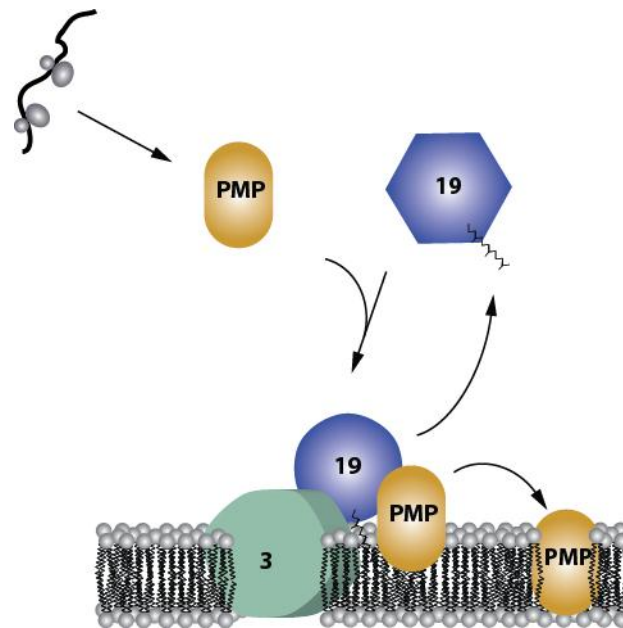


Figure 1.5 Model for transport of class I peroxisomal membrane proteins. The shuttling receptor and chaperone for class I PMPs, the farnesylated protein Pex19p, binds the PMP cargo in the cytosol and docks to the integral membrane protein Pex3p. Via an unknown mechanism the PMP cargo is inserted into the peroxisomal membrane and Pex19p reenters the cytosol.

Together with Pex3p and Pex16p Pex22p is known as class II PMP which are distinguished from class I PMPs by their Pex19p-independent peroxisomal targeting. Pex16p co-translationally inserts into the endoplasmic reticulum (ER) and is later transferred to peroxisomes. Pex3p and Pex22p possess an N-terminal mPTS but without a binding site for Pex19p (Halbach et al., 2009). Recent studies have assigned a more general role for the ER-involving route with several PMPs typically travelling via this pathway (van der Zand et al., 2010; van der Zand et al., 2012), however, regulation and processes in traffic between ER and peroxisome still remain to be elucidated.

1.1.6 The peroxisomal membrane protein receptor Pex19p

The central component of PMP transport, the 33 kDa protein Pex19p, shares structural and functional properties with its equivalent in peroxisomal matrix transport, Pex5p. First, both proteins are organized in a bipartite manner with a disordered N-terminal part and a folded C-terminal domain where they recognize their individual cargo. Second, Pex5p and Pex19p are temporarily found at the peroxisomal membrane. Third, the receptor proteins operate in a cycling manner and return to the cytosol after cargo delivery. Compared to the functions known for Pex5p the different nature of the transported proteins requires an additional task for Pex19p. Due to the hydrophobicity of the shuttled PMPs Pex19p also has to ensure

solubility of PMPs in the cytosol and therefore serves as a PMP-specific chaperone (Jones et al., 2004). A role for Pex19p in the insertion of PMPs into the membrane has also been suggested

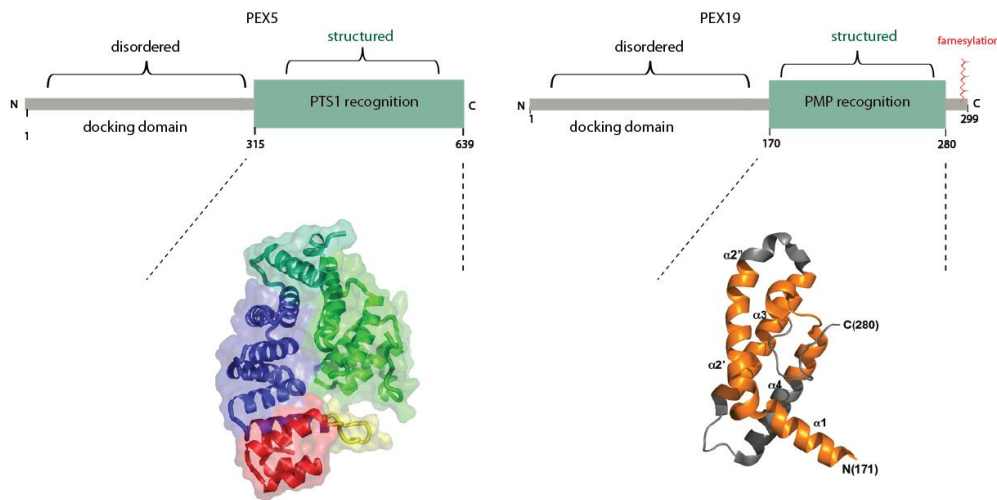


Figure 1.6 Domain composition and structures of PEX5 and PEX19. Both proteins share a similar organization into a disordered N-terminal part for docking to the peroxisome and a structured C-terminus for cargo binding. Crystal structures of C-terminal fragments of human PEX5 (left; (Stanley and Wilmanns, 2006)) and PEX19 (right; (Schueller et al., 2010)).

Docking of the Pex19p-PMP complex to Pex3p at the peroxisomal membrane and therefore peroxisomal targeting is mainly mediated by the Pex19p N-terminus. Human PEX3 is anchored to the peroxisomal membrane with the first 33 amino acids forming a transmembrane domain. The residual part is soluble, faces the cytosol and harbors the PEX19 binding site. While the amino-terminal half of PEX19 is generally unstructured with low sequence conservation its PEX3 binding site from residue 17 to 31 is highly conserved. The crystal structure of PEX3 without the transmembrane domain was solved in complex with the peptide Met1 – Ala44 from PEX19 (Sato et al., 2010; Schmidt et al., 2010). This region in PEX19 does not contain any secondary structure in aqueous solution but is α -helical when bound to PEX3. The hydrophobic environment in the complex seems to favor this conformation as an increased content of methanol also induces a higher content of helical structure as shown by circular dichroism analysis. Hydrophobic interactions from both PEX3 and PEX19 residues contribute to a tight and highly specific interaction with an affinity of 3 nM (Schmidt et al., 2010).

The N-terminus of Pex19p is also required for binding of Pex14, a component of peroxisomal matrix import and most likely an essential part of the transient pore. As the NMR solution structure of Pex14p N-terminus in complex with peptide s from Pex5p and Pex19p shows the peptide bind to the same hydrophobic interface via conserved aromatic residues but in opposite directionality. The affinity of Pex14p for a binding peptide from Pex5p (108-127) is 70 nM and therefore clearly higher than for the core binding motif from Pex19p (66-77) with 9 μ M (Neufeld et al., 2009).

With the exception of these two binding partners the main protein-protein-interaction domain is found in the C-terminus of Pex19p. The functional distribution is reflected by a two-part topology. Limited proteolysis yielded a stable fragment starting from residue 156 to 296 while no N-terminal regions were protected from proteolytic digest in the N-terminus. CD spectra of the full-length protein show a considerable percentage of unfolded protein and a predominantly α -helical conformation of the C-terminus. Taken together, these data indicate a Pex19p organization into an intrinsically unstructured N-terminus and a folded C-terminal domain (Shibata et al., 2004).

The crystal structure of a C-terminal fragment (residues 171-283) of human PEX19 confirms that this region is well ordered and comprises four α -helices with only few loop regions. This region is sufficient to recognize mPTS peptides from PEX13 and PEX11 with affinities of 8 and 12 μ M as determined by fluorescence polarization experiments (Schueller et al., 2010). PMP binding is most likely not reduced to the presence of a certain local binding site but rather seems to require an overall structural integrity of the C-terminus (Fransen et al., 2004). However, an essential role in PEX19-PMP interactions was assigned to conserved aliphatic residues in helix α 1 (residues 172-183) as it contains a hydrophobic surface and insertion of proline residues as well as truncation of the helix completely abolish PMP binding (Schueller et al., 2010). Pex19p is extraordinary soluble up to concentrations more than 200 mg/ml (Shibata et al., 2004). Pex19p is posttranslationally modified by farnesylation at a C-terminal cysteine, C296. Biochemical and cell-based studies of *S. cerevisiae* Pex19p provide evidence that Pex19p is only fully functional when farnesylated (Rucktaschel et al., 2009) which will be discussed in detail in 1.1.7.

1.1.7 Posttranslational lipid modifications

Posttranslational modifications (PTMs) like phosphorylation, glycosylation or lipidation have emerged as one of nature's most variable tools to alter protein properties. Whereas changes in amino acid sequence occur on the basis of mutations and hence are permanent PTMs do not require changes on the genetic level are often reversible and therefore provide many possibilities for the regulation of cellular processes on protein level. A number of lipid PTMs has been discovered in the past decades which can be classified according to the different chemistry of the attached lipid.

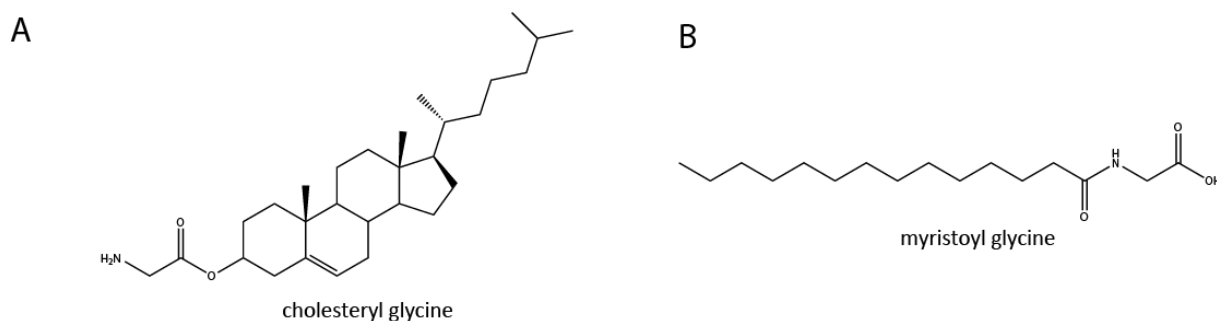


Figure 1.7 Glycine lipidation. A glycine residue can be modified C-terminally with a cholesteryl moiety (A) as known for the Hedgehog protein family (Hall et al., 1997) or with an N-terminally attached myristoyl group (B) like in the ADP ribosylation factor (ARF) (Martin et al., 2011). The figure was prepared with ChemDraw Ultra 12.0 (CambridgeSoft).

1.1.7.1 Cholesterol modifications

A rare case of lipidation, the attachment of a cholesteryl moiety, has only been discovered for the Hedgehog protein family involved in developmental regulation (Hall et al., 1997). Topologically, they are divided into an N-terminal signaling domain and an autoprocessing C-terminal part. An autocatalytic splicing reaction from the C-terminus splits the two halves between a glycine (N-terminus) and a cysteine (C-terminus) and a cholesteryl ester is formed with the free carboxyl of the N-terminal glycine. Subsequently, the original N-terminus is palmitoylated and the two hydrophobic appendents allow for either oligomerization of Hedgehog molecules or insertion into vesicles for further transport (Mann and Beachy, 2000).

1.1.7.2 Myristoylation

Myristoylation describes the attachment of the 14-carbon saturated fatty acid to an N-terminal glycine in an irreversible reaction (Martin et al., 2011). Myristoyl-CoA:protein N-myristoyltransferase (NMT) transfers the lipid moiety from myristoyl-CoA to a protein with the consensus sequence MGXXS/T by forming an amide bond (Zha et al., 2000). The substrate proteins can be modified during their synthesis (co-translationally) or posttranslationally after cleavage of the initial methionine as found for a number of proteins involved in apoptosis. The myristoyl group adds hydrophobicity and is mostly involved in membrane attachment but myristoylation alone is not sufficient to anchor the protein permanently to the lipid. Hence, myristoylation often coincides with either additional lipidation like palmitoylation (described below) or a membrane-binding protein domain. The weak membrane association offers possibilities for regulating the intracellular localization of proteins by “myristoyl switches”. Such a mechanism has been reported for e. g. the ADP ribosylation factor (ARF) where the myristoyl is bound inside the protein, becomes exposed upon ligand binding and subsequently mediates membrane targeting (Ames et al., 1996). For MARCKS protein, phosphorylation of serine residues reducing the positive charge of a basic amino acid stretch which binds phospholipids is sufficient to trigger its release from the membrane (Seykora et al., 1996). In spite of its irreversibility myristoylation therefore allows for a highly diverse and flexible application spectrum.

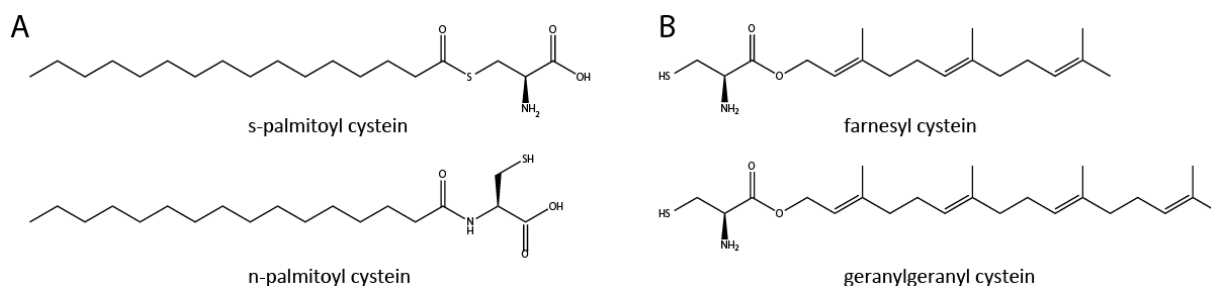


Figure 1.8 Cysteine lipidation. (A) Palmitoylation is formed either via an amide (n-palmitoylation) or a thioester (s-palmitoylation) bond to a cysteine residue. (B) Isoprenylation includes farnesylation and geranylgeranylation via a thioether bond (Magee and Seabra, 2005). The figure was prepared with ChemDraw Ultra 12.0 (CambridgeSoft).

1.1.7.3 Palmitoylation

Palmitate, a C:16 saturated fatty acid, is transferred from palmitoyl-CoA to a cysteine in the target protein. with a thioester- or amide bond. The responsible enzymes, S-palmitoyl transferases, contain a DHHC (aspartate-histidine-histidine-cysteine) domain and are polytopic membrane proteins. Often affiliated with intracellular sorting processes palmitoylated proteins do not share a specific amino acid sequence but rather properties like additional lipidation, a neighboring stretch of basic and hydrophobic amino acids or a transmembrane domain close to the modified cysteine. As the membrane affinity of palmitoyl adds up with the mentioned aspects palmitoylated proteins are normally stably associated with the membrane and preferably found in cholesterol-rich membrane domains (Salaun et al., 2010). However, palmitoylation is the only form of lipidation which can easily be reversed. Although the enzymes for depalmitoylation have not been identified yet information is available for the dynamics in palmitoylation-depalmitoylation of e. g. the Ras protein. Previously farnesylated Ras only weakly interacts with Golgi membranes but becomes permanently membrane-bound upon palmitoylation. It is delivered to the plasma membrane via vesicular transport where the palmitoyl group is removed and Ras is released to the cytosol and the cycle can be repeated (Eisenberg and Henis, 2008).

1.1.7.4 Isoprenylation

Among prenylated proteins the family of small GTPases is certainly the most prevalent and the lipidation in most cases is essential for their cellular function. Prenylation describes two different lipid modifications i. e. the covalent attachment of either a farnesyl or a geranylgeranyl group to a cysteine in the protein (Magee and Seabra, 2005). The reaction is catalyzed by prenyl transferases which recognize a conserved amino acid sequence termed CaaX box where “C” is the modified cysteine and “a” any aliphatic amino acid. The residue at the terminal position X decides about the nature of the isoprenoid. Serine, threonine, glutamine, alanine or methionine are normally converted by farnesyl transferase whereas phenylalanine or leucine will recruit geranylgeranyl transferase (Lane and Beese, 2006). These enzymes transfer the isoprene moiety of farnesyl pyrophosphate, a C15 or geranylgeranylphosphate, a C20 isoprenoid to the target protein. If one of the two enzymes is blocked “cross-prenylation” can occur, i. e. the target protein can also accept the other

isoprenoid, respectively. The reaction is fueled by hydrolysis of pyrophosphate yielding a very stable thioether bond and is considered irreversible (Crowell, 2000).

As pointed out above prenylation does not necessarily transform a soluble to a membrane-bound protein as especially farnesylation only slightly enhances lipophilicity (Silvius and l'Heureux, 1994). Geranylgeranylation can be sufficient for membrane anchorage; however, prenylation is often combined with additional modifications. Many prenylated proteins for example undergo CaaX processing in which the three carboxyterminal amino acids are cleaved off and the carboxyl group of the farnesylated cysteine is methylated. These post-prenylation events contribute significantly to the hydrophobicity of the modified protein and stabilize membrane association. Whereas prenyl transferases are cytosolic the prenyl-dependent CaaX protease and prenylcysteine carboxyl methyltransferase are bound to the ER membrane (Bracha-Drori et al., 2008). But prenylation can also trigger also another prenylation or additional palmitoylation of the same protein. Several members of the Ras protein family, e. g. N-Ras or H-Ras, are first farnesylated and undergo post-farnesylation processing, then it is palmitoylated at one or two additional cysteine residues (Ahearn et al., 2012). The C-terminus of K-RasB contains a basic amino acid stretch which interacts with the negatively charged plasma membrane. In both cases the low membrane affinity due to farnesylation is supported by an additional mechanism to promote stable membrane association (Brunsveld et al., 2009).

1.1.8 Pex19p farnesylation

Pex19 was originally discovered in a screening for farnesylated proteins. Incubation of Chinese hamster ovary cells with [³H] mevalonate, the precursor for farnesyl pyrophosphate and subsequent separation by two-dimensional SDS-PAGE identified a novel farnesylated protein PxF found at the peroxisomal membrane (James et al., 1994). Orthologs of the protein were discovered in many organisms including human HK33 and *S. cerevisiae* Pex19p (Gotte et al., 1998; Kammerer et al., 1997). A chimeric protein consisting of the Pex19p N-terminus with the C-terminus of HK33 was able to complement the defects in peroxisomal biogenesis of a Δ pex19 mutant *S. cerevisiae* strain which further supported the functional similarity of the proteins (Gotte et al., 1998). The members of the peroxin-19 family share the conserved farnesylation motif with only one exception, PEX19 from *Trypanosoma brucei* (Banerjee et al., 2005).

Several studies have investigated the role of farnesylation in different organisms with partially controversial results. Weaker growth on oleate and defects in peroxisomal protein import were demonstrated for *S. cerevisiae* Pex19p mutants with the farnesylation site C347 mutated to serine or arginine and with a deletion of the CaaX box (Gotte et al., 1998). A human PEX19 variant with a mutation of the farnesylated cysteine to alanine, C296A, was capable to restore about 80% complementation compared to wildtype PEX19 in PEX19-deficient human fibroblasts as judged from the number of formed peroxisomes and localization of the peroxisomal marker catalase (Sacksteder et al., 2000). A similar binding behavior was observed for non-farnesylated and partially *in vitro* farnesylated GST-PEX19 to PEX5, PEX14 and PEX13 (Fransen et al., 2004). Additionally, no effects for the inhibition of farnesyl transferase and enzymes from post-farnesylation processing events on peroxisomal biogenesis in human fibroblasts were detected (Fransen et al., 2004). A study by Rucktäschel *et al* (Rucktaschel et al., 2009) demonstrated that farnesylation enhances the binding of ScPex19p to PMP cargo from a K_D of 64 nM to 7.6 nM by a factor of 10 and both a C347R and Δ CaaX genomic mutation cause defects in peroxisomal matrix protein import. Structural changes upon farnesylation have been suggested on the basis of CD data; however, the molecular details are still unknown.

1.2 Nuclear magnetic resonance spectroscopy (NMR)

1.2.1 Basic principles of NMR

NMR is based on the fact that nuclei with a spin quantum number unequal to zero possess an intrinsic nuclear angular momentum which can interact with an external magnetic field. Spin $\frac{1}{2}$ nuclei like the stable isotopes ^1H , ^{13}C and ^{15}N can adopt two different states with a certain energy level separated by a discrete energy difference. The energy difference corresponds to a distinct frequency, the Larmor frequency, which depends on the gyromagnetic ratio γ and the strength of the external magnetic field B_0 as given by Eq. I.

Eq. I

$$\Delta E = \gamma \hbar B_0 = m \hbar \omega_0$$

with γ =gyromagnetic ratio; \hbar =reduced Planck constant; B_0 =magnetic field strength; ω_0 =Larmor frequency

The population of the energy states follows the Boltzmann equation (Eq II).

Eq. II

$$\frac{N_\alpha}{N_\beta} \approx 1 - \frac{\gamma \hbar B_0}{kT}$$

with N_α , N_β =populations of the respective state; k =Boltzmann constant; T =temperature

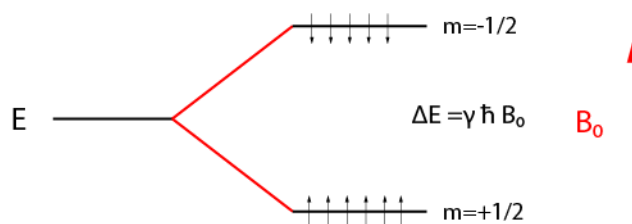


Figure 1.9 Energy levels for spin $\frac{1}{2}$ nuclei in presence of an external magnetic field. In an external magnetic field B_0 two energy levels exist for spin $\frac{1}{2}$ nuclei with a distinct energy associated with each spin state. The population of the lower energy state is higher which gives rise to a net magnetization along the external magnetic field.

The behavior of the sum of a large ensemble of spins in the magnetic field can be described in the vector model. This approach describes the orientation of the bulk magnetization in respect to a coordinate system in which the orientation of the external magnetic field corresponds to the z axis. In equilibrium, that is the situation where the magnetic moment of the spins can align with the magnetic field without additional external influences the

populations of the two spin states follows Eq. II. The difference between N_α and N_β creates a net magnetization M_z along the direction of the magnetic field (s. Fig. 1.6). The angular momentum of the spins causes a precession around the z-axis with the Larmor frequency. The x- and y-components are randomly distributed and therefore level out to zero in the transverse plane.

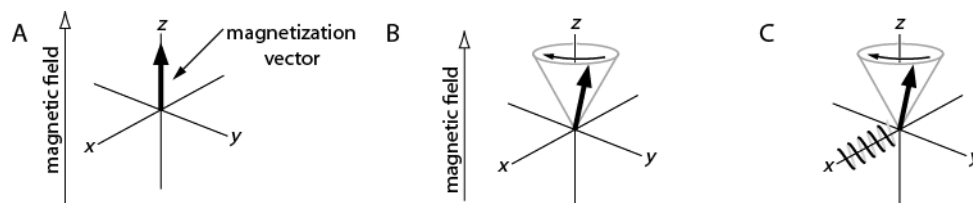


Figure 1.10 The vector model. (A) The bulk magnetization can be described as a vector with an orientation in respect to the orientation of the external magnetic field. (B) A change of the orientation of the magnetization causes a precession of the vector around the z-axis. (C) The magnetization in the xy-plane can be detected in the NMR spectrometer (adapted from (Keeler, 2005)).

The orientation of the bulk magnetization can be manipulated by applying an electromagnetic field B_1 in the transverse plane. In an NMR spectrometer, such a B_1 field is generated by radiofrequency (*rf*) irradiation, an *rf* pulse. A pulse along the x-axis causes a rotation of the magnetization around the x-axis and thus the bulk magnetization is oriented towards the y-axis which gives rise to the free induction decay (FID). The measured FID is a time-domain signal which contains the sum of cosine waves corresponding to all the frequencies present in the sample. The included frequencies can be transferred into the frequency domain by Fourier Transformation. An NMR spectrum shows signals in this frequency-domain representation.

The Larmor frequencies of certain nuclei such as ^1H and ^{15}N vary depending on the individual gyromagnetic ratio. For example, a magnetic field strength of 14.1 Tesla corresponds to a proton Larmor frequency of 600 MHz and a ^{15}N Larmor frequency of 60 MHz. However, nuclei of the same type within a molecule possess distinct resonance frequencies called the chemical shift due to the different electron density in their individual environment. These changes in frequency are relatively small and given in units of ppm (parts per million) in respect to a reference compound which is tetramethylsilane, TMS, for ^1H NMR (Eq. III).

Eq. III

$$\delta\text{ppm} = 10^6 \times \frac{\nu - \nu_{\text{TMS}}}{\nu_{\text{TMS}}}$$

1.2.2 Relaxation

Relaxation in NMR describes the return of the spins into the equilibrium state which is a net magnetization along the z-axis according to the Boltzmann distribution. If the equilibrium is disturbed by rotating the magnetization away from the z-axis two processes will govern the relaxation of the spins: T_1 or spin-lattice relaxation along the z-axis which describes the recovery of the initial z-magnetization M_0 and T_2 or spin-spin relaxation in the transverse or xy plane which causes a decay of the transverse magnetization. M_z recovery follows an exponential growth with the time constant T_1 while M_{xy} exponentially decays with the time constant T_2 as described in Eq III and Eq IV.

Eq III

$$\frac{dM_z(t)}{dt} = -\frac{1}{T_1} [M_z(t) - M_z^0]$$

Eq IV

$$\frac{dM_{xy}(t)}{dt} = -\frac{1}{T_2} M_{xy}(t)$$

The time constants T_1 and T_2 depend on the rotational motion of a molecule. This molecular tumbling is related to the size of the molecule. The larger the molecule, the faster the transverse magnetization will decay. Cross-relaxation of spins describes the exchange of magnetization via dipolar coupling. This magnetization transfer through space depends on the distance r between the two nuclei and declines with r^{-6} . This phenomenon is described as the nuclear Overhauser effect (NOE).

1.2.3 NMR of proteins

The concepts outlined above have been successfully applied to study structure and dynamics of biological macromolecules such as nucleic acids and proteins on atomic level. NMR analysis of proteins is limited by two main factors: First, the large number of nuclei of the same atom type leads to signal overlap. Early experiments in protein NMR were limited to measurements of the naturally abundant NMR-active isotope ^1H in one-dimensional spectra and did not provide a sufficient resolution of the signals. Second, the large size of proteins and nucleic acids causes fast transverse relaxation rates. Progress has been achieved both with molecular biology methods and advances in NMR technology. The recombinant expression of proteins in bacteria enables the production of proteins enriched by the NMR-active nuclei ^{13}C and ^{15}N . These samples are used for multidimensional heteronuclear NMR experiments providing the required resolution. Expression in a partially deuterated or perdeuterated background has proven useful as the proton density, a major source of relaxation, is reduced and thus larger molecules are accessible for NMR analysis. Deuteration in combination with specific labeling schemes to introduce only certain isotope labeled amino acids or chemical groups contributes to the simplification of protein spectra. At the same time, the magnetic field strength of NMR spectrometers available continuously rises. Cryoprobes additionally enhance the sensitivity of the machines. These ongoing advances in NMR allow studies of biomolecules with sizes larger than 300 kDa.

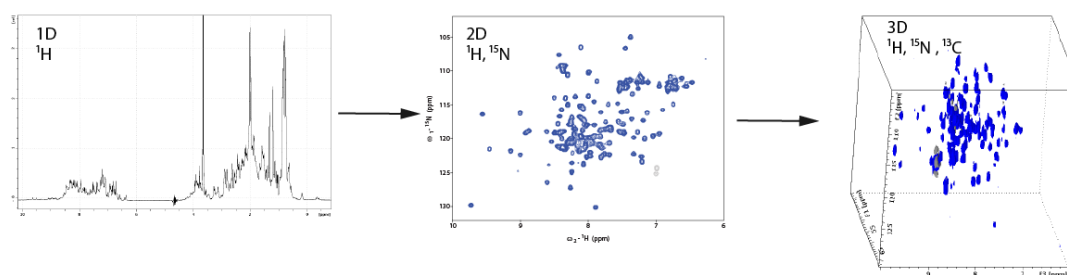


Figure 1.11 Typical protein NMR spectra. Signal overlap in a 1D spectrum (left) is reduced by heteronuclear multidimensional NMR experiments. The “fingerprint” ^1H , ^{15}N HSQC spectrum (middle) detects amide protons and is characteristic for a protein. ^{15}N , ^{13}C labeled samples are used for triple resonance experiments like an HNCA (right) for backbone assignments. The spectra show measurements of PEX19 CTD.

In a one-dimensional ^1H spectrum of a protein, lineshape and dispersion of the signals allow first conclusions about the structural integrity of the protein. For example, methyl groups in the protein core are often shifted upfield as they have a distinct chemical environment, thus,

these signals indicate proper folding. A two-dimensional ^1H , ^{15}N heteronuclear single quantum correlation spectrum (HSQC) detects proton and nitrogen frequencies of an amide group so that essentially the backbone amide of every amino acid (with the exception of proline) gives rise to one signal in the spectrum. The signal dispersion and individual frequencies are characteristic for every protein, thus, the ^1H , ^{15}N HSQC spectrum is often referred to as the “fingerprint” spectrum.

To assign the signals to individual amino acids a set of triple resonance experiments is recorded (Sattler et al., 1999). In these experiments, the frequency of the amide proton is correlated with those of the scalar coupled carbon atoms of the amino acid. The scalar couplings between these atoms are used to transfer magnetization to the CO, C α or C β of the same amino acid or the previous one in the amino acid sequence. As the carbon resonance frequencies are characteristic for an amino acid the information obtained in these experiments allows for sequential backbone assignment of a protein. TOCSY experiments correlate the ^1H and ^{13}C frequencies of all atoms within a residue and thus are used for the assignment of the side chain atoms.

In NOESY experiments, polarization is transferred by dipolar interactions between atoms close in space. To provide sufficient resolution, isotope-edited NOESY-HSQC spectra are recorded in which magnetization is transferred to protons nearby and the HSQC sequence selects protons bound to either ^{15}N or ^{13}C . Information from backbone and side-chain experiments is combined to obtain complete resonance assignments of proteins. The NOESY experiments additionally contain information about the distances between specific atoms which is the basis for structure determination by NMR (s. also I.2.6).

NMR of proteins also allows for studying the dynamic properties of proteins. Measurements of ^{15}N relaxation provide information about backbone dynamics covering a picosecond to second timescale. The longitudinal and transverse relaxation rates T_1 and T_2 which are specific for a molecule and correlated with its size can be determined experimentally. Dynamics on the pico- to microsecond timescale like molecular tumbling and internal motion are reflected by T_1 . T_2 is additionally influenced by dynamics in the micro- to millisecond timescale and thus sensitive to chemical exchange. The correlation time τ_c describes molecular tumbling and can be calculated from the ratio between both relaxation rates including information about the ^{15}N frequency. In $\{^1\text{H}\}$ - ^{15}N heteronuclear NOE experiments,

motions of distinct N-H bond vectors are sampled. τ_c and $\{^1\text{H}\}\text{-}^{15}\text{N}$ heteronuclear NOE values below the average indicate protein regions with high backbone dynamics.

Residual dipolar couplings (RDCs) are influenced by the angles between internuclear bond vectors. While molecular tumbling in solution averages these dipolar couplings to zero they are detectable in weakly aligned molecules. Various media like phage or bicelles which induce a preference for the orientation of a molecule allow for the alignment of proteins in an NMR sample. RDCs are useful to determine the orientation of secondary structure elements or protein domains towards each other (Prestegard et al., 2004).

1.2.4 Ligand binding

NMR is a valuable tool to detect protein-ligand interactions such as protein-protein and protein-nucleic acid interactions as well as binding of small molecules. The most common and fastest approach is to record a series of ^1H , ^{15}N HSQC spectrum of the protein in presence of increasing ligand concentrations. Interactions with the ligand are detected by chemical shift perturbations of the amide proton signals of involved residues. The changes observed in the spectrum depend on the exchange rates between free and ligand-bound state in respect to the difference in resonance frequencies for both states, $\Delta\nu$. The different exchange regimes are defined as

$\Delta\nu \gg k_{ex}$ slow exchange

$\Delta\nu \approx k_{ex}$ intermediate exchange

$\Delta\nu \ll k_{ex}$ fast exchange

with k_{ex} =association rate k_{on} + dissociation rate k_{off}

Ligand binding in slow exchange will give rise to two separate signals with intensities corresponding to the percentage of free and bound protein. Intermediate exchange induces line broadening and thus decreased signal intensity. For interactions in fast exchange, signals possess an average chemical shift between free and bound state weighted by the population of each state, thus, the position of the peak is gradually shifted until saturation. NMR titrations thus allow for a quick and residue-specific determination of the ligand interaction site in proteins.

1.2.5 Paramagnetic effects

Paramagnetic effects are caused by the dipolar interactions between a nucleus and the unpaired electron of a paramagnetic center as for example a paramagnetic metal ion (Bertini et al., 2005). While the NOE caused by the weak dipolar couplings between spins is limited to a distance of up to 6 Å the large gyromagnetic ratio of an unpaired electron can affect nuclei in a distance of more than to 40 Å (Otting, 2008). The strength of the paramagnetic interaction is given by the magnetic susceptibility tensor χ . Paramagnetic relaxation enhancement (PRE) describes the enhancement of the relaxation rates of nuclear spins within the interaction radius due to the large gyromagnetic ratio of the unpaired electron. The PRE effect on transverse relaxation is quantified as

Eq V

$$\Gamma_2 = R_2^{para} - R_2^{dia} = \frac{1}{5\pi r^6} B_0^2 \gamma^2 \chi^2 \tau_c$$

with R_2^{para} and R_2^{dia} = the transverse relaxation rates in the para- and diamagnetic state; B_0 =magnetic field strength; γ =gyromagnetic ratio; χ =magnetic susceptibility tensor; τ_c =molecular rotational correlation time (John and Otting, 2007)

If the χ tensor includes an anisotropic component $\Delta\chi$ the signals will also undergo pseudocontact shifts (PCSs), large changes in the chemical shift of affected signals given by

Eq VI

$$\Delta\delta^{PCS} = \frac{1}{12\pi r^3} \left[\Delta\chi_{ax} (3\cos^2\theta - 1) + \frac{3}{2} \Delta\chi_{rh} \sin^2\theta \cos 2\varphi \right]$$

with $\Delta\delta^{PCS}$ =chemical shift difference between diamagnetic and paramagnetic sample; r =distance between spin and paramagnetic center; $\Delta\chi_{ax}$ and $\Delta\chi_{rh}$ =axial and rhombic components of the $\Delta\chi$ tensor; θ and φ =polar coordinates of the spin defined by the principal axes of the $\Delta\chi$ tensor (Otting, 2008)

Notably, the magnitude of paramagnetic effects is proportional to the distance between nucleus and paramagnetic center r and declines with r^{-6} for PRE and with r^{-3} for PCS.

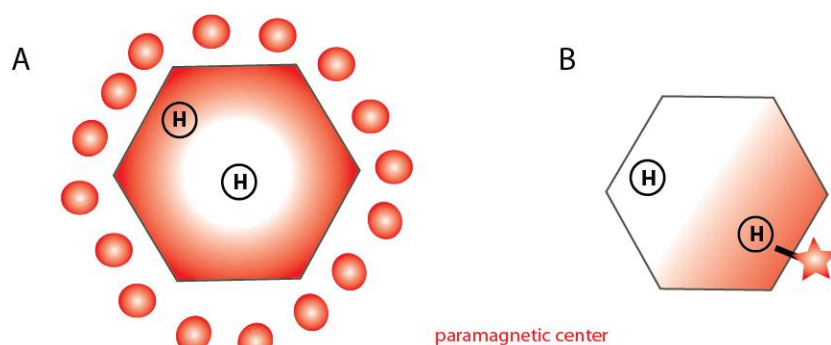


Figure 1.12 Paramagnetic relaxation enhancement. Schematic representation of paramagnetic relaxation enhancement effects on proteins with (A) a paramagnetic co-solute or (B) the attachment of a paramagnetic spin label to a fixed position in the protein.

In protein NMR, this phenomenon was first exploited in metal binding proteins with e. g. a Fe^{2+} as a natural paramagnetic ligand (Weiner, 1986). A more general approach is enabled by the site-specific attachment of paramagnetic centers to proteins. Common spin labels are nitroxide stable radicals such as iodoacetamido proxyl which can be attached to the protein via cysteine residues (Su and Otting, 2010). The PRE effect on distinct amide protons is quantified by comparing signal intensities in ^1H , ^{15}N HSQC spectra of the protein with the spin label in the oxidized (paramagnetic) and reduced (diamagnetic) state. Mapping of the PRE effects allows for example conclusions about domain-domain contacts or transient interactions (Clore and Iwahara, 2009) and the PRE rates can also be included into NMR structure calculations. However, this technique requires that the protein of interest contains one solvent-accessible cysteine residue and thus normally requires mutations of the protein. No biochemical modifications are required when using paramagnetic cosolutes. PCSs induced by complexed lanthanide ions like Dy(DTPA) can help to resolve spectral overlap (Sattler and Fesik, 1997). Gd(DTPA-BMA) exerts strong PRE effects but no PCSs and can thus be used to probe protein surfaces and protein-protein interaction sites by measuring solvent PREs. For this approach, longitudinal relaxation rates are determined in presence of increasing Gd(DTPA-BMA) concentrations. Solvent PREs can be included in structure calculations or used to validate a given structure by comparing experimental with back-calculated values (Madl et al., 2009; Simon et al., 2010).

1.2.6 Structure calculation

In the past decades, NMR has emerged as the second pillar of structure biology next to x-ray crystallography as only these two methods provide structural information on atomic level.

NMR structure calculations require complete assignments of resonances within a protein. The chemical shift already contains useful structural information. $^{13}\text{C}\alpha$ and $^{13}\text{C}\beta$ resonances of a specific amino acid have characteristic values given for a random coil environment. In structured regions the chemical shift of $^{13}\text{C}\alpha$ and $^{13}\text{C}\beta$ deviates from the random coil values depending on the secondary structure. This difference is termed secondary chemical shift. In an α -helix, $^{13}\text{C}\alpha$ carbons experience a downfield and $^{13}\text{C}\beta$ an upfield shift (Wishart 1992, 1994) while opposite effects are observed for carbon atoms in a β -sheet. For that reason, positive values of the difference of $^{13}\text{C}\alpha$ and $^{13}\text{C}\beta$ secondary chemical shift indicate α -helical and negative values β -sheet conformation. The chemical shifts of atoms from the protein backbone are used to predict backbone torsion angles e.g. by the program TALOS+ (Shen et al., 2009). The signal intensity of cross-peaks in NOESY spectra depends on the distance between the atom pair and therefore is the basis for NMR structure calculations as the peak volume can be correlated to a distance between the two atoms. Additionally, experimental data such as RDCs or PRCs can be included into structure calculations.

NMR structure determination is based on a restrained molecular dynamics simulation using a target function which combines different potential energy functions. The target function includes energy terms for known parameters as bond lengths, angles, van der Waals- and electrostatic forces, the so-called force field. Additionally, energy functions for NMR data such as distance restraints from NOEs and torsion angles derived from chemical shift and sequence information are incorporated. Local energy minima are avoided by starting with approximately 100 randomized structures at high temperature. In the following steps of the calculation the temperature is lowered and the different restraints are varied randomly to reduce violations and minimize the target function in a simulated annealing process. Due to the large number of signals in NOESY spectra peak assignments are often ambiguous. The concept of using these ambiguous NOEs in an automated iterative assignment and structure calculation process was first implemented in the program ARIA (Ambiguous Restraints for Iterative Assignment (Nilges et al., 1997)). The program CYANA (Schmucki et al., 2009) also combines structure calculation with automatic assignments in an iterative process starting with unambiguous NOEs. In the subsequent cycles both the energy of the system and the ambiguity of the assignments are reduced. The obtained structures can be subjected to a final refinement in explicit solvent to improve surface electrostatics, e.g. by the program

CNS/ARIA (Linge et al., 2003). The 20 lowest energy structures are included in an NMR structure ensemble.

The precision of the output structure is given by the root mean square coordinate deviation (RMSD) between the structures in the final ensemble and depends on the precision and number of the experimental NMR data. A low number of restraints, low resolution or signal-to-noise in the spectra is reflected by a higher RMSD and thus a low precision of the structure. High precision is not correlated with a high accuracy as mistakes in data interpretation such as misassignments of resonances give rise to precise but inaccurate structure (Clore et al., 1993). Accuracy of the structure is judged by the absence of substantial violations for distance restraints, in bond length or in the Ramachandran plot. Structure validation tools like the iCING server (Doreleijers et al., 2012) allow for the assessment of both accuracy and precision of an NMR structure which analyzes the described parameters for the described criteria in a residue-specific manner.

1.3 Scope of the Thesis

The organization of cellular processes relies on a complex interplay of proteins which has to be tightly regulated in time and space. Posttranslational protein modifications like phosphorylation, glycosylation and lipidation are very versatile tools to modulate protein-protein interactions or subcellular localization. In the peroxisomal system, a dynamic network of numerous protein components ensures the specific recognition and delivery of peroxisomal proteins to the organelle. During the past decades, the understanding of the involved factors and processes has expanded but especially the molecular details of the transport of peroxisomal membrane proteins (PMPs) remain largely unknown.

The main focus of this study was on the investigation of an essential factor for peroxisomal biogenesis, PEX19, which undergoes farnesylation *in vivo*. PEX19 as the central component of PMP transport binds and stabilizes PMPs (Halbach et al., 2009; Jones et al., 2004) and targets them to the peroxisomal membrane where the complex associates with the docking protein PEX3 (Fang et al., 2004). After insertion of the cargo protein into the membrane PEX19 is released to the cytosol. The role of farnesylation for PEX19 functions as a chaperone and shuttling receptor in PMP transport has been discussed controversially (Fransen et al., 2004; Gotte et al., 1998), however, a more recent study demonstrates an important function (Rucktaschel et al., 2009).

It was therefore the aim of this project to obtain structural information about PEX19 and the effects of farnesylation and to correlate these results with implications on PEX19 functions. When this project was started structural information was limited to a crystal structure of a C-terminal fragment of non-farnesylated PEX19, determined by collaboration partners at the EMBL Hamburg (Schueller et al., 2010). Their attempts to crystallize farnesylated PEX19 failed. Therefore, solution state NMR was chosen to study PEX19, its farnesylation and PMP binding properties. For quantitative analysis of PMP binding, MST assays were performed. To use structural findings as the basis for additional biochemical and cell-based characterization the study included a close collaboration with Robert Rucktäschel and Wolfgang Schliebs at the Ruhr-Universität Bochum.

Additionally, this thesis includes structural studies of two proteins from the *S. cerevisiae* matrix protein transport machinery, Pex4p and Pex22p involved in Pex5p ubiquitination in collaboration with Chris Williams (EMBL Hamburg). As crystallization was only successful for the complex (Williams et al., 2012) the individual proteins were investigated by NMR.

As part of another collaboration with Dr. Y. Hong and Prof. Dr. H. S. Soon, School of Biological Sciences, Nanyang Technological University, Singapore, solvent PRE measurements were performed to study intramolecular interactions within with the peptidyl prolyl *cis/trans* isomerase FKBP.

2. Materials and Methods

2.1 Materials

2.1.1 Bacterial strains and vectors

Table 2.1 Bacterial strains

Strain	Genotype
<i>E. coli</i> BL21 (DE3)	F ⁻ ompT gal dcm lon hsdS _B (r _B ⁻ m _B ⁻) λ(DE3 [lacI lacUV5-T7 gene 1 ind1 sam7 nin5])
<i>E. coli</i> XL1-Blue	endA1 gyrA96(nal ^R) thi-1 recA1 relA1 lac glnV44 F'[::Tn10 proAB ⁺ lacI ^q Δ(lacZ)M15] hsdR17(r _K ⁻ m _K ⁺)

Table 2.2 Plasmids

Plasmid	Vector	Insert	Reference
pex19 fl	pETM-11	His ₆ -PEX19 1-299	(Schueller et al., 2010)
pex19-7	pETM-11	His ₆ -PEX19 115-299	(Schueller et al., 2010)
pCW131	pETM-11	His ₆ -GST Pex4p 15-183	(Williams et al., 2012)
pCW218	pETM-11	His ₆ -GST Pex22p 54-180	(Williams et al., 2012)
FTase	pETM-11	His ₆ -RAM1 RAM2	provided by Dr. S. Holton, EMBL Hamburg
pex19 CTD	pETM-11	His ₆ -PEX19 161-299	(Schueller et al., 2010)
pex19 CTD Δc/S205C	pETM-11	His ₆ -PEX19 161-299 C226A C229A S205C	this study
pex19 CTD Δc/S286C	pETM-11	His ₆ -PEX19 161-299 C226A C229A/S286C	this study
pex19 CTD Δc/ΔF/S205C	pETM-11	His ₆ -PEX19 161-299 C226A C229A C296 S205C	this study
pex19 CTD Δc/ΔF/S286C	pETM-11	His ₆ -PEX19 161-299 C226A C229A C296S 286C	this study
pex19 CTD F1	pETM-11	His ₆ -PEX19 161-299 M179R	this study
pex19 CTD F2	pETM-11	His ₆ -PEX19 161-299 I195K	this study
pex19 CTD F3	pETM-11	His ₆ -PEX19 161-299 M255R	this study
pex19 pep13	pETM-11	His ₆ -PEX19 161-299 with N-terminally added amino acids HFTKVFSAFALVRTIR	this study

2.1.2 Media and buffers

Chemicals were purchased from VWR international, isotopically labeled chemicals from Sigma-Aldrich and enzymes from New England Biolabs unless otherwise specified.

2.1.2.1 Media and solutions for protein expression

Table 2.3 Media for protein expression

Medium	Component	Amount per liter
LB (lysogeny broth) rich medium	tryptone	10 g
	NaCl	10 g
	yeast extract	5 g
M9 minimal medium	Na ₂ HPO ₄	6 g
	KH ₂ PO ₄	3 g
	NaCl	0.5 g
	¹⁵ NH ₄ Cl	0.5 g
	glucose	4 g
	or U-[¹³ C]-D-glucose	2 g
	or U-[² H]-D-glucose	2 g
	MgSO ₄ (1M)	1 ml
	CaCl ₂ (1M)	1 ml
	biotin	1 mg
	thiamin	1 mg
100x trace elements stock solution (s. below)	10 ml	
100x trace elements stock solution	EDTA, pH 7.5	5 g
	FeCl ₃ x 6 H ₂ O	0.83 g
	ZnCl ₂	84 mg
	CuCl ₂ x 2 H ₂ O	13 mg
	CoCl ₂ x 6 H ₂ O	10 mg
	H ₃ BO ₃	10 mg
	MnCl ₂ x 6 H ₂ O	1.6 mg

All expression media were supplemented with 50 mg/l kanamycin and sterile filtrated with a 0.22 µM filter (Millipore). For perdeuterated expression all components were lyophilized and dissolved in D₂O prior to sterile filtration.

2.1.2.2 Buffers for protein purification

Table 2.4 PEX19 purification buffers

Buffer	Component	Concentration
lysis buffer	NaCl	300 mM
	Tris/HCl, pH 8.0	30 mM
	imidazole	10 mM
	β -mercaptoethanol	1 mM
	DNase (SERVA)	1.5 μ g/ml
	protease inhibitor mix HP (SERVA)	according to the manufacturer's instructions
	lysozyme (Roth)	spatula-tip
wash buffer 1	NaCl	700 mM
	Tris/HCl, pH 8.0	30 mM
	imidazole	10 mM
	β -mercaptoethanol	1 mM
wash buffer 2	NaCl	700 mM
	Tris/HCl, pH 8.0	30 mM
	imidazole	25 mM
	β -mercaptoethanol	1 mM
elution buffer	NaCl	150 mM
	Tris/HCl, pH 8.0	30 mM
	imidazole	400 mM
	β -mercaptoethanol	1 mM
storage buffer	NaCl	150 mM
	Tris/HCl, pH 8.0	30 mM
	imidazole	10 mM
	β -mercaptoethanol	1 mM
NMR buffer	sodium phosphate solution, pH 6.5	20 mM
	NaCl	50 mM

Table 2.5 Pex4p/Pex22p purification buffers

Buffer	component	concentration
lysis buffer	NaCl	100 mM
	Tris/HCl, pH 7.5	50 mM
	imidazole	10 mM
	β -mercaptoethanol	3 mM
	DNase (SERVA)	1.5 μ g/ml
	protease inhibitor mix HP (SERVA)	according to the manufacturer's instructions
	lysozyme (Roth)	spatula-tip
wash buffer	NaCl	500 mM
	Tris/HCl, pH 7.5	50 mM
	imidazole	10 mM
	β -mercaptoethanol	3 mM
elution buffer	NaCl	100 mM
	Tris/HCl, pH 7.5	50 mM
	imidazole	400 mM
	β -mercaptoethanol	3 mM
storage buffer	NaCl	100 mM
	Tris/HCl, pH 7.5	50 mM
	imidazole	10 mM
	β -mercaptoethanol	3 mM
NMR buffer	sodium phosphate solution, pH 6.5	20 mM
	NaCl	50 mM
	DTT	5 mM

Table 2.6 Farnesyl transferase (RAM 1/2) purification buffers

Buffer	component	concentration
lysis buffer	NaCl	300 mM
	Hepes, pH 7.5	50 mM
	imidazole	10 mM
	β -mercaptoethanol	2 mM
	DNase (SERVA)	1.5 μ g/ml
	protease inhibitor mix HP (SERVA)	according to the manufacturer's instructions
	lysozyme (Roth)	spatula-tip
wash buffer 1	NaCl	500 mM
	Hepes, pH 7.5	50 mM
	imidazole	10 mM
	β -mercaptoethanol	2 mM
wash buffer 2	NaCl	500 mM
	Hepes, pH 7.5	50 mM
	imidazole	25 mM
	β -mercaptoethanol	2 mM
elution buffer	NaCl	200 mM
	Hepes, pH 7.5	50 mM
	imidazole	500 mM
	β -mercaptoethanol	2 mM
dialysis buffer	NaCl	200 mM
	Hepes, pH 7.5	50 mM
	glycerol	10 %
	β -mercaptoethanol	2 mM

NMR spectra of FKBD and NTD were recorded in 20 mM potassium phosphate buffer; pH 6.5, with 50 mM NaCl and 1 mM DTT. All NMR samples contained 10 % D₂O.

2.2 Biochemical methods

2.2.1 Cloning

To introduce point mutations primers were designed using the QuikChange Primer Design Program by Agilent Technologies and purchased from Eurofins MWG Operon. pETM-11 pex19 CTD was amplified in a polymerase chain reaction (PCR) using these primers coding for the intended amino acid substitutions. PCR sample composition and PCR program are listed in Table 2.7 and 2.8. The PCR products were incubated with 1 μ l *DpnI* for 1h at 37 °C. After heat inactivation at 80 °C for 20 min 20 μ l of the sample were transformed into *E. coli* XL1-Blue cells.

Table 2.7 PCR sample composition

component	concentration/volume
template plasmid	40-80 ng
primer forward	10 pmol
primer reverse	10 pmol
<i>Pfu</i> DNA polymerase (Promega)	1.5 U
dNTPs	0.2 mM each
<i>Pfu</i> reaction buffer (10x, Promega)	5 μ l
total volume	50 μ l

Table 2.8 PCR program for site-directed mutagenesis

Temperature (°C)	Time	Setting
95	2 min	1 cycle
95	1 min	
58	1 min	18 cycles
68	12 min	
68	12 min	1 cycle
10	hold	

To clone a peptide to PEX19 CTD complementary oligonucleotides were designed coding for a 15 amino acid peptide from the PEX19 binding site in PEX13 and containing a *NcoI* cleavage site. The oligonucleotides were annealed for 1 min at 65°C and digested with *NcoI* for 1h at 37 °C. pETM11 pex19 CTD was digested with *NcoI* and dephosphorylated with alkaline phosphatase for 1 h at 37 °C. The restriction digests were purified using the Wizard® SV Gel and PCR Clean-Up System (Promega). Vector and insert were mixed in a 1:2 molar ratio and ligated overnight with T4 ligase (Promega) at 4°C. All plasmids were purified using the Wizard® Plus SV Minipreps DNA Purification System (Promega) and sequenced at GATC Biotech. The plasmids generated in this study are included in Table 2.2.

2.2.2 Protein expression and isotope labeling

All proteins used in this study were expressed from pETM-11 vectors in *E. coli* BL21 (DE3) in LB medium or minimal medium for isotope labeling (s. 2.1.2.1). For growth in LB or M9 medium, expression was induced with 0.5 mM IPTG at an OD₆₀₀ of 0.6 for 20 - 24 h at 20 °C. For stereospecific assignments the cultures were grown in 10% U-[¹³C]-D-glucose and 90% unlabeled glucose (Neri et al., 1989). For specific labeled proteins the cultures were grown in perdeuterated medium supplied with U-[²H]-D-glucose to an OD₆₀₀ of 0.5 at 37 °C, then 50 mg of the labeled amino acid or 150 mg of the respective precursor was added. The selectively labeled amino acids and precursors used in this study are listed in Table 2.9. The culture was kept at 37 °C for 1 h, afterwards incubated at 20 °C for 15 min and then induced with 0.5 mM IPTG. After expression overnight at 20 °C the cells were harvested by centrifugation at 5000 rpm in a Evolution RC zentrifuge with an SLC 6000 rotor (Thermo Scientific Sorvall) for 15 min at 4 °C. After washing with PBS buffer the cell pellets were frozen in liquid nitrogen and stored at -80 °C.

Table 2.9 Selective Isotope Labeling

Precursor for expression	Labeling of U-[²H], U-[¹⁵N] -PEX19 CTD
¹³ C, ¹⁵ N leucine (Isotec)	¹³ C, ¹⁵ N leucine
¹³ C, ¹⁵ N isoleucine (CortecNet)	¹³ C, ¹⁵ N isoleucine
Phenylalanine (unlabeled)	Phenylalanine protons
¹³ Cε methionine (Cambridge Isotope Laboratories)	¹³ Cε methionine
α-ketobutyric acid ¹³ C ₄ , 3, 3-d ₂ (Isotec)/	(¹ H-1δ methyl)-isoleucine/
2-keto 3-methyl ¹³ C-butyric 4- ¹³ C, 3d (Isotec)	(¹ H-1δ methyl)-leucine, (¹ H-1γ methyl)- valine
2-(¹³ C) methyl-4-(² H ³)-acetolactate (Gans et al., 2010)	leu/val - [¹³ C, ¹ H ₃]-proS

2.2.3 Protein purification

The buffers used for purification are listed in 2.1.2.2. Cell pellets of 1 liter culture were resuspended in 30 ml lysis buffer, incubated on ice for 30 min and lysed by sonication. The lysate was centrifuged at 14000 g in a F-34-6-38 rotor in a 5810 R centrifuge (Eppendorf) for 60 min at 4 °C. The supernatant was loaded onto Ni-NTA agarose (Qiagen), washed with 30 ml wash buffer or 30ml of wash buffer 1 and 2 each, respectively. The proteins were eluted with 10 ml elution buffer and cleaved overnight at 4 °C by His₆-TEV protease (approximately 250 µg TEV for 10 mg protein). The buffer was exchanged to storage buffer via Amicon Ultra-15 Centrifugal Filter Units (MWCO 3kDa; Millipore) and the solution was loaded onto Ni-NTA resin to remove the His₆-TEV and the His₆-expression tag. Subsequent size-exclusion chromatography was performed in the ÄKTA Purifier system using a HiLoad 16/60 Superdex 75 µg column (GE Healthcare) with the respective NMR buffer.

Specific changes in the purification procedure for the different proteins used in this study are given below:

The fact that PEX19 CTD reversibly unfolds at 85 °C was used for an additional purification step: the flow-through of the second Ni-NTA resin was heated to 85 °C, incubated for 10 min and centrifuged at 13200 rpm in a Pico 21 Microcentrifuge (Heraeus Thermo Scientific) for 10 min at room temperature. The supernatant contains highly pure PEX19 CTD. Farnesylation (s. 2.2.4) was carried out after the heat treatment and the farnesylated proteins were subjected to size-exclusion chromatography.

In farnesyl transferase purification, the His-tag was not removed by TEV cleavage. After the first Ni-NTA column the protein was dialyzed overnight in dialysis buffer and subsequently subjected to size-exclusion chromatography in the same buffer.

PEX19 CTD harboring the point mutations described in 3.3.1 was not heated to 85 °C due to the increased instability of the mutated proteins. To achieve an equal degree of purity the PEX19 CTD variants were subjected to ion exchange chromatography using a Resource Q column with a NaCl gradient from 0 to 1 M for elution before performing size-exclusion chromatography.

2.2.4 *In vitro* farnesylation

The sample composition for *in vitro* farnesylation (Caplan et al., 1992) of PEX19 is given in Table II.10. The samples were incubated at 37 °C for 1 h. To remove the His₆-FTase the samples were loaded on Ni-NTA resin. The flow-through was collected and the buffer was exchanged to NMR buffer using a Amicon Ultra-15 Centrifugal Filter Unit (MWCO 3kDa; Millipore). Farnesylated proteins are abbreviated as “_{farn}”.

Table 2.10 Sample composition for *in vitro* farnesylation

component	concentration/volume
PEX19 in storage buffer	1-100 µM
Farnesyl pyrophosphate	1.2 excess of the protein concentration
FTase	1 µM
MgCl ₂	5 mM
ZnCl ₂	10 µM
β-mercapto ethanol	3.5 mM
Tris/HCl, pH 8.0	50 mM
add H ₂ O	10 ml

2.2.5 Microscale thermophoresis assays

MST assays (Jerabek-Willemsen et al., 2011) were performed at NanoTemper technologies, Munich, using an N-terminally fluorescein-labeled PEX11 peptide LALKLRLQVLLARV (Peptide Specialty Laboratories GmbH, Heidelberg). The peptide was dissolved to a concentration of 200 nM in 20 mM potassium phosphate; pH 6.5, 50 mM NaCl with 20 % methanol and 0,1% Tween. Unlabeled Pex19 CTD with or without farnesylation was serially diluted in the same buffer to concentrations from 612 μ M to 18 nM for wildtype PEX19 CTD and from 100 μ M to 6 nM for PEX19 CTD M179R, I195K and M255R. 10 μ l protein and 10 μ l peptide solution were mixed and subsequently centrifuged at 5000 rpm in a Micro 200R centrifuge (Hettich) for 5 min. The supernatant was transferred to MST capillaries and measured with a NanoTemper Monolith NT 0.15T. Normalized fluorescence values from three separate measurements for PEX19 CTD wildtype and two measurements for PEX19 CTD harboring the respective mutations were used to determine K_D values. As a negative control IPSE, a structurally and functionally unrelated glycoprotein from *Schistosoma mansonii*, was used in a dilution series from 500 μ M to 10 nM.

2.2.6 Spin labeling

The spin label 3-(2-iodoacetamido)-PROXYL (Sigma-Aldrich), a stable nitroxide radical, was attached to single cysteine variants of PEX19 CTD. The variants PEX19 CTD cys which keeps the farnesylation site and PEX19 CTD cys/ Δ F in which the farnesylation site is mutated to serine were generated as described in 2.2.1. Single cysteine residues were introduced into both variants at position S205 and S286, respectively (s. Table 2.2). 15 N labeled protein samples were expressed and purified as described in 2.2.2 and 2.2.3. PEX19 CTD cys was farnesylated according to 2.2.4. The NMR buffer was adjusted to 50 mM DTT to ascertain a complete reduction of the cysteine. The buffer was exchanged to 200 mM Tris; pH 8.0 using a PD-10 desalting column (GE Healthcare). A five-fold excess of iodoacetamide proxyl was added and incubated protected from light at 4 °C overnight. To completely remove unbound spin label the buffer was exchanged to NMR buffer via a PD-10 desalting column (GE Healthcare) and concentrated in an Amicon Ultra-15 Centrifugal Filter Units (Millipore) to 100 μ M. After recording a 1 H, 15 N HSQC spectrum in the oxidized state the spin label was reduced by adding a three-fold excess of ascorbate; pH 6.5, and incubating between 20 min and 2 h. Another 1 H, 15 N HSQC spectrum was measured and the PRE effect on backbone

amide protons was determined by calculating the signal intensities in the spectra as $\frac{I_{ox}}{I_{red}}$ with I_{ox} the signal intensity in the oxidized and I_{red} the signal intensity in the reduced state. Spectra were recorded on a Bruker Avance III 750 MHz spectrometer at 298 K.

2.2.7 Hydrophobic interaction chromatography

Hydrophobic interaction chromatography analysis was performed by Dr. Robert Rucktäschel (Ruhr-Universität Bochum). 500 μ g of PEX19 CTD and PEX19 CTD variants M179R, I195K and M255R farnesylated and non-farnesylated form in NMR-buffer additionally containing 650 mM $(\text{NH}_4)_2\text{SO}_4$ were applied to a Butyl Sepharose FF column (GE Healthcare) equilibrated in 50 mM sodium phosphate buffer containing 50 mM NaCl and 650 mM $(\text{NH}_4)_2\text{SO}_4$. The proteins were eluted using a linear decreasing gradient from 650 to 0 mM $(\text{NH}_4)_2\text{SO}_4$. The eluted proteins were detected by absorption at 280 nm.

2.2.8 Peroxisomal protein import assay in fibroblasts

Cell-based peroxisomal import assays were carried out by Elisabeth Becker (Ruhr-Universität Bochum). pIRES2-HsPEX19-EGFP-PTS1 was constructed by replacing the open reading frame of PEX14 in the bicistronic expression plasmid coding for EGFP-PTS1 and non-tagged PEX14 (pMF1220; (Huybrechts et al., 2009)) with a DNA-cassette encoding the full-length open reading frame of human PEX19 as derived from *Bam*HI/*Sall* digestion of pAH05 (Saveria et al., 2007). Single point mutations were introduced into the PEX19 sequence by Quickchange XL Site-directed Mutagenesis kit (Stratagene) as described in 2.2.1.

The bicistronic expression vectors coding for PEX19 variants and EGFP-PTS1 were transfected into the human cell-line Δ PEX19 T derived from PEX19-deficient Zellweger patient fibroblasts (Schueller et al., 2010). Seventy-two hours after transfection, fluorescence and immunofluorescence microscopy were performed using polyclonal antiserum against human PEX14 (Will et al., 1999). Statistical analysis is based on three independent transfection experiments of each pIRES-PEX19-EGFP-PTS1 expression plasmid. Approximately 100 cells of each assay were divided into three categories according to the appearance of EGFP-PTS1 fluorescence pattern: first, full complementation of peroxisomal import indicated by a punctuate staining pattern, second, partial complementation when a diffuse cytosolic background staining with few dots was detected and third, no complementation due to exclusively cytosolic background staining. All micrographs were

recorded on a Zeiss Axioplan 2 microscope with a Zeiss Plan-Apochromat 63 × /1.4 oil objective and an Axiocam MR digital camera and processed with AxioVision 4.6 software (Zeiss, Jena, Germany). The steady-state level of PEX19 expression was detected by immunoblot analyses using monoclonal mouse antibodies against HsPEX19 (BD Biosciences).

2.3 NMR techniques

2.3.1 Resonance assignments

Standard triple resonance experiments (Sattler et al., 1999) HNCA, HNCACB, CBCA(CO)NH and HNC(O) were recorded at 298 K on a Bruker Avance III 750 MHz spectrometer on 1 mM samples of PEX19 CTD and PEX19 CTD_{farn}. Complete backbone resonance assignments were obtained for PEX19 CTD and PEX19 CTD_{farn}. (H)CC(CO)NH-TOCSY and H(CC)(CO)NH-TOCSY spectra were acquired on a Bruker Avance III 600 MHz spectrometer with a TCI cryo-probe head. Stereospecific assignments were extracted from ¹H, ¹³C HSQC and (H)CC(CO)NH-TOCSY using samples that were randomly fractionally isotope-labeled with 10% U-[¹³C]-D-glucose (s. 2.2.2).

¹³C- and ¹⁵N- edited NOESY-HSQC spectra with a mixing time of 70 ms were recorded on uniformly ¹⁵N, ¹³C labeled PEX19 CTD and PEX19 CTD_{farn} on a Bruker Avance 900 spectrometer with a TXI cryo-probe head. Isotope-edited constant-time NOESY-HSQC spectra with mixing times of 100 - 150 ms were recorded on perdeuterated selectively labeled PEX19 CTD_{farn} samples (s. II.2.2) on a Bruker Avance 900 spectrometer with a TXI cryo-probe head or a Bruker Avance III 800-MHz spectrometer with a TCI cryo-probe head. To detect protein-farnesyl NOEs 2D isotope-filtered NOESYs and TOCSYs with a mixing time of 70 ms or 100 ms and 3D isotope-filtered ¹³C- edited NOESY-HSQC spectra with a mixing time of 100 ms sampling the aliphatic region were used for assignment of the farnesyl ¹H resonances.

¹³C resonances of the farnesyl group were detected in natural abundance ¹H, ¹³C HSQC spectra of 2 mM farnesyl pyrophosphate in methanol and perdeuterated U-[²H]-D-glucose labeled PEX19 CTD_{farn} in NMR buffer on a 500 MHz Bruker Avance III spectrometer with a TCI cryo-probe.

All spectra were processed using the NMRPipe software package (Delaglio et al., 1995). Analysis and assignments of the spectra were performed with Sparky (Goddard and Kneller). Backbone assignment was supported by semiautomatic assignments obtained from MARS (Jung and Zweckstetter, 2004).

HNCA and HNCACB spectra of 400 μM Pex4p were recorded on a Bruker Avance 900 spectrometer with a TXI cryo-probe head.

2.3.2 Secondary chemical shift analysis and chemical shift perturbations

$^{13}\text{C}\alpha$ and $^{13}\text{C}\beta$ secondary chemical shifts of PEX19 CTD and PEX19 CTD_{farm} were calculated according to

$$\Delta\delta (^{13}\text{C}\alpha, ^{13}\text{C}\beta) = (\delta^{13}\text{C}\alpha(\text{obs}) - \delta^{13}\text{C}\alpha(\text{rc})) - (\delta^{13}\text{C}\beta(\text{obs}) - \delta^{13}\text{C}\beta(\text{rc}))$$

with $\delta^{13}\text{C}(\alpha,\beta)(\text{obs})$ = experimentally observed chemical shift and $\delta^{13}\text{C}(\alpha,\beta)(\text{rc})$ = random coil chemical shift values (Wishart and Sykes, 1994).

Chemical shift perturbations of signals in ^{15}N , ^1H HSQC spectra were calculated according to

$$\Delta\delta (\text{NH}) = (\Delta\delta^1\text{H})^2 + \left(\frac{\Delta\delta^{15}\text{N}}{6}\right)^2$$

with $\Delta\delta$ = chemical shift difference of the signal in the different spectra.

2.3.3 Peptide titrations

The different peptides from peroxisomal membrane proteins which were chosen for NMR titrations on the basis of previous studies (Halbach et al., 2005; Schueller et al., 2010) are listed in Table 2.11.

Table 2.11 PMP peptides

Peptide from	Sequence	Length (aa)
PEX13	HFTKVFSAFALVRTIR	16
PEX11	LALKLRLQVLLLARV	15
PEX11ext	QLALKLRLQVLLLARVLR	18
PEX26-2	PSSLHFLYKLAQLFR	15
PEX26-1	KKSLAALILCLLVVR	16
ALDP	NRVFLQRLWLLRLLFPR	18

For titrations with the PEX13 peptide the peptide was dissolved to a concentration of 3.1 mM in NMR buffer. PEX11 and PEX11b peptides were dissolved to 1 and 5.9 mM concentrations in methanol. Peptides were titrated to samples of ^{15}N labeled PEX19 full-length, PEX19 full-length_{farm}, PEX19 CTD and PEX19 CTD_{farm} in NMR-buffer, pH 6.5. Pex26-2

was dissolved to 10 mM in NMR-buffer with pH 5.8 and titrated to PEX19 CTD_{farn} in NMR-buffer, pH 5.8. To form a PEX19 CTD_{farn}-peptide complex a 70 μM PEX19 CTD_{farn} sample in NMR-buffer, pH 5.8, was mixed with 90 μM PEX26-2 peptide in a total volume of 1 ml and concentrated to 250 μl in an Amicon Ultra-15 Centrifugal Filter Units (Millipore). ¹⁵N, ¹H HSQC spectra were recorded at 298 K on a Bruker Avance III 750-MHz spectrometer or a Bruker Avance III 600 MHz spectrometer.

2.3.4 Relaxation analysis

¹⁵N relaxation NMR experiments were recorded on a Bruker Avance III 750-MHz spectrometer on uniformly ¹⁵N, ¹³C labeled samples of PEX19 CTD (340 μM) and PEX19 CTD_{farn} (800 μM). {¹H}-¹⁵N heteronuclear NOE data were recorded according to (Farrow et al., 1994). Values were determined from the ratio between signal intensity in the experiment with and without saturation with the error calculated from experimental noise. T₁ and T_{1ρ} relaxation times were determined from pseudo-3D saturation-recovery HSQC experiments recorded in an interleaved fashion with 12 different recovery delays of 21.6 to 1782 ms for T₁ and 8 different recovery delays from 5 to 140 ms for T_{1ρ}. Two delays in each experiment were recorded in duplicates to define the experimental error. Spectra were processed with NMRPipe (Delaglio et al., 1995) and R₁ and R_{1ρ} rates were calculated by fitting peak intensities to an exponential curve in NMRViewJ (Johnson and Blevins, 1994) using a three-parameter fit.

Calculation of the error combines the experimental error from the time points recorded in duplicate with the fitting error in a Monte Carlo simulation. R₂ was extracted from R_{1ρ} according to (Massi et al., 2004). The correlation time τ_c was calculated as

$$\tau_c \cong \frac{1}{2\pi\nu^{15N}} \sqrt{\left(\frac{3}{2}\right) \left(\frac{R_2}{R_1} - \frac{7}{6}\right)}$$

with ν¹⁵N = the resonance frequency of ¹⁵N in Hz.

2.3.5 Residual dipolar couplings

Residual dipolar couplings were measured on samples on a Bruker Avance III 750-MHz spectrometer. ^1HN - ^{15}N J-couplings were extracted from doublet-separated sensitivity-enhanced HSQC experiments (Cordier et al., 1999). ^1HN - ^{13}CO and ^{13}CO - ^{15}N J-couplings were measured in a 3D TROSY-based HNC0 experiment (Yang et al., 1999). Experiments were recorded on a 1.25 mM uniformly ^{15}N , ^{13}C labeled PEX19 CTD and a 300 μM uniformly ^{15}N , ^{13}C labeled PEX19 CTD_{farn} and repeated after addition 18 mg/ml (PEX19 CTD) or 17 mg/ml (PEX19 CTD_{farn}) of Pf1 phage (ASLA^{biotech}), respectively. Data analysis was carried out with Sparky (Goddard and Kneller) and MODULE (Dosset et al., 2001).

2.3.6 Structure calculation

Assignments for PEX19 CTD_{farn} resonances were obtained as described in 2.3.1. Structure calculation and automatic NOE assignment were performed with CYANA 3.0 (Guntert, 2009). Backbone torsion angles predicted by TALOS+ (Shen et al., 2009) and RDCs (s. 2.3.6) were used as additional restraints in the structure calculation. Iterative calculation cycles were carried out from 100 randomly generated. The 20 lowest energy structures of each cycle were used to generate 100 starting structures for the following cycle. The CYANA output was used for water refinement with ARIA 1.2/CNS (Linge et al., 2003). Structure validation was performed with iCING (Doreleijers et al., 2012).

2.3.7 Solvent PREs

To measure solvent PREs saturation recovery ^{15}N , ^1H HSQC experiments (Madl et al., 2009) with recovery times of 0.01 to 3 s were recorded at 298 K on a Bruker Avance III 750-MHz spectrometer. Gd(DTPA-BMA) was added in concentrations of 0, 1, 2, 3, 5, 7 and 10 mM to a 1.2 mM sample of uniformly ^{15}N , ^{13}C labeled PEX19 CTD and in concentrations of 0, 1, 2, 3, 5 and 7 mM to a 800 μM sample of uniformly ^{15}N , ^{13}C labeled PEX19 CTD_{farn}. Spectra were processed with NMRPipe (Delaglio et al., 1995) and analyzed with Sparky (Goddard and Kneller). R_1 rates were calculated using NMRViewJ (Johnson and Blevins, 1994) as described in 2.3.5. R_1 values were plotted against the Gd(DTPA-BMA) concentrations and the PRE was extracted from the slope of the relaxation rates. The error was calculated as error propagation of the individual fitting errors for each Gd(DTPA-BMA) concentration (Madl et al., 2009).

Solvent PRE measurements on FKBD and NTD were recorded at 303 K on a 750 MHz spectrometer with sample concentrations of 230 μM for FKBD and 110 μM for NTD. Gd(DTPA-BMA) was added in concentrations up to 7 mM for FKBD and, due to the lower protein concentration, up to 5 mM for NTD.

3. Results

3.1 Structural analysis of PEX19 farnesylation

3.1.1 Comparison of PEX19 constructs

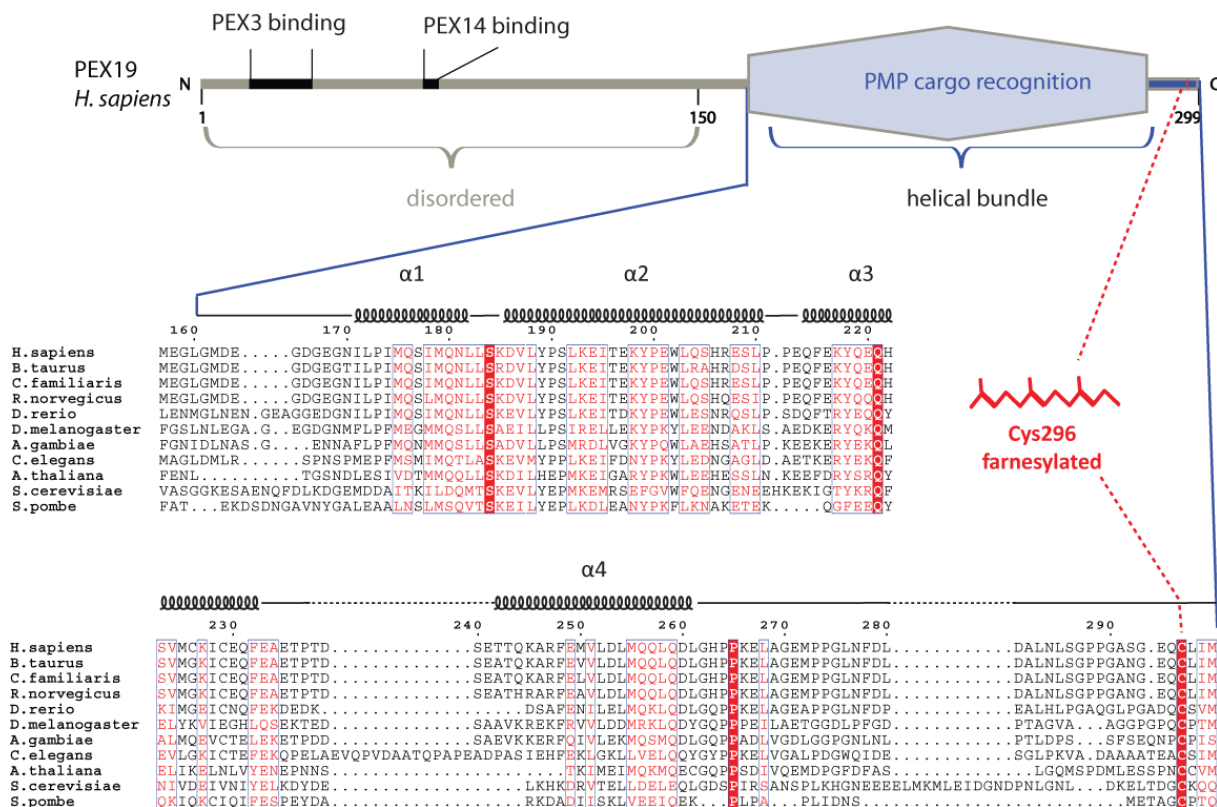


Figure 3.1 Domain structure of PEX19. The unfolded N-terminus of PEX19 interacts with the peroxisomal membrane proteins PEX3 and PEX14, the C-terminus harbors the α -helical cargo binding region and the farnesylation site. Sequence conservation is mainly limited to residues in the structured area and to the farnesylated cysteine (labeled in red). Sequences were aligned using the program Clustal Omega (Sievers et al., 2011) and analyzed using the program ESript (Gouet et al., 1999).

A multiple sequence alignment of the PEX19 C-terminus performed with Clustal Omega (Sievers et al., 2011) shows that sequence conservation is mainly limited to the α -helical regions and the farnesylation site (Fig. 3.1). An N-terminal stretch of approximately 15 residues including helix $\alpha 1$, partially helix $\alpha 2$ and the short loop connecting the two helices contains a number of highly conserved mostly aliphatic amino acids. The four C-terminal residues which form the farnesylation signal sequence, the CaaX box, are equally conserved, the farnesylated cysteine is invariant.

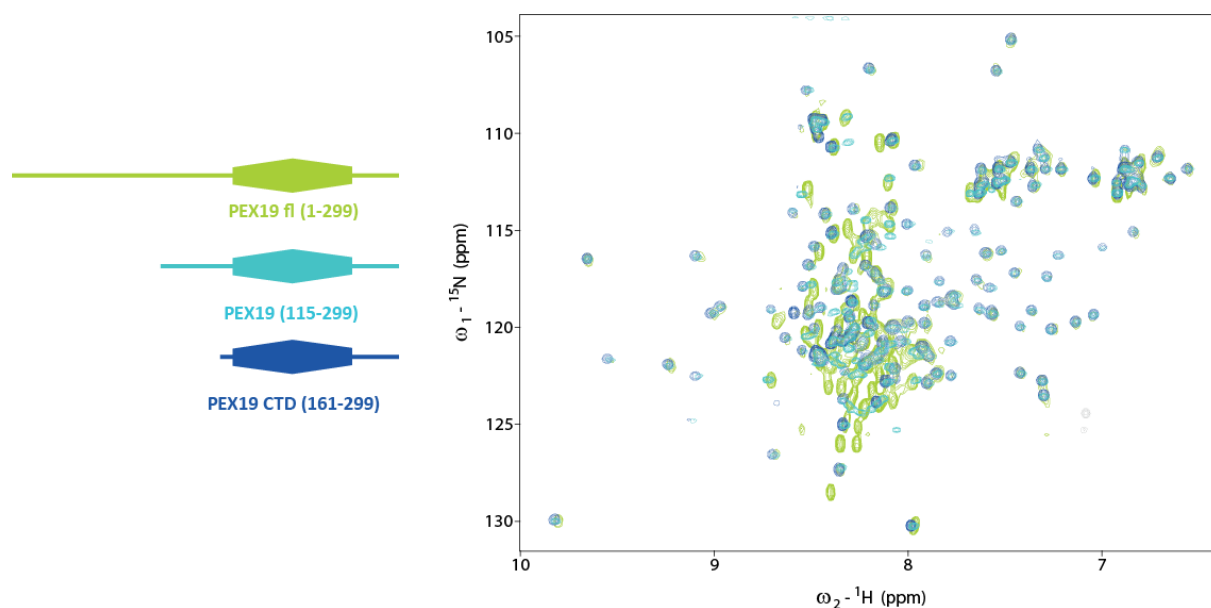


Figure 3.2 Overlay of the ^1H ^{15}N HSQC spectra of full-length PEX19 (1-299; light green) with PEX19 (115-299, cyan) and the PEX19 C-terminus (161-299; blue). Signals from the disordered N-terminus between residues 1 and 160 cluster in the center of the spectrum. The chemical shifts for the dispersed resonances from the C-terminus correlate well between the three constructs.

^1H , ^{15}N HSQC NMR spectra were recorded on PEX19 constructs with different boundaries. The majority of the signals in the ^1H , ^{15}N HSQC NMR spectrum of the full-length protein with 299 amino acids and a molecular weight of 33 kDa clusters in the center of the spectrum around 8 to 8.5 ppm as typically seen for unfolded proteins. A comparison of the ^1H , ^{15}N HSQC NMR spectrum of an intermediate construct (residues 115-299) with that of a C-terminal construct (residues 161-299, referred to as PEX19 CTD) shows that only amino acids from the C-terminus of PEX19 correspond to well-dispersed peaks. Additional N-terminal residues give rise to signals in the center of the spectrum and do not induce chemical shift perturbations of resonances in the C-terminal part. Thus, there are no strong interactions between the N- and C-terminus of PEX19.

3.1.2 Farnesylation of PEX19

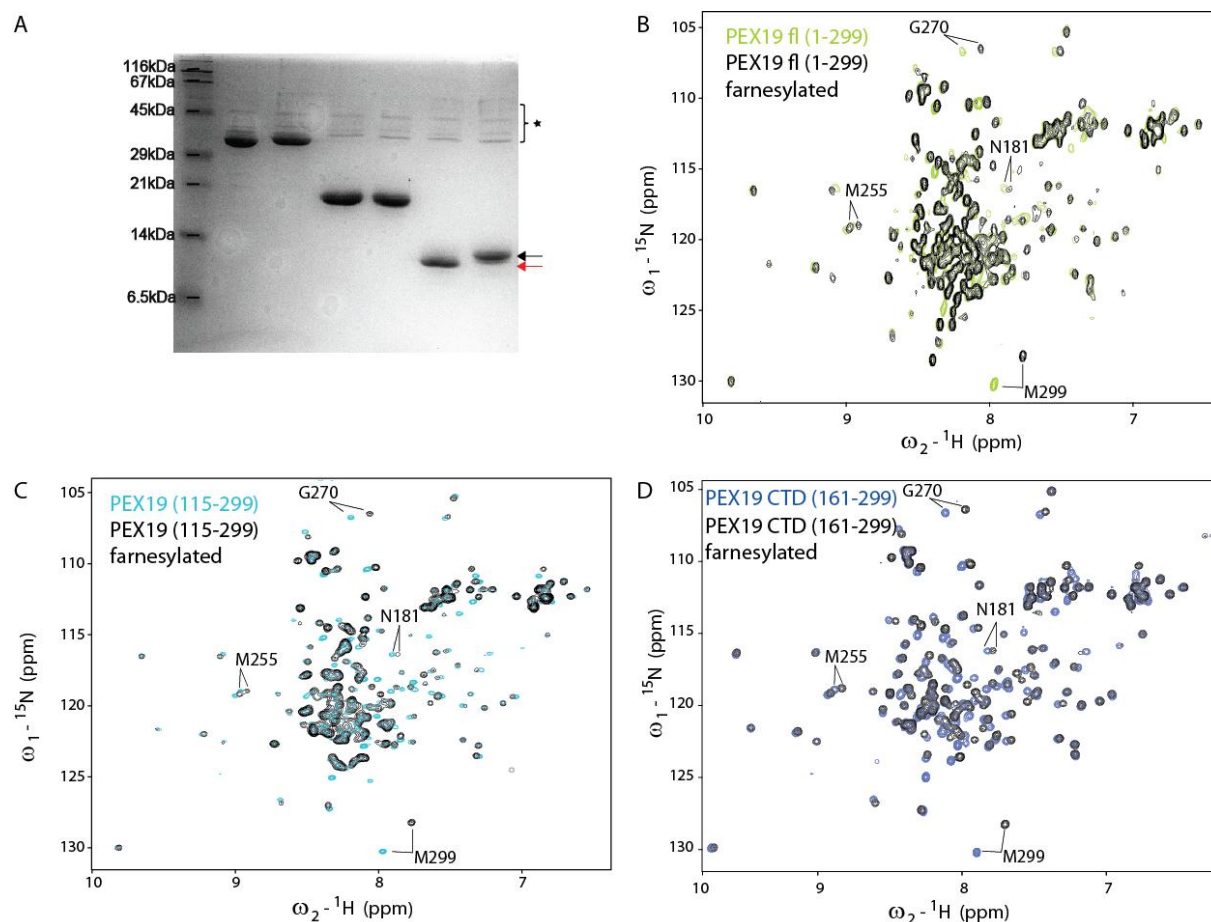


Figure 3.3 *In vitro* farnesylation of PEX19. SDS-PAGE analysis of farnesylation of PEX19 fl (1-299), PEX19 (115-299) and PEX19 CTD (161-299). Lanes (10-14 μ g protein): 1 = marker, 2 = PEX19 full-length farnesylated, 3 = PEX19 full-length, 4 = PEX19 (115-299) farnesylated, 5 = PEX19 (115-299), 6 = PEX19 CTD farnesylated, 7 = PEX19 CTD. The farnesylated proteins migrate faster on the gel as is representatively labeled for farnesylated PEX19 CTD (*red arrow*) and non-farnesylated PEX19 CTD (*black arrow*). The second lane for each construct shows the negative control without farnesyl pyrophosphate. The bracket and the asterisk indicate bands from the different subunits of the farnesyl transferase. (B-D) Chemical shift perturbations upon farnesylation of PEX19. Overlay of ^1H ^{15}N HSQC spectra of PEX19 fl (1-299) (B), PEX19 (115-299) (C) and PEX19 CTD (161-299) (D) with (black) and without (colored) farnesylation. As shown for the representatively labeled peaks the same residues undergo chemical shift perturbations in all PEX19 proteins.

In vitro farnesylation of PEX19 yields a homogeneously modified sample and slightly enhances the electrophoretic mobility as shown by SDS-PAGE analysis (Fig. 3.3A). PEX19 proteins maintain their solubility regardless of presence or absence of farnesylation. A comparison of ^1H , ^{15}N HSQC spectra of farnesylated and non-farnesylated PEX19 demonstrates a number of chemical shift perturbations. PEX19 is completely farnesylated *in vitro* as no signals corresponding to the non-farnesylated protein are detected. Backbone

assignments were obtained for farnesylated and non-farnesylated PEX19 CTD. Transfer of the assignments of the resolved signals to longer PEX19 constructs demonstrate that chemical shift perturbations in ^1H , ^{15}N HSQC spectra of resolved signals coincide for PEX19 full-length, PEX19 (115-299) and PEX19 CTD. Within PEX19 CTD the chemical shift perturbations are not limited to the farnesylation site but scattered throughout the amino acid sequence and mainly affect the region around helix $\alpha 1$ and the C-terminal 30 residues (Fig. 3.4).

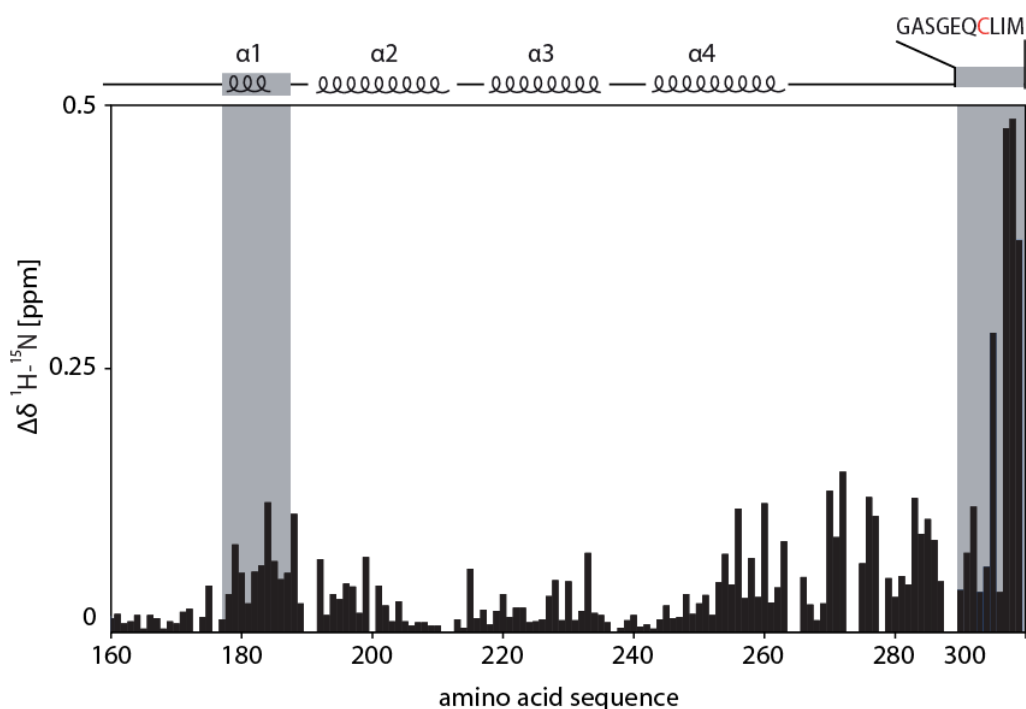


Figure 3.4 Chemical shift perturbations upon farnesylation of PEX19 CTD. (A) Amide proton chemical shift differences between farnesylated and non-farnesylated PEX19 CTD plotted against the amino acid sequence. The secondary structure is indicated on top and the amino acid sequence is given for the C-terminal ten residues with the farnesylated cysteine in red. C-terminal residues which undergo the most prominent changes and affected residues in helix $\alpha 1$ are highlighted with a grey box.

3.1.3 NMR analysis of secondary structure and relaxation properties of PEX19 CTD with and without farnesylation

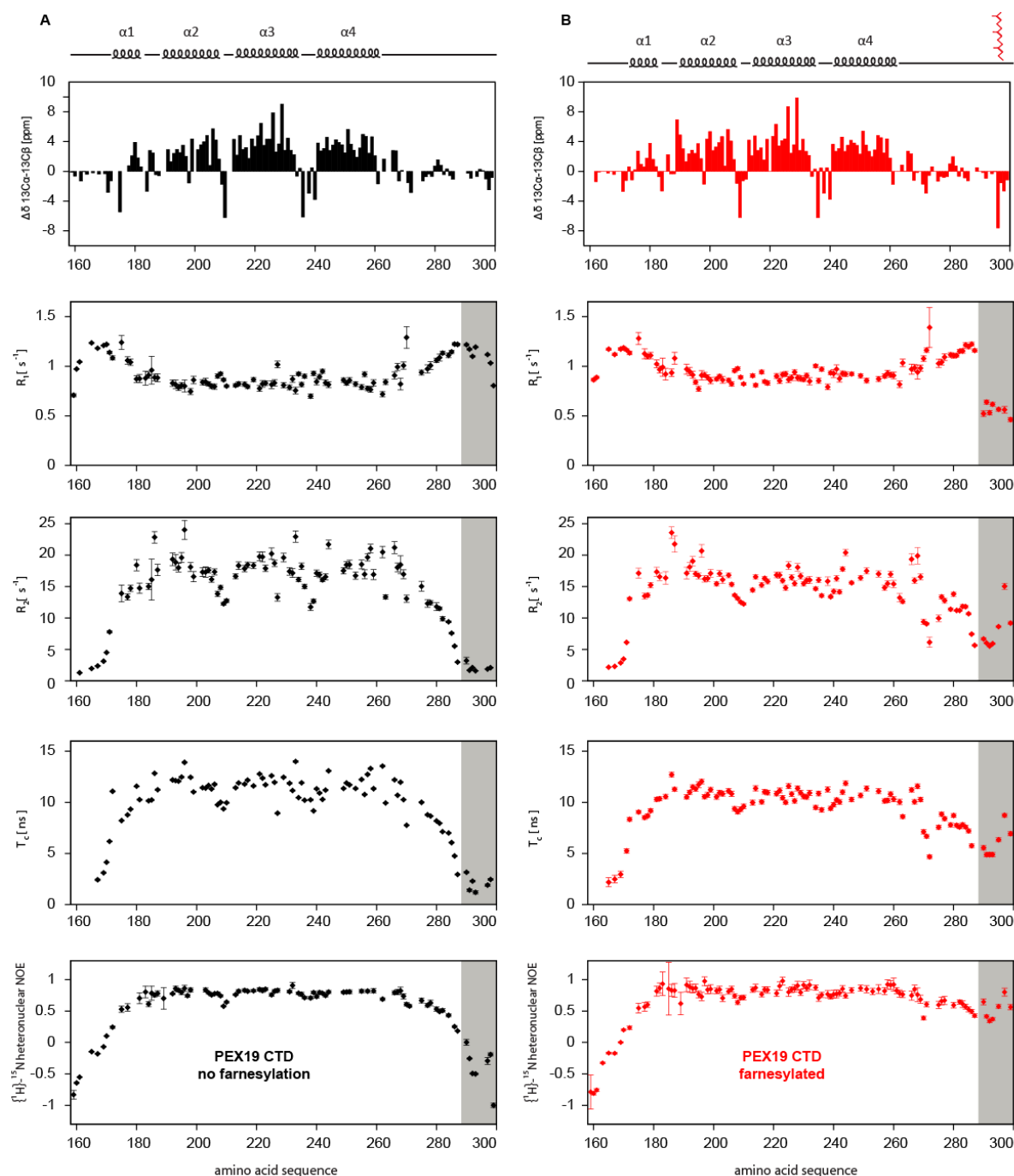


Figure 3.5 Secondary chemical shift analysis and ^{15}N relaxation studies of PEX19 CTD without and with farnesylation plotted against the amino acid sequence. The $^{13}\text{C}^\alpha - ^{13}\text{C}^\beta$ secondary chemical shifts of PEX19 CTD (upper panel) indicate four α -helices for the non-farnesylated (A, black) and the farnesylated (B, red) protein. R_1 and R_2 rates, the correlation time τ_c and $\{^1\text{H}\}-^{15}\text{N}$ heteronuclear NOE values in panel 2, 3, 4 and 5 change upon farnesylation for the C-terminal residues highlighted with grey boxes. Secondary structure elements as well as the farnesylation site are indicated on top.

$^{13}\text{C}^\alpha$ - $^{13}\text{C}^\beta$ secondary chemical shifts of PEX19 without farnesylation indicate four α -helices between residues 171 and 260 and an unstructured stretch from residue 261 to 299. Farnesylation does not considerably affect the $^{13}\text{C}^\alpha$ - $^{13}\text{C}^\beta$ secondary chemical shifts with the exception of the farnesylated cysteine (Fig. 3.5, upper panel).

Dynamic properties of PEX19 CTD were analyzed by measuring R_1 and R_2 relaxation rates as well as the $\{^1\text{H}\}$ - ^{15}N heteronuclear NOE. Due to signal overlap in ^1H , ^{15}N HSQC spectra quantitative evaluation was limited to approximately 70% of the peaks. R_1 relaxation rates of non-farnesylated PEX19 CTD are very similar between residues 180 and 265 and increased for amino acids N- and C-terminal of these boundaries. In farnesylated PEX19 CTD R_1 rates are unchanged for residues 161 to 290 compared to non-farnesylated PEX19 CTD but significantly reduced for the ten C-terminal residues (Fig. 3.5, second panel). R_2 relaxation rates are low for the N-terminus and slightly reduced in the loop regions connecting the four α -helices in PEX19 CTD with and without farnesylation. Low values are measured for the ten C-terminal residues in non-farnesylated PEX19 CTD which are increased upon farnesylation (Fig. 3.5, third panel). These residues also have an increased correlation time in farnesylated PEX19 CTD (Fig. 3.5, fourth panel). The overall correlation time τ_c for both non-farnesylated (11.4 ns) and farnesylated (10.5 ns) PEX19 CTD corresponds to monomeric tumbling of PEX19 CTD with and without farnesylation. For both non-farnesylated and farnesylated PEX19 CTD $\{^1\text{H}\}$ - ^{15}N heteronuclear NOE data describe a rigid core domain with values of approximately 0.8 and a flexible N-terminal stretch from residue 161 to 171 with very low rates between 0.5 to -0.9 which is indicative for dynamics on a picosecond to nanosecond timescale. The C-terminal 16 residues are equally flexible in absence of farnesylation; however, attachment of the farnesyl group significantly increases the $\{^1\text{H}\}$ - ^{15}N heteronuclear NOE values indicating that this region becomes rigid upon farnesylation (Fig. 3.5, lowest panel).

3.1.4 Spin labeling

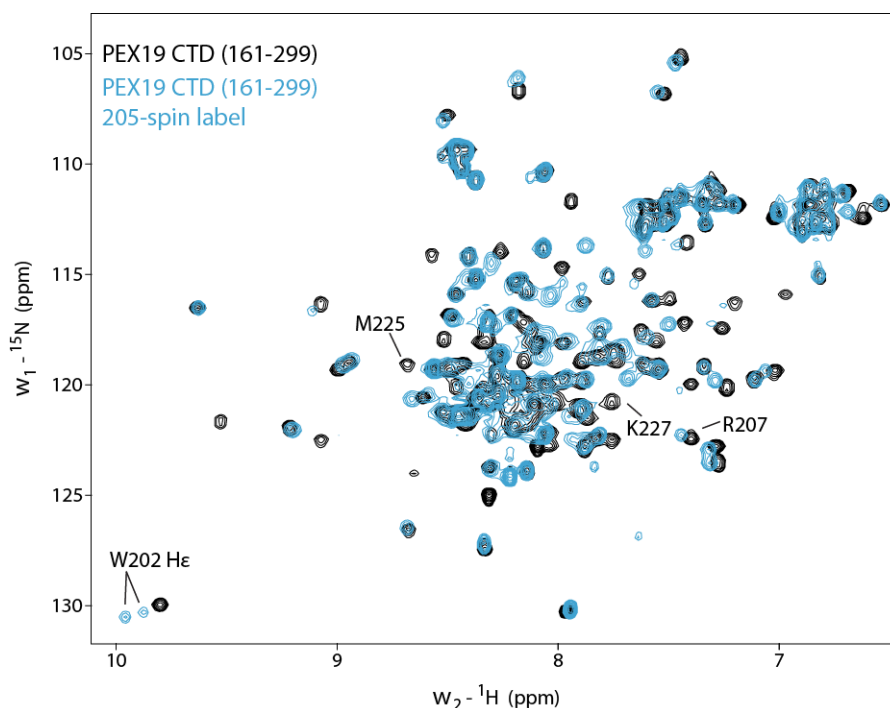


Figure 3.6 Overlay of the ^1H ^{15}N HSQC spectra of PEX19 CTD and PEX19 CTD with a spin label at position 205.

The single cysteine variant PEX19 CTD $\Delta\text{c/S205C}$ with iodoacetamide proxyl in the reduced state attached to C205 (cyan) shows local chemical shift perturbations compared to wildtype PEX19 CTD (black).

Paramagnetic relaxation enhancement was measured for a iodoacetamide proxyl spin label attached to the farnesylated and non-farnesylated single cysteine variants S205C and S286C in PEX19 CTD. Exchange of the two native cysteine residues 226 and 229 against alanine induces local chemical shift perturbations of several resonances which could not be unambiguously assigned to a certain amide proton in the ^1H , ^{15}N HSQC of the mutated proteins. The side chain amide proton of W202 gives rise to two signals in the ^1H , ^{15}N HSQC spectra of PEX19 CTD with the spin label attached to position 205 indicative of a second conformation (Fig. 3.6).

For the spin label at position 205 the $I_{\text{ox}}/I_{\text{red}}$ ratio is strongly reduced for amide protons between residue 194 and 213 and additionally from residue 266 to 275. The pattern is highly similar for farnesylated and non-farnesylated PEX19 CTD (Fig. 3.7A). Attachment of the spin-label to position 286 in a segment with relatively high backbone dynamics lowers the $I_{\text{ox}}/I_{\text{red}}$ ratio for the residues 257 to 299 adjacent to the spin-label position and for amide protons in helix $\alpha 1$ (Fig. 3.7B). For both spin label positions the PRE effects are similar for farnesylated and non-farnesylated PEX19 CTD with the exception of M299 with a significantly reduced

ratio when PEX19 CTD is farnesylated (Fig. 3.7B). Mapping of the PRE effects on the solution structure of farnesylated PEX19 CTD (s. 3.1.8) shows that the affected residues are located within the expected distance to the spin label (Fig. 3.7C and D).

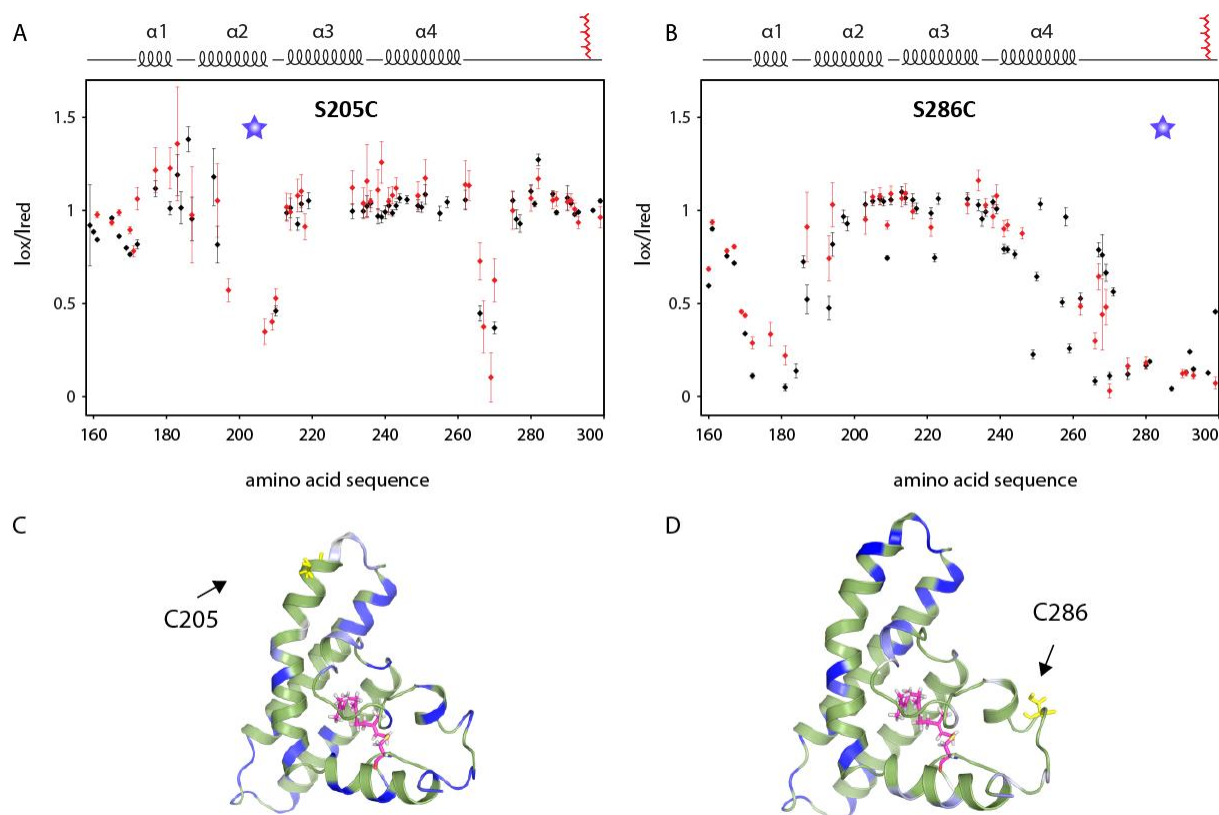


Figure 3.7 Paramagnetic relaxation enhancement of PEX19 CTD with and without farnesylation with a spin-label at residue 205 and 286. I_{ox}/I_{red} ratios of amide protons with the spin label at position 205 (A) and 286 (B) of non-farnesylated (black) and farnesylated (red) PEX19 CTD plotted against the amino acid sequence. The position of the spin label is indicated with a purple asterisk. (C-D) Mapping of I_{ox}/I_{red} ratios of farnesylated PEX19 CTD with a spin label at 205 (C) and at 286 (D) on the NMR solution structure of farnesylated PEX19 CTD using a white-blue gradient with blue corresponding to a ratio of 1. The serine residue at the spin label position is shown in stick representation and highlighted in yellow. Residues which were not analyzed due to signal overlap are colored in olive.

3.1.5 Solvent paramagnetic relaxation enhancement

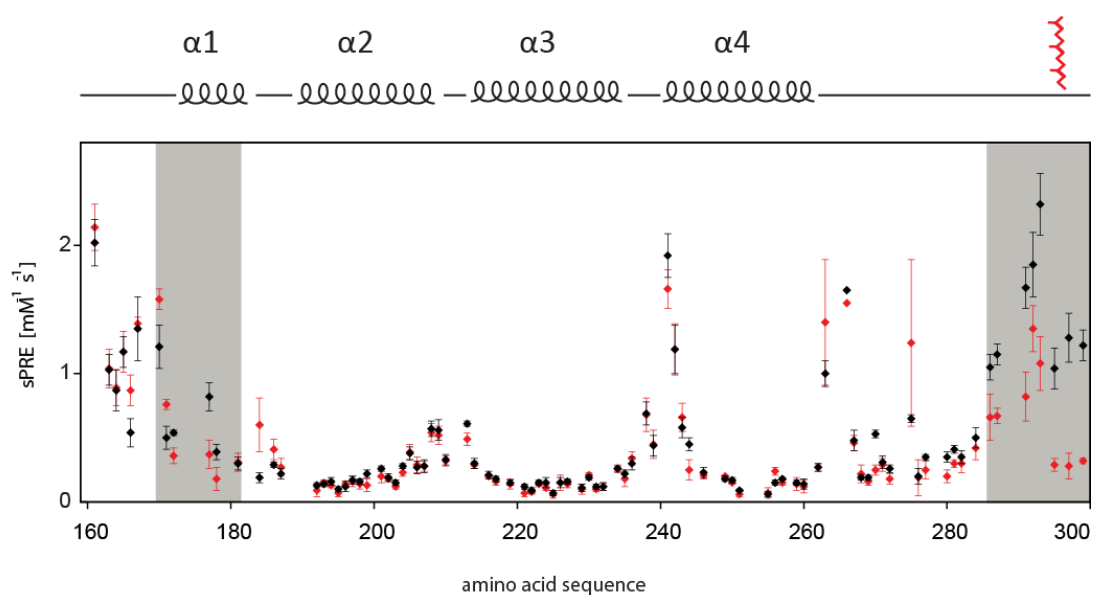


Figure 3.8 Solvent PRE rates of backbone amide protons of farnesylated and non-farnesylated PEX19 CTD.

Solvent PRE rates of backbone amide protons are shown for PEX19 CTD with (red) and without (black) farnesylation. The secondary structure and the farnesylated cysteine are indicated on top. Regions which undergo the most prominent changes upon farnesylation are highlighted with grey boxes.

Solvent PRE rates for amide protons in PEX19 CTD are low within the four α -helical regions for the farnesylated and the non-farnesylated protein. Flexible sections at the N-terminus (residues 161-171) and the short linker between helices α 2 and α 3 (residues 208-213) and helix α 3 and α 4 (residues 238-243) show a high relaxation enhancement. Values for residues 192-284 are highly similar between farnesylated and non-farnesylated PEX19 CTD. The pattern for amide protons in helix α 1 changes upon farnesylation. Additionally, solvent PRE rates are significantly reduced for residues between 286 and 293. The most prominent effects are observed for the amide protons of Q295, I298 and M299 which are solvent exposed in absence of farnesylation but become shielded when the farnesyl is attached (Fig. 3.8).

3.1.6 Farnesyl spectra and assignments

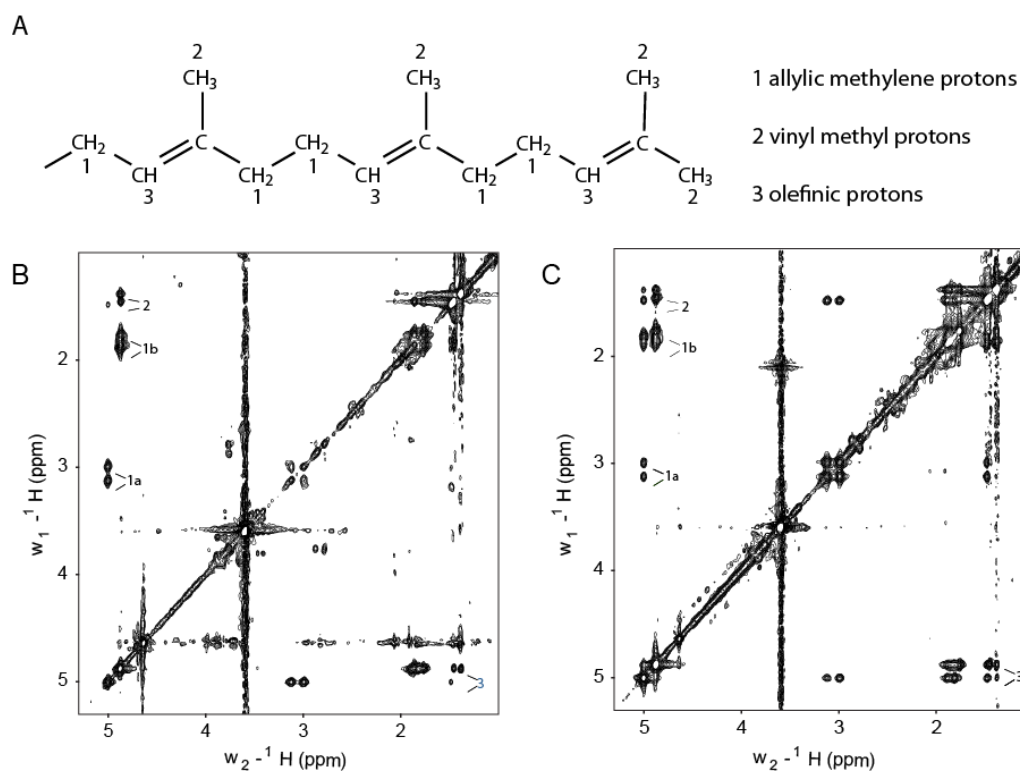


Figure 3.9 Farnesyl protons. (A) Chemical structure of the farnesyl with the chemically different groups of aliphatic protons highlighted. Figure prepared with ChemDraw Ultra 12.0 (CambridgeSoft). (B) ¹⁵N, ¹³C filtered TOCSY and (C) NOESY spectra of farnesylated PEX19 CTD. Representatively labeled cross-peaks: 1a=resonances from allylic methylene protons directly attached to the cysteine, 1b=allylic methylene protons, 2= vinyl methyl protons, 3=olefinic protons

Farnesyl, a C₁₅ isoprenoid, contains three chemically different groups of aliphatic protons, i. e. allylic methylene protons, vinyl methyl protons and olefinic protons (Fig. 3.9A). The proton frequencies of the farnesyl group were detected by two-dimensional double-filtered TOCSY and NOESY spectra of ¹³C, ¹⁵N labeled farnesylated PEX19 CTD (Fig. 3.9B and C). Resonances from the two allylic methylene protons adjacent to the C296 sulfur are separated; however, overlap between the residual farnesyl resonances does not allow for unambiguous assignments on the basis of these homonuclear spectra. As ¹³C labeled farnesyl is not commercially available natural abundance ¹H ¹³C HSQC spectra were recorded. ¹H ¹³C HSQC spectra of farnesyl were measured on farnesyl pyrophosphate in methanol and farnesylated PEX19 CTD. Signals from allylic methylene and vinyl methyl protons cluster in the same region as resonances from aliphatic amino acids in PEX19 CTD. In the natural abundance ¹H ¹³C HSQC spectrum of U-[²H], U-[¹³C] glucose labeled farnesylated PEX19 CTD signals from

the farnesyl cannot be identified unambiguously because of background signals from residual protonation of the protein (Fig. 3.10).

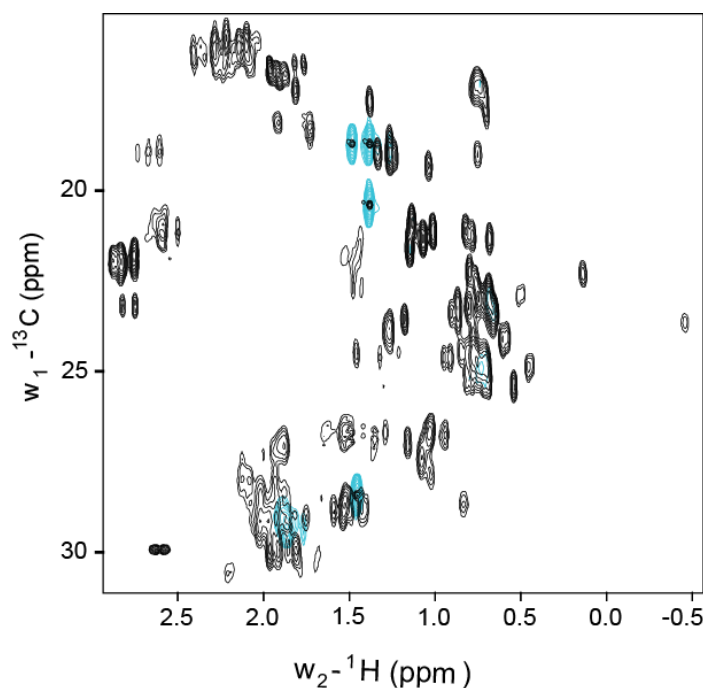


Figure 3.10 Natural abundance ^1H , ^{13}C HSQC spectra of farnesyl pyrophosphate (cyan) and farnesylated PEX19 CTD labeled with $\text{U}-[^2\text{H}]$, $\text{U}-[^{13}\text{C}]$ glucose (black). Background signals from the protein due to the residual glucose protonation overlap with farnesyl signals.

In the natural abundance ^1H ^{13}C HSQC spectrum of farnesylated PEX19 CTD labeled with $\text{U}-[^2\text{H}]$ -D-glucose only signals from the farnesyl group with few background signals are detected. With the exception of two of the three olefinic protons all carbon frequencies are resolved for the farnesyl attached to PEX19 CTD. Only the three farnesyl protons which are closest to the cysteine undergo significant chemical shift perturbations when comparing the farnesyl group attached to the protein with farnesyl pyrophosphate in methanol (Fig. 3.11).

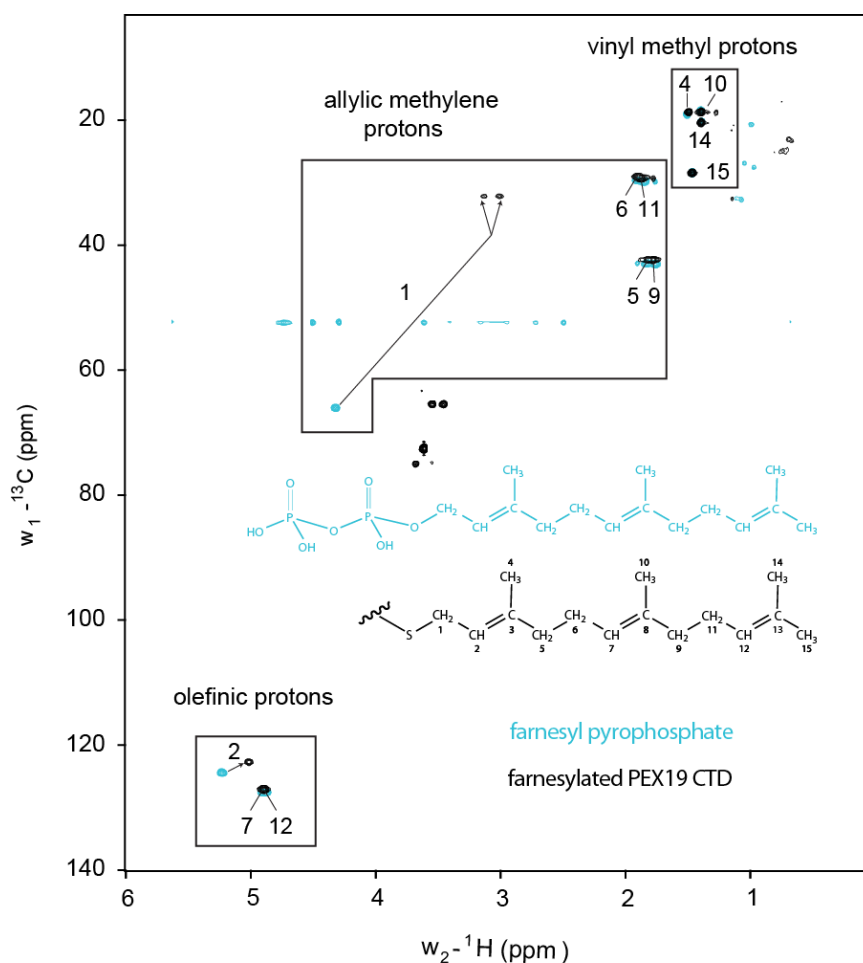


Figure 3.11 Proton and carbon resonances of the farnesyl group. Comparison of natural abundance ^{13}C , ^1H HSQC spectra of farnesyl pyrophosphate in methanol (cyan) and farnesyl attached to perdeuterated PEX19 CTD via a thioether (black). Arrows indicate chemical shift changes between atoms in free and bound farnesyl.

3.1.7 Specific labeling strategies

Substantial overlap in the methyl region of spectra of uniformly ^{13}C labeled PEX19 CTD due to a high content of aliphatic amino acids - 17 leucine, six isoleucine and nine methionine residues – was resolved by specific isotope labeling. In spectra of farnesylated PEX19 CTD labeled with ^{13}C methionine or ^{13}C isoleucine all signals are sufficiently separated whereas resonances of a sample with uniformly ^{13}C labeled leucine are not. ^{13}C methyl-labeled (^1H - 1δ methyl)-isoleucine, (^1H - 1δ methyl)-leucine and (^1H - 1γ methyl)-valine) and stereospecifically methyl-labeled (^{13}C , $^1\text{H}_3$]-proS labeled leucine and valine) farnesylated PEX19 CTD samples provide the required simplification of the spectra (Fig. 3.12).

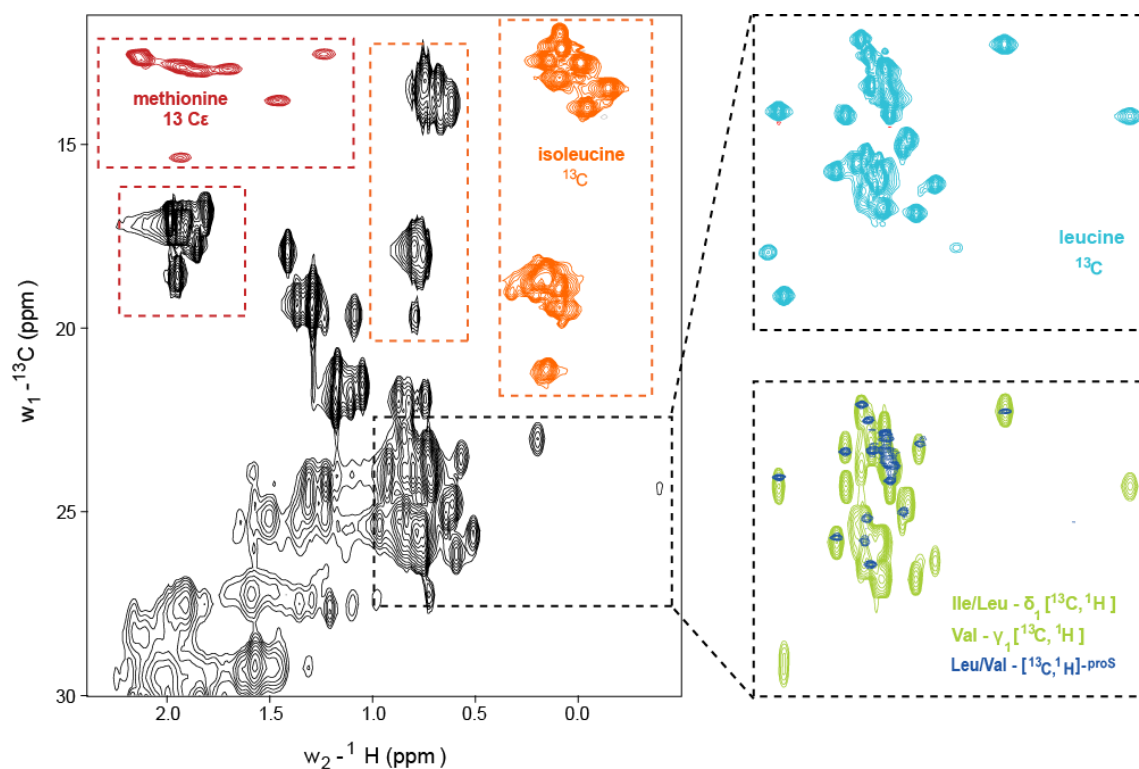


Figure 3.12 Selective labeling of aliphatic amino acids in PEX19 CTD. Methyl region of a ^{13}C ^1H HSQC spectrum of uniformly ^{13}C labeled farnesylated PEX19 CTD (black). ^{13}C ^1H HSQC spectra of perdeuterated farnesylated PEX19 CTD isotope enriched for specific amino acids or chemical groups coloured as follows: $^{13}\text{C}\epsilon$ methionine = dark red; ^{13}C ^1H labeled isoleucine = orange; ^{13}C ^1H labeled leucine = cyan; overlay of (^1H - 1δ methyl)-isoleucine, (^1H - 1δ methyl)-leucine, (^1H - 1γ methyl)-valine labeled PEX19 CTD (green) with pro-S specific ^{13}C ^1H leucine/valine methyl labeling (blue)

Resonances of aromatic amino acids in farnesylated PEX19 CTD, especially of the four phenylalanine and three tyrosine residues, are poorly dispersed (Fig. 3.13A). In a 2D homonuclear NOESY spectrum of farnesylated PEX19 CTD reverse labeled with phenylalanine these frequencies are resolved. NOESY cross peaks to the farnesyl are observed for F278 as the only aromatic residue (Fig. 3.13B).

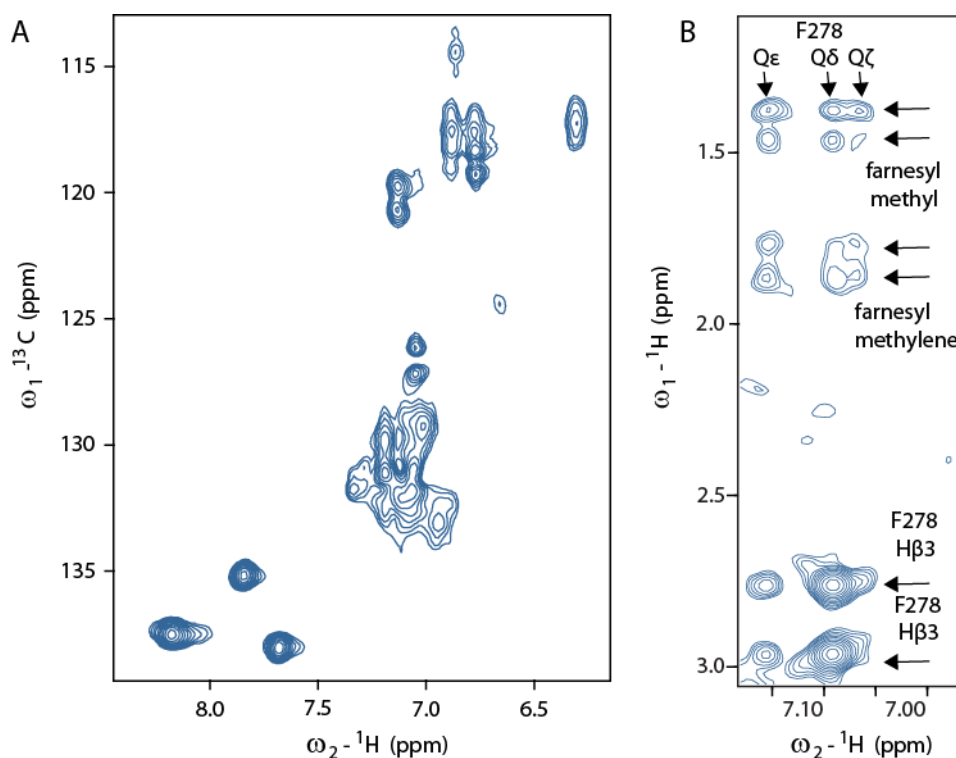


Figure 3.13 Reverse labeling of phenylalanine in farnesylated PEX19 CTD. (A) ^1H , ^{13}C HSQC spectra of the aromatic region of farnesylated PEX19 CTD. (B) Strip of a 2D homonuclear NOESY spectrum of farnesylated perdeuterated PEX19 CTD reverse labeled with phenylalanine with NOEs between F278 and the farnesyl group labeled.

The limited number of resonances in ^{13}C edited NOESY-HSQC experiments of the selectively labeled farnesylated PEX19 CTD samples reduces the signal overlap in the methyl region and allows for the identification of farnesyl-protein NOESY cross peaks. Ambiguities from samples containing uniformly ^{13}C labeled isoleucine or leucine are resolved by comparison with spectra of methyl-labeled protein (Fig. 3.14).

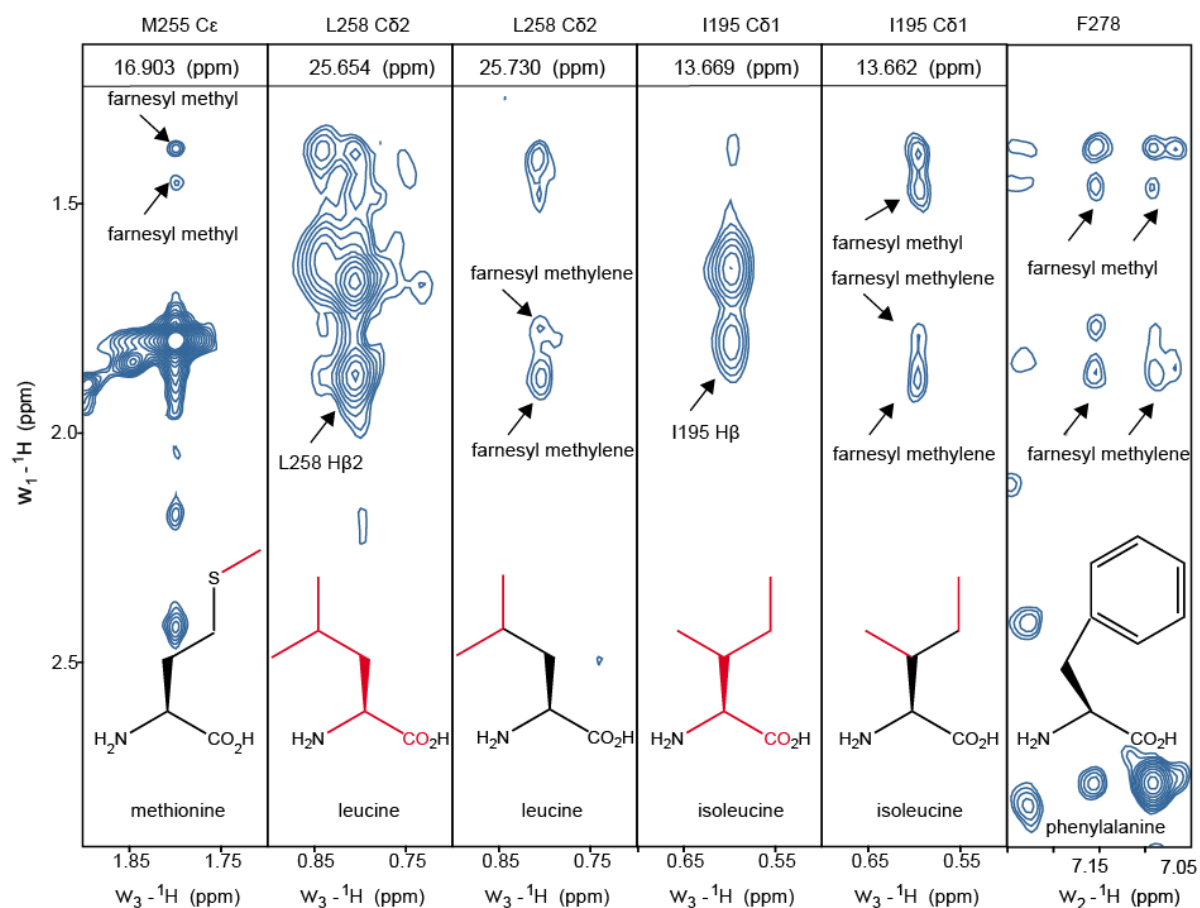


Figure 3.14 Protein-farnesyl NOESY cross peaks between specifically labeled farnesylated PEX19CTD. Representative farnesyl NOESY cross peaks are labeled in strips of ^{13}C edited HSQC NOESY spectra of the differently labeled samples. ^{13}C enriched positions are highlighted in red in the chemical formula of the respective amino acids.

3.1.8 NMR solution structure of farnesylated PEX19 CTD

Table 3.1 Structural statistics of farnesylated PEX19 CTD

NOE-based distance restraints	
total number of NOEs	3728
intraresidual, sequential	823
medium range ($2 \leq i-j \leq 4$)	1002
long range ($ i-j \geq 5$)	600
protein-farnesyl	203
other restraints	
total number of dihedral angle restraints	187
Φ	91
Ψ	96
total number of RDCs (H^N-N , $N-C'$, H^N-C')	136
Q^{RDC} (%)	28
average pairwise r.m.s. deviation	
backbone (\AA)	0.45 ± 0.09
heavy atom (\AA)	0.85 ± 0.11
violations (mean \pm s. d.)	
distance restraints (\AA)	0.018 ± 0.00
max. distance restraint violation (\AA)	0.46
dihedral angle restraints ($^\circ$)	0.913 ± 0.06
max. dihedral angle violation ($^\circ$)	4.75
deviations from idealized geometry	
bond lengths (\AA)	0.003 ± 0.00
bond angles ($^\circ$)	0.511 ± 0.07
impropers ($^\circ$)	1.175 ± 0.04
Ramachandran plot	
most favoured regions (%)	91.5
allowed regions (%)	8.2
generously allowed regions (%)	0.2
disallowed regions (%)	0.1

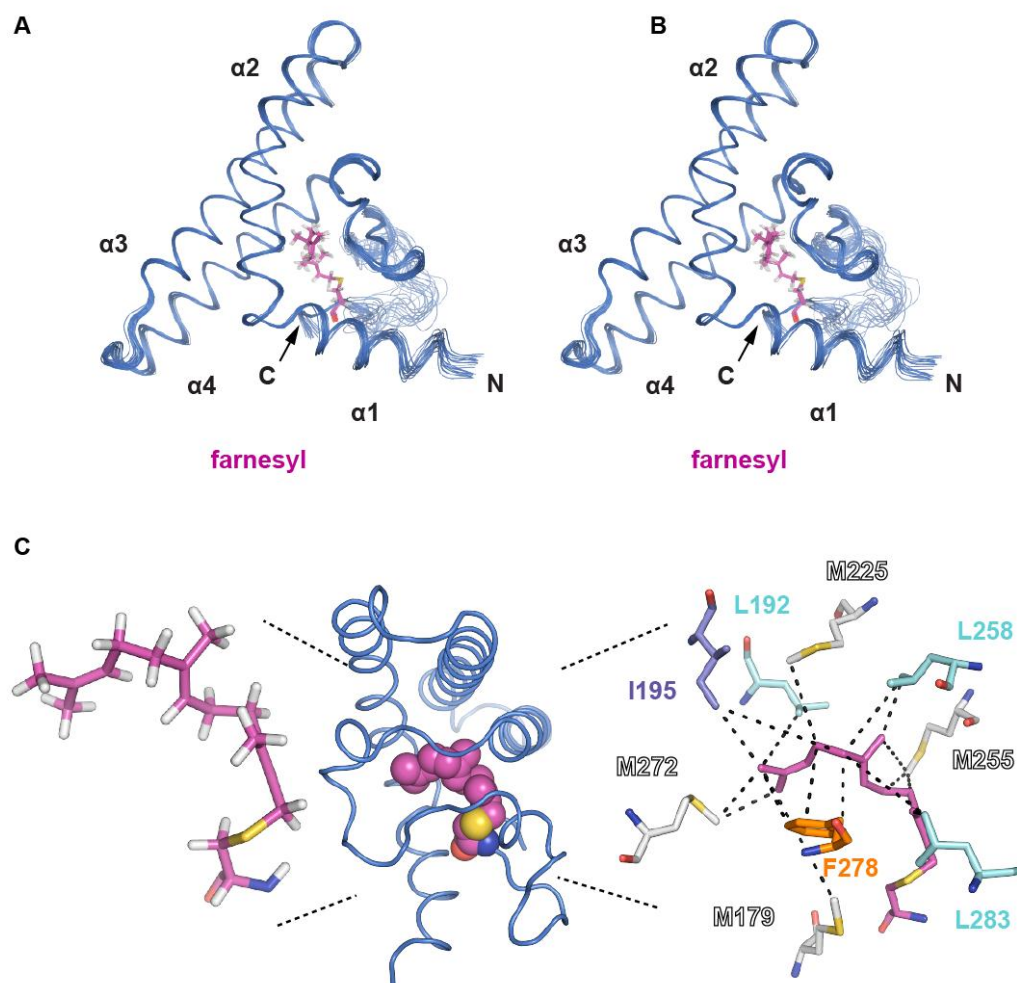


Figure 3.15 Farnesyl recognition in PEX19 CTD (a) Stereoview of the ensemble of the 20 lowest energy NMR structures. The farnesyl moiety (pink) is buried within the PEX19 CTD structure. (B) Cartoon representation of farnesylated PEX19 CTD with the the farnesyl highlighted in pink. Left: Stick representation of the farnesylated cysteine. The farnesyl adopts a bent conformation. Right: Close-up view of the farnesyl binding pocket with representative farnesyl binding amino acids shown as sticks. Cyan: leucine; white: methionine; violet: isoleucine; orange: phenylalanine.

The NMR solution structure of farnesylated PEX19 CTD was calculated as described in 2.3.1 and 2.3.6. Structure statistics after water refinement are listed in Table 3.1. PEX19 CTD is composed of four α -helices with the three α -helices from residue 185 to 270 organized in a cylindrical bundle. This bundle surrounds a large hydrophobic cavity where the farnesyl group is bound by numerous aliphatic residues. Additional contacts to the farnesyl are found in the hydrophobic surface of helix $\alpha 1$ (171-182). A loop from the unstructured C-terminal residues 270-299 forms a lid structure which covers the upper surface of the farnesyl so that the lipid is completely buried inside the protein (Fig. 3.15A and B) and adopts a bent

conformation within the hydrophobic cavity (Fig. 3.15C, left). The farnesyl recognition site in PEX19 CTD is defined by 203 NOEs between protein and isoprenoid and is mainly composed of aliphatic amino acids as there are six leucine (L183, L188, L192, L258, L283 and L297), two isoleucine (I195 and I298) and four methionine (M179, M225, M255 and M299) residues. Only one aromatic amino acid, phenylalanine 278, participates in isoprenoid binding (Fig. 3.15C, right).

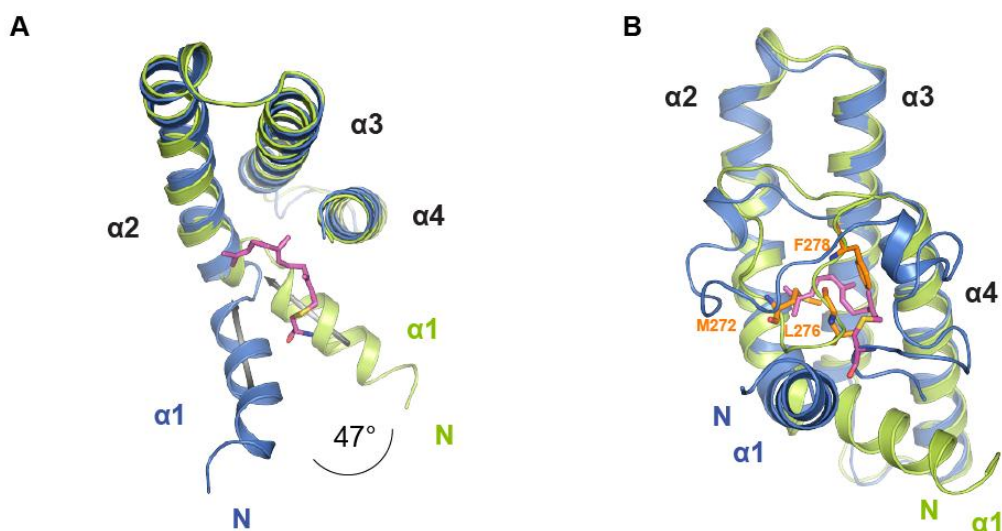


Figure 3.16 Comparison of the NMR solution structure of farnesylated PEX19 CTD with the crystal structure of PEX19 (171-283). Residues 260-280 in the crystal structure and 260-299 in PEX19 CTD are not shown for clarity. (A) Farnesylation changes the orientation of helix $\alpha1$ by an angle of 47° . (B) Several C-terminal residues in the crystal structure occupy a part of the farnesyl recognition site and shield the hydrophobic cavity.

Compared to the crystal structure of PEX19 (171-283) the central cylindrical bundle surrounding the farnesyl binding pocket does not change as shown by the r.m.s.d. of $0.84 \pm 0.06 \text{ \AA}$ for backbone atoms of residues 187-261 between the two structures. However, the orientation of helix $\alpha1$ changed by an angle of 47° as it is tilted towards the protein core by interactions with the farnesyl moiety (Fig. 3.16A). Furthermore, several residues such as M272, L276 and F278 in the C-terminus of the crystal structure partially occupy the farnesyl recognition site, thus shielding the hydrophobic cavity in absence of the farnesyl moiety (Fig. 3.16B).

3.1.9 Discussion: Farnesyl recognition in PEX19

The NMR solution structure of farnesylated PEX19 CTD presented in this thesis shows that the covalently attached farnesyl group is bound in a large cavity inside the protein and covered by a C-terminal loop region. A major challenge was to obtain the assignments for the farnesyl group as ^{13}C labeled farnesyl pyrophosphate is not available and homonuclear ^1H spectra of farnesyl protons do not provide sufficient resolution. ^{13}C resonance frequencies could only be detected by using the natural abundance of 1.1% ^{13}C in unlabeled farnesyl. To obtain information for farnesyl resonances when bound to the protein it was necessary to separate signals from protein and isoprenoid. For this purpose, fully deuterated PEX19 was expressed using U- ^2H , U- ^{13}C glucose as sole carbon source. However, deuteration of the commercially available U- ^2H , U- ^{13}C glucose is only 97% with 3% residual ^{13}C -bound protons for the protein which results in high background signals from residual protein protonation. For natural abundance ^1H ^{13}C HSQC spectra of farnesylated PEX19 CTD the amount of ^{13}C -bound protons in PEX19 CTD had to be reduced compared to the farnesyl group, thus, PEX19 CTD was expressed in a perdeuterated background with U- ^2H -D-glucose which reduces the statistic occurrence of ^{13}C -bound protons in the protein to 0.03% and is thus negligible compared to the farnesyl. Implementation of this labeling scheme succeeded to resolve the ^1H and ^{13}C resonance frequencies of the farnesyl group attached to the protein (s. 3.1.6).

A structural impact of farnesylation is probably limited to the structured C-terminus of PEX19 as farnesylation mainly induces chemical shift perturbations in ^1H , ^{15}N HSQC spectra in residues between position 161 and 299 (s. 3.1.2). Furthermore, the NMR solution structure of farnesylated PEX19 CTD shows that the farnesyl is entirely buried within the protein where it is placed in an uncommon binding site. The α -helices of PEX19 CTD form a large hydrophobic cavity which serves as a pocket for the isoprene group and do not match the sequence or secondary structure of other farnesylated proteins like Ras (Ismail et al., 2011) or transducin (Loew et al., 1998). An overall structural similarity can be found in the protein family of the CaaX prenyltransferases, like geranylgeranyltransferase type I (GGTase-I) and farnesyltransferase (FTase). In spite of only 25 % sequence conservation the β subunits form the same α - α barrel structure harboring the isoprenoid binding site. In both enzymes, conserved aromatic amino acids in a hydrophobic cavity of about 15 Å width and 14 Å depth interact with the isoprene units of the substrate while a positively charged patch

binds the pyrophosphate. The farnesyl is coordinated in an extended conformation. While the first three isoprene units of geranylgeranyl align with the farnesyl the additional fourth unit is bent in a right angle with respect to the preceding ones. In PEX19, the farnesyl is arranged by aliphatic instead of aromatic residues as in the farnesyl transferase complexes and adopts a bent conformation within PEX19, probably due to the smaller size of the 15.6 kDa PEX19 CTD compared to the 94 kDa prenyl transferases (Lane and Beese, 2006) (Fig. 3.17A and B). The farnesyl group is endowed with sufficient conformational flexibility to arrange the isoprenoid in a curved form as has also been observed in sesquiterpene cyclases which catalyze the cyclization of farnesyl pyrophosphate (McAndrew et al., 2011) (Fig. 3.17C).

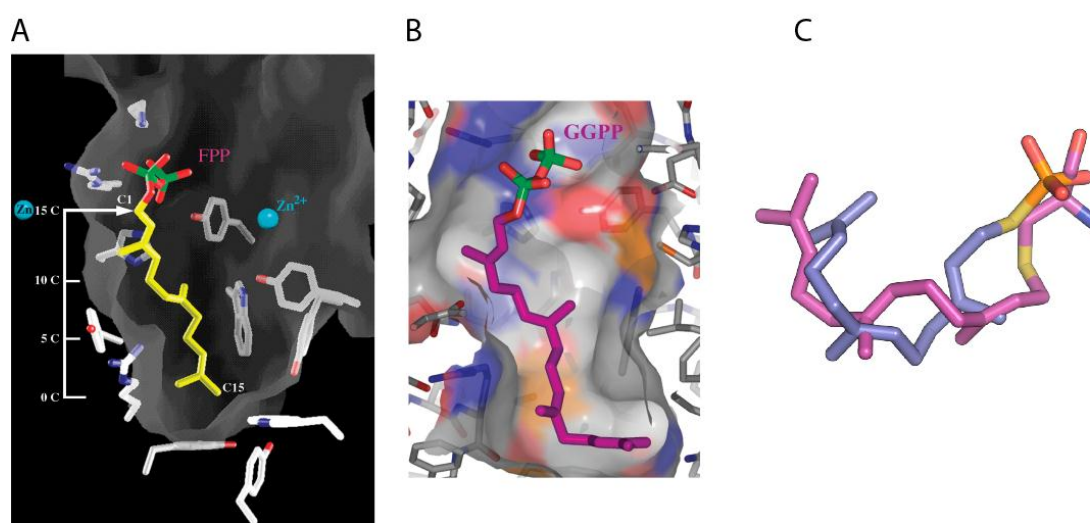


Figure 3.17 Isoprenoid conformations. Farnesyl transferase binds farnesyl pyrophosphate in an extended conformation, coordinated by aromatic amino acids (Lane and Beese, 2006) (A). The terminal isoprene unit of geranylgeranyl phosphate is kinked (B). Both farnesyl pyrophosphate bound by sesquiterpene synthase (McAndrew et al., 2011) (violet) and the farnesyl group in PEX19 (magenta) adopt a bent conformation

3.2 PEX19-PMP interactions

3.2.1 PEX19-PMP NMR titrations

NMR titrations were performed with different peptides from various PMPs which are listed in Table 2.11. A 1D spectrum of the PEX13 peptide in the same phosphate buffer used for NMR studies of PEX19 shows that the peptide is at least partially soluble (Fig. 3.18A). However, NMR titrations of PEX19 CTD with the PEX13 peptide induce rapid precipitation and aggregation of protein and peptide as can be seen by a general decrease in signal intensity in ^1H , ^{15}N HSQC spectra. The effect is more pronounced for the farnesylated protein. For both farnesylated and non-farnesylated full-length PEX19 the same aggregation and precipitation effects as for PEX19 CTD are observed, again with stronger effects on the farnesylated protein. The signal dispersion of residues N-terminally from PEX19 CTD in the ^1H ^{15}N HSQC is not improved upon peptide addition either (Fig. 3.18B-F).

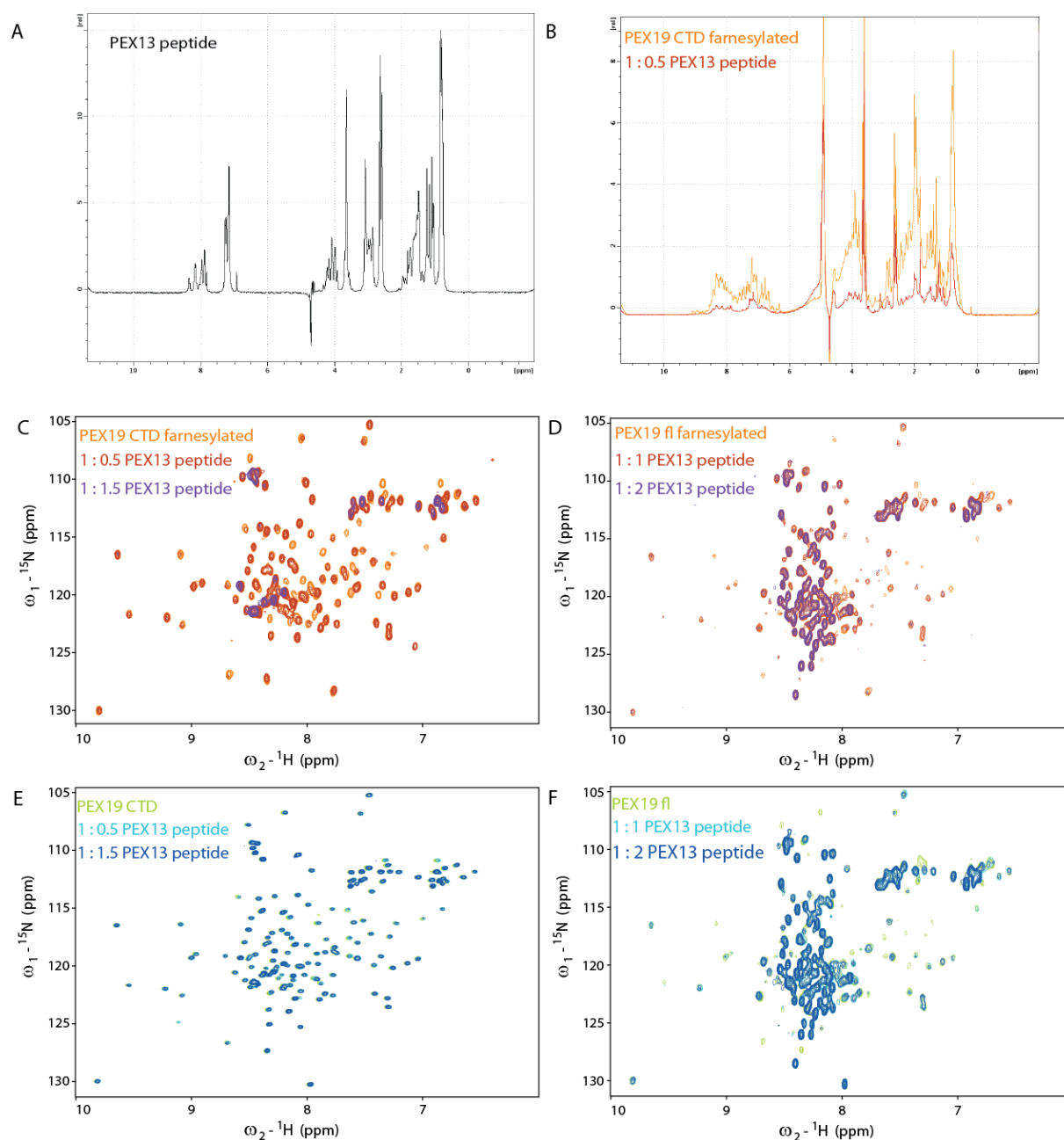


Figure 3.18 NMR titration experiments of PEX19 with a PEX13 peptide. (A) 1D ^1H NMR spectrum of a 15 amino acid PEX13 peptide. (B) Overlay of 1D ^1H NMR spectra of farnesylated PEX19-CTD without PEX13 peptide (orange) and in presence of 1.5fold excess of PEX13 peptide (red). (C-F) ^1H ^{15}N HSQC spectra of farnesylated PEX19 CTD. (C) farnesylated full-length PEX19 (D), non-farnesylated PEX19 CTD (E) and non-farnesylated full-length PEX19 (F) with increasing PEX13 concentrations. Addition of the PMP peptide decreases signal intensities in all spectra with a more pronounced influence on the farnesylated proteins.

The two peptides from PEX11 were only soluble in methanol. Chemical shift perturbations in ^1H ^{15}N HSQC spectra upon titration of the peptides in methanol overlay with the control in which only methanol was added (Fig. 3.19A and B). A peptide from PEX26 was mixed in lower concentrations with farnesylated PEX19 CTD and subsequently concentrated. The ^1H ^{15}N HSQC spectrum of this sample shows few chemical shift perturbations but also strong aggregation (Fig. 3.19C). A titration performed with the same peptide at 318 K equally demonstrates aggregation of the protein (Fig. 3.19D). Specific and evaluable chemical shift perturbations were not detected in any of the chosen experimental setups.

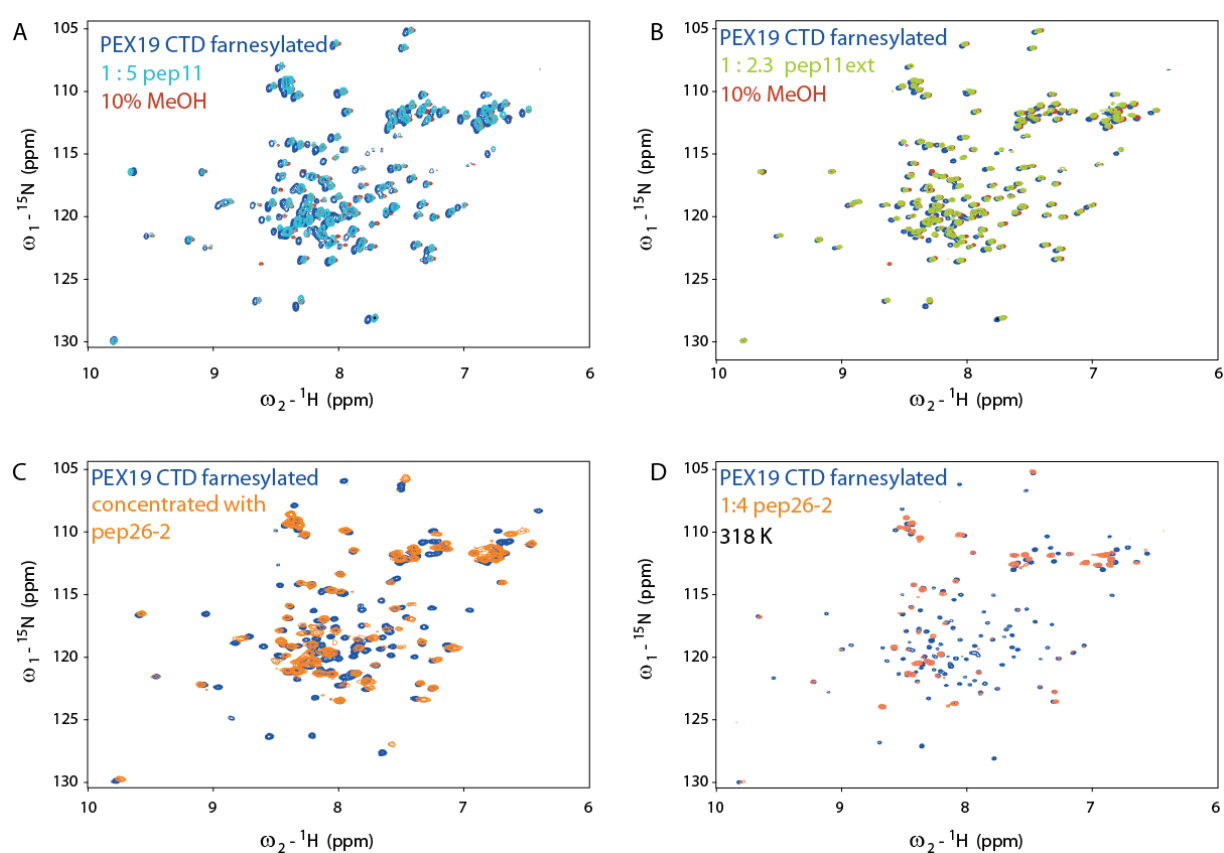


Figure 3.19 NMR titration experiments of farnesylated PEX19 CTD with PMP peptides. Addition of the PEX11 (A) and the PEX11ext peptide (B) dissolved in methanol induces the same chemical shift perturbations as the control titration with methanol. (C) A dilute mixture of farnesylated PEX19 CTD and the PEX26-2 peptide was concentrated subsequently. The corresponding ^1H ^{15}N HSQC spectrum (orange) indicates aggregation effects as seen from the overlay with the one of farnesylated PEX19 CTD (blue) (D) A titration of farnesylated PEX19 CTD with the PEX26-2 peptide at 318K shows loss of signal upon peptide addition.

3.2.2 Fusion construct of PEX19 CTD and a PMP peptide

To improve the solubility of the PEX19-PMP peptide complex a 15 amino acid sequence from PEX11 peptide was cloned to the N-terminus of PEX19 CTD. The peptide sequence is separated from the PEX19 CTD helical bundle by the intrinsically unstructured residues 161-171 in the native PEX19 sequence. The fusion protein PEX11 peptide-PEX19 CTD is soluble during expression and purification but with a strong tendency for aggregation. A comparison of the ^1H ^{15}N HSQC spectrum of PEX11 peptide-PEX19 CTD in presence of 0.1 mM DPC and PEX19 CTD without the peptide sequence shows that signals from the peptide cluster in the center of the spectrum while the PEX19 CTD resonances do not shift significantly. Titrations of PEX11 peptide-PEX19 CTD with DPC to concentrations above the critical micelle concentration do not abolish aggregation and only induce few apparently non-specific chemical shift perturbations in PEX19 CTD (Fig. 3.20).

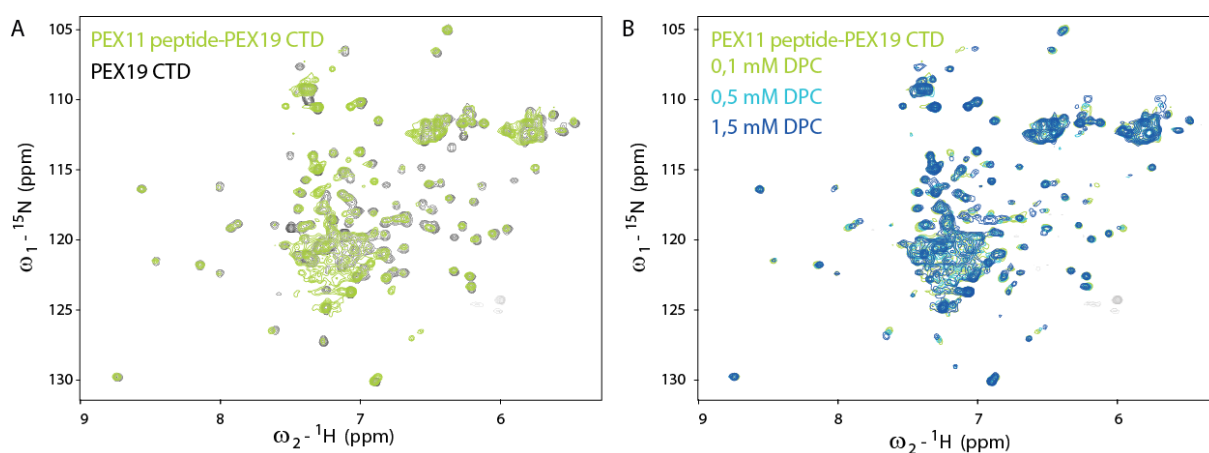


Figure 3.20 ^1H ^{15}N HSQC spectra of PEX11 peptide-PEX19 CTD. (A) Overlay of PEX19 CTD (black) with the fusion construct of a PEX11 peptide and PEX19 CTD in presence of 0.1 mM DPC. The well-dispersed peaks overlay in both spectra. The signals from the peptide sequence cluster in the center of the spectrum. (B) Titration of PEX11 peptide-PEX19 CTD with DPC induces few chemical shift perturbations.

3.2.3 Flotation assays

Interactions between PEX19 with a PEX11 peptide with liposomes were examined in flotation assays performed by Dr. R. Rucktäschel at the Ruhr-Universität Bochum. Full-length PEX19 both with and without farnesylation associates with liposomes only in presence of the PEX11 peptide. A considerable percentage of farnesylated full-length PEX19 is also detected in fractions with intermediate density between unbound and liposome-attached protein. This fraction is reduced for the non-farnesylated protein (Fig. 3.19A). Farnesylated and non-farnesylated PEX19 CTD is found at liposomes upon addition of the PEX11 peptide but not in intermediate fractions (Fig. 3.19B)

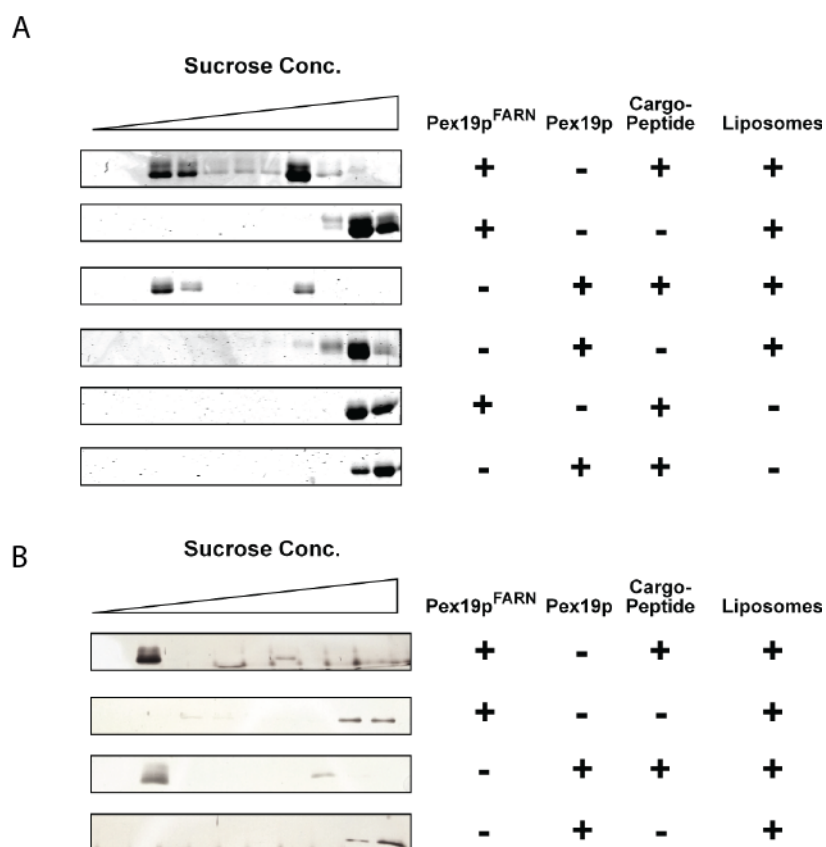


Figure 3.21 Flotation assays of PEX19. Flotation assays were performed by Dr. R. Rucktäschel, Ruhr-Universität Bochum. (A) Both farnesylated and non-farnesylated full-length PEX19 associate with liposomes upon addition of PEX11 peptide (row 1 and 3). Fractions with intermediate density also contain full-length PEX19 with higher protein content for farnesylated PEX19. (B) Farnesylated and non-farnesylated PEX19 CTD also binds to liposomes in presence of PEX11 peptide.

3.2.4 Microscale thermophoresis assays

Microscale thermophoresis assays (Jerabek-Willemsen et al., 2011) were used to determine binding affinities for PEX19 CTD with and without farnesylation to a FITC-labeled PEX11 peptide. The K_D of $29.8 \pm 1.6 \mu\text{M}$ for non-farnesylated PEX19 CTD is increased to $6.1 \pm 0.4 \mu\text{M}$ for PEX19 CTD with farnesylation (Fig. 3.21). Thus, the K_D is lowered by a factor of 4.9 confirming that farnesylation significantly improves PMP cargo recognition of PEX19.

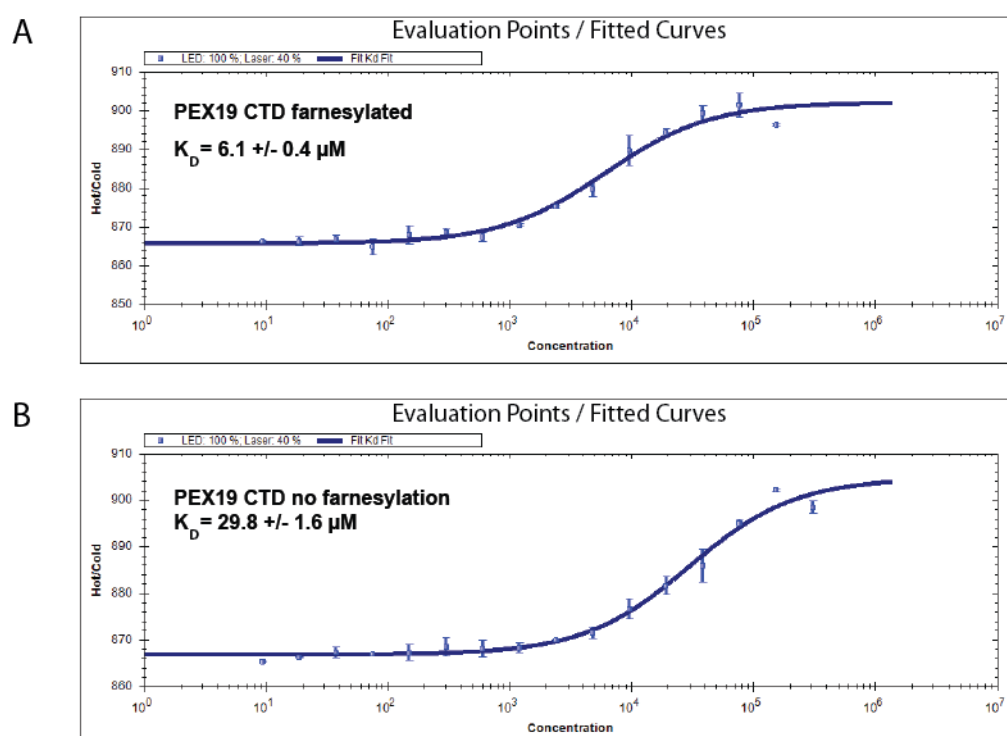


Figure 3.22 Microscale thermophoresis measurements of PEX19 CTD. Thermophoresis was measured on a FITC-labeled peptide from PEX11 with a serial dilution of PEX19 CTD with (A) and without (B) farnesylation. Farnesylation enhances the affinity for the peptide by approximately a factor of 5 from $29.8 \pm 1.6 \mu\text{M}$ to $6.1 \pm 0.4 \mu\text{M}$.

3.2.5 Discussion: The influence of farnesylation on PMP interactions and PEX19 membrane association

Previous studies have shown a positive effect of farnesylation on PEX19-PMP interactions (Rucktaschel et al., 2009). Structural and biochemical analysis presented here offer a molecular explanation: The core domain of PEX19 CTD in the NMR solution structure consisting of helix $\alpha 2$, $\alpha 3$ and $\alpha 4$ which form the farnesyl binding pocket superimposes well with the same fragment in the crystal structure but the orientation of helix $\alpha 1$ is changed (s. 3.1.8). The position in the crystal structure most likely represents a crystallization artifact as PEX19 (171-283) crystallized as a tetramer with this N-terminal helix $\alpha 1$ packing against the helix $\alpha 1$ of another PEX19 molecule but oligomerization of PEX19 has not been observed in solution (Schueller et al., 2010). ^{15}N NMR relaxation data for farnesylated and non-farnesylated PEX19 CTD presented in this work also corresponds to monomeric molecules (s. 3.1.3). Nevertheless, helix $\alpha 1$ could be rearranged in non-farnesylated PEX19 CTD in solution for several reasons. First, chemical shift perturbations upon farnesylation affect amide protons in helix $\alpha 1$ (s. 3.1.2). Second, the position of the helix is strongly influenced by contacts to the farnesyl group as seen from farnesyl-protein NOEs to M179 and L183 (s. 3.1.8). Third, solvent PRE rates document a different solvent accessibility for amide protons in helix $\alpha 1$ in farnesylated and non-farnesylated PEX19 CTD (s. 3.1.5). Expected solvent PRE rates for the farnesylated PEX19 CTD solution structure and for the crystal structure were back-calculated by Dr. T. Madl (Technische Universität München) and compared to the experimentally determined values for farnesylated and non-farnesylated PEX19 CTD (Fig 3.23). In loop regions, the experimentally determined values are generally higher than the back-calculated ones due to exchange contributions in the experimental data. Values for the core domain are in good agreement and the C-terminal amide protons reflect the difference in shielding between the farnesylated and the non-farnesylated protein. Experimental solvent PRE rates in helix $\alpha 1$ in non-farnesylated PEX19 CTD neither match the back-calculated values from the crystal structure nor the farnesylated NMR structure indicating a third and different arrangement of this region in solution.

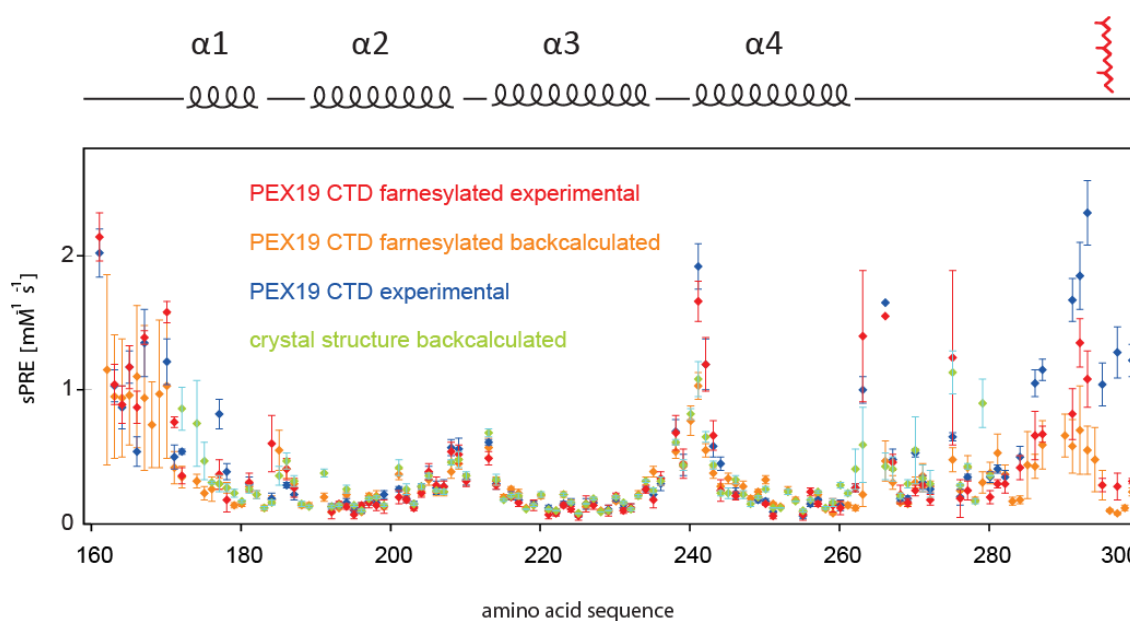


Figure 3.23 Comparison of back-calculated with experimental solvent PRE rates. Experimental solvent PRE rates of backbone amide protons of PEX19 CTD (blue) and farnesylated PEX19 CTD (red) and back-calculated solvent PRE rates from the crystal structure of PEX19 171-283 (light green) and the NMR structure of farnesylated PEX19 CTD (orange). Back-calculations were performed by Dr. T. Madl (Technische Universität München).

The nanomolar affinity of *S. cerevisiae* Pex19p for a Pex13p peptide is improved by a factor of 10 (Rucktaschel et al., 2009). Studies on non-farnesylated human PEX19 show binding affinities for PMP peptides in the micromolar range with only a slight improvement for the full-length protein compared to the C-terminus (Schueller et al., 2010). A comparison of MST data with farnesylated and non-farnesylated human PEX19 CTD collected in this study demonstrates a five-fold enhanced affinity for a PEX11 peptide in the farnesylated protein and thus corroborate a positive influence of farnesylation on PEX19-PMP interactions (s. 3.2.4). Direct farnesyl-PMP contacts are unlikely as the lipid is buried and not accessible on the protein surface. Assuming that the interface for the cargo proteins involves helix $\alpha 1$ and given the rearrangement in this region upon farnesylation the enhanced affinity could result from a reduction of the conformational multiplicity of the PMP binding site. Thus, the equilibrium of conformations in solution could be shifted towards a state with higher affinity for the PMP cargo which would also explain that binding activity, although weakened by a factor of 5, is detected for the non-farnesylated protein.

Although predominantly localized in the cytosol PEX19 is also found at the peroxisomal membrane together with the PMP cargo and the docking transmembrane protein PEX3 (Matsuzono and Fujiki, 2006). NMR titrations presented in this work document the transition

from highly soluble PEX19 alone to a hydrophobic and aggregating complex when a PMP peptide is added (s. 3.2.1). Both full-length and C-terminus of PEX19 associate with liposomes depending on the presence of a PEX11 peptide as shown in flotation assays (s. 3.2.3). *In vitro* membrane targeting therefore neither requires farnesylation nor PEX3 suggesting that the hydrophobic peptide could function as a membrane anchor and PEX3 ascertain the organelle-specific trafficking. This assumption is further supported by NMR analysis of a fusion construct of PEX19 CTD and a PEX11 peptide: Addition of the PMP sequence does not induce chemical shift perturbations in PEX19 CTD but the fusion protein is prone to aggregation (s. 3.2.2). If this construct mimics PMP binding larger structural changes in PEX19 CTD for membrane attachment are unlikely. However, the linker between protein and peptide sequence might be too short to allow for correct PMP binding and the binding studies were performed with a short peptide instead of a folded PMP domain. Thus, these results need additional efforts and controls to examine the specificity of the interactions.

The NMR structure of farnesylated PEX19 CTD offers possible explanations for the mechanism of membrane targeting. Correlating the surface charge with the sequence conservation shows an overall negative charge of farnesylated PEX19 CTD with the exception of a highly conserved positive patch at the N-terminus of the hydrophobic helix $\alpha 1$ (Fig. 3.24). The PEX19-cargo complex could thus interact with the membrane by contacts between the hydrophobic PMP cargo and the membrane with additional contributions from electrostatic interactions to the negatively charged headgroups of phospholipids in the peroxisomal membrane. A possible role for the farnesyl will be discussed in 4.

Farnesylated proteins can undergo post-farnesylation modification events (Bracha-Drori et al., 2008): after attachment of the farnesyl group to the cysteine in the signal sequence, the CaaX box, the C-terminal three amino acids following the modified cysteine are cleaved off by a prenyl-dependent CaaX protease and the farnesylated cysteine is subsequently carboxymethylated by a prenylcysteine carboxymethyltransferase. Additionally, prenylation and post-prenylation events can also trigger further lipid modifications, like palmitoylation in N-Ras or H-Ras. These modifications enhance the hydrophobicity of the prenylated protein and lead to a stable membrane association. None of these modifications has been shown for PEX19. Functionally, a high membrane affinity would complicate the release back to the

cytosol and is therefore difficult to reconcile with the role of PEX19 as a shuttling receptor. Thus, PEX19 might not undergo further post-farnesylation events.

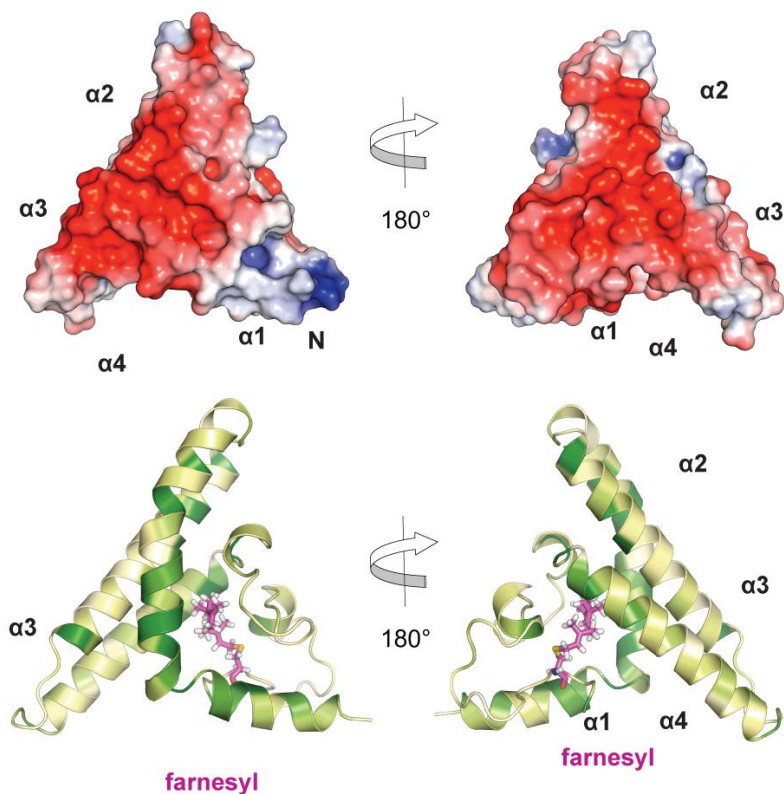


Figure 3.24 Surface charge and sequence conservation in PEX19 CTD. (A) Surface of farnesylated PEX19 CTD colored according to the electrostatic surface potential (red=negative, blue=positive). (B) Sequence conservation as calculated by ConSurf (Ashkenazy et al., 2010) mapped on the structure. Gradient: beige=low sequence conservation; green: high amino acid conservation. PEX19 CTD is mainly negatively charged with a conserved positive area in the PMP-binding helix $\alpha 1$.

3.3 *In vitro* and *in vivo* analysis of mutations in the farnesyl recognition site

3.3.1 Design and NMR analysis of structure-based mutations

Structure-based mutations of aliphatic residues interacting with the farnesyl to positively charged amino acids were designed to interrupt farnesyl recognition of PEX19 CTD and change the position of the farnesyl moiety (Fig. 3.25A). Amino acid substitutions were introduced both inside the cavity (I195K in helix $\alpha 2$ and M255R in helix $\alpha 4$) and in the preceding helix $\alpha 1$ (M179R).

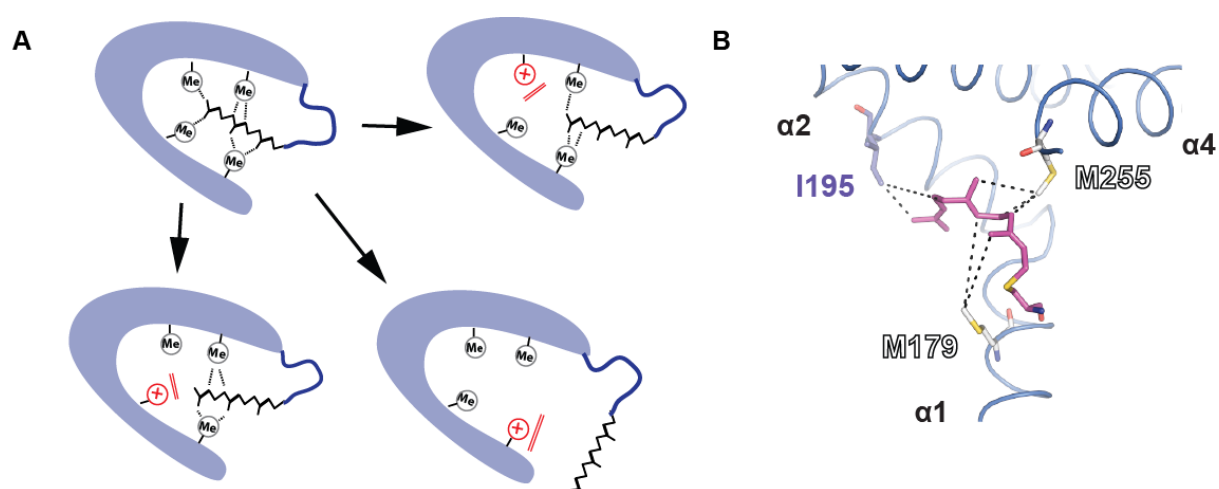


Figure 3.25 Structural basis for the design of point mutations in the farnesyl recognition site. (A) Schematic representation of the farnesyl coordination inside PEX19 CTD by methyl groups from aliphatic amino acids (Me = methyl). Introduction of large positively charged amino acids at different positions should block protein-farnesyl interactions and thus change the binding mode or expel the isoprenoid from the binding cavity. (B) Position of the mutated residues in the NMR structure of farnesylated PEX19 CTD. Representative NOE-based distance restraints are indicated with dashed lines.

All PEX19 CTD variants are soluble and can be purified in yields comparable to the wildtype protein but are more sensitive for aggregation indicating a reduced stability due to the mutations. To ascertain the structural integrity of the PEX19 variants harboring the described mutations ^1H , ^{15}N HSQC spectra with and without farnesylation were recorded which show that all variants maintain the overall fold. Mainly minor local effects in residues adjacent to the mutation site are found for non-farnesylated M179 and I195K mutations like a chemical shift change for the K185 amide proton. About 50% of the backbone resonances were reassigned for PEX19 CTD M255R as the M255R mutation in helix $\alpha 4$ induces more

extensive chemical shift perturbations, e. g. a shift of the amide proton of L203 in helix α_2 (Fig. 3.26A).

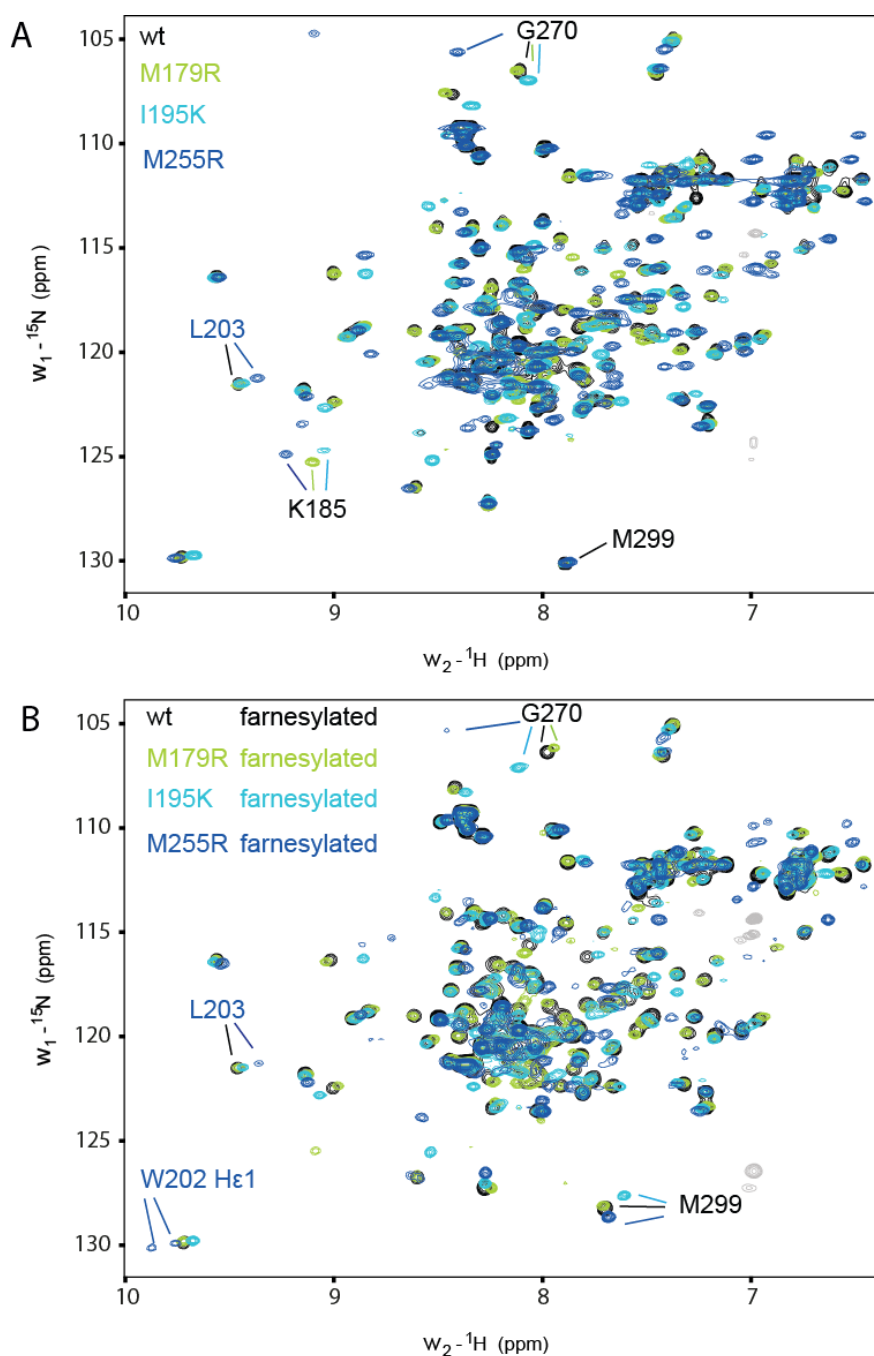


Figure 3.26 NMR spectra of wild type and mutant PEX19 CTD. (A) ^1H , ^{15}N HSQC spectra of M179R and I195K mutations show mainly local chemical shift perturbations for the M179R and I195K variants and more extended changes for the M255R mutation. (B) Chemical shift perturbations upon farnesylation are different among PEX19 CTD variants. Farnesylated PEX19 CTD M255R becomes inhomogeneous as several signals are split (representatively labeled for W202 H ϵ 1).

Although completely farnesylated *in vitro* the farnesylation-induced chemical shift perturbations upon farnesylation vary between the PEX19 CTD variants as can be seen from the example of M299 which experiences the largest chemical shift perturbation in the wildtype protein. Unlike the M299 amide proton frequency in the non-farnesylated proteins the chemical shift of the M299 amide proton is different for every PEX19 CTD variant indicating that the influence of the farnesylation on this residue is altered (Fig. 3.26B). Signals of farnesylated PEX19 CTD M255R are partially split as shown for W202 He1 which suggests a second conformation. $\{^1\text{H}\}\text{-}^{15}\text{N}$ heteronuclear NOE values for the core domain are in good agreement with the wildtype protein, however, the increase in the values upon farnesylation for the C-terminal residues is reduced for the M255R variant and thus this stretch retains a higher flexibility in the mutated protein (Fig. 3.27).

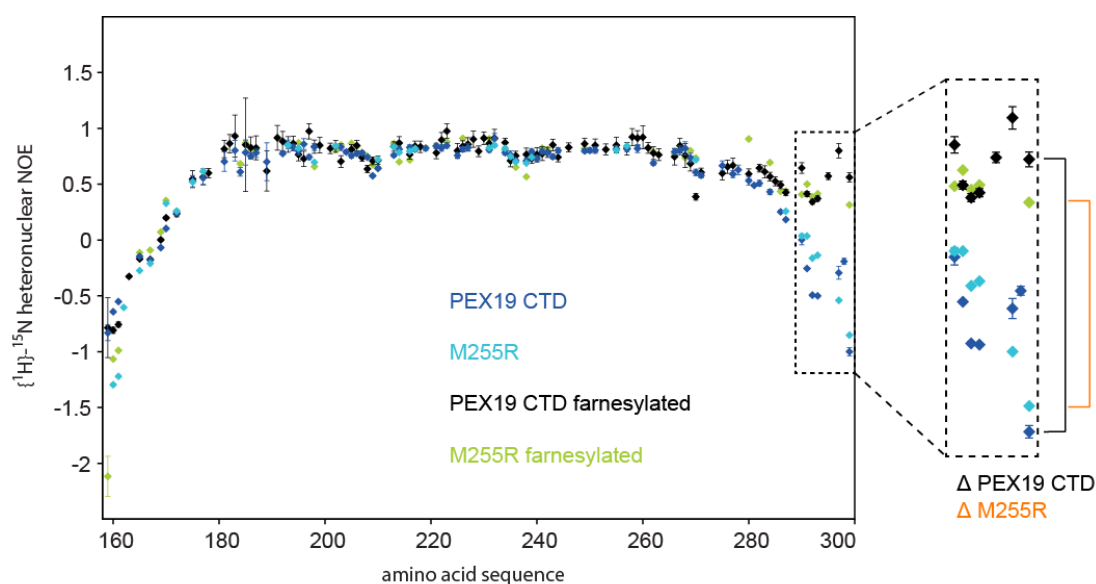


Figure 3.27 $\{^1\text{H}\}\text{-}^{15}\text{N}$ heteronuclear NOE values of PEX19 CTD and PEX19 CTD M255R. The reduction of backbone flexibility upon farnesylation is less pronounced for the M255R variant than for wildtype PEX19 CTD.

3.3.2 Hydrophobic interaction chromatography

In collaboration with Dr. R. Rucktäschel at the Ruhr-Universität Bochum PEX19 CTD wildtype and farnesyl-recognition variants were analyzed by hydrophobic interaction chromatography. The results show that each of the proteins is more hydrophobic when farnesylated which is reflected by the increased elution volume for the farnesylated protein (Fig. 3.28A). Relative to PEX19 CTD wildtype the difference in the elution volume between the farnesylated and the non-farnesylated protein is slightly enlarged for PEX19 CTD M179R and even more for PEX19 CTD I195K. A 2.4-fold increase is observed for PEX19 CTD harboring the M255R substitution (Fig. 3.28B). The farnesylation-induced change in hydrophobicity is thus increased for the mutated proteins.

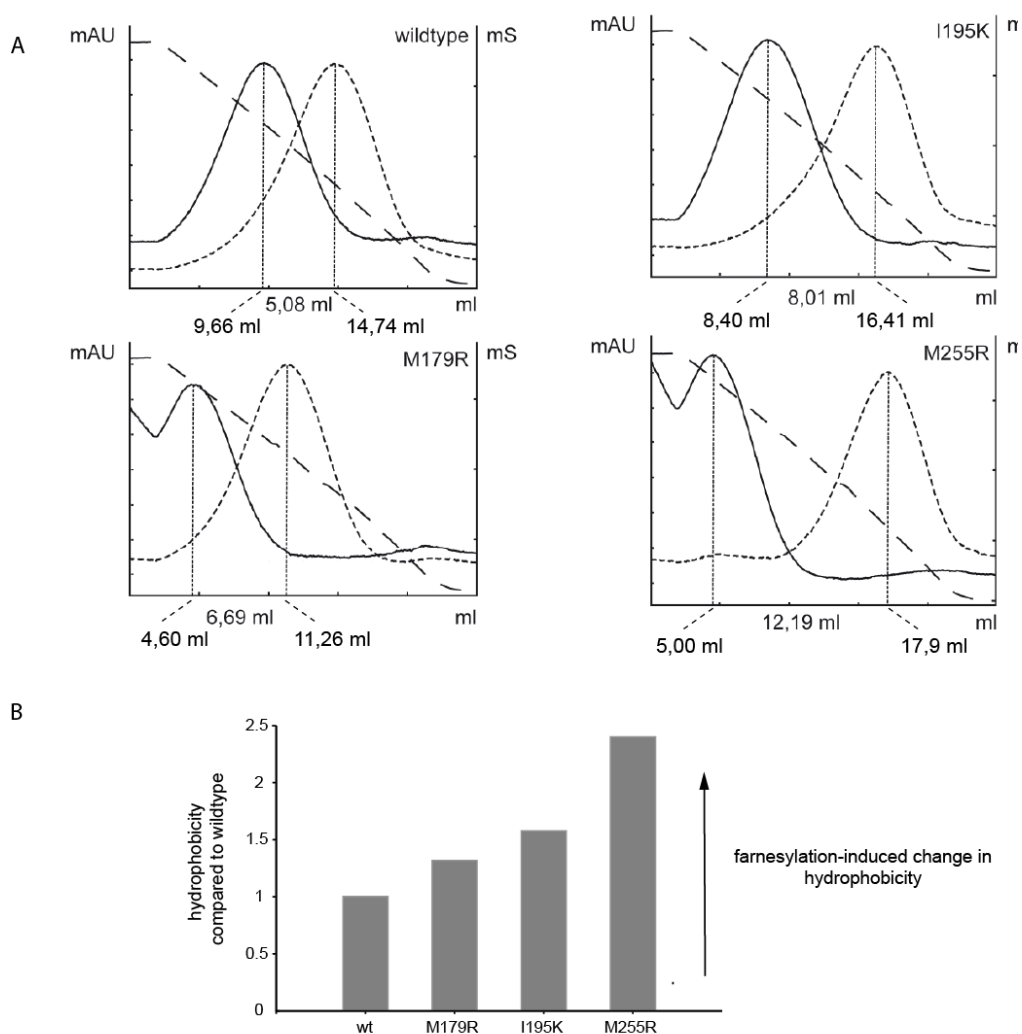


Figure 3.28 Hydrophobic interaction chromatography. (A) The elution profile of PEX19 CTD wildtype and mutated variants from a butyl sepharose column with a linear decreasing $(\text{NH}_4)_2\text{SO}_4$ concentrations shows that all

proteins are more hydrophobic when farnesylated. (B) Difference between the farnesylated and the non-farnesylated protein proportional to wildtype PEX19 CTD. The increase in hydrophobicity is higher for PEX19 CTD with mutations in the farnesyl recognition site.

3.3.3 PMP binding of the mutated PEX19 CTD variants

The effect of the point mutations in the farnesyl recognition site on PMP interactions were addressed by MST assays. The experimental setup was adapted to the reduced stability compared to wildtype PEX19 CTD by reducing the protein concentrations (s. 2.2.5). Under these experimental conditions, no binding was detected for M179R. Due to large variations between the two measurements for farnesylated M179R a binding affinity of $8.1 \mu\text{M} \pm 0.58$ was derived from one experiment. However, the fit quality of 0.82 is rather low and the result needs further validation (Fig. 3.29).

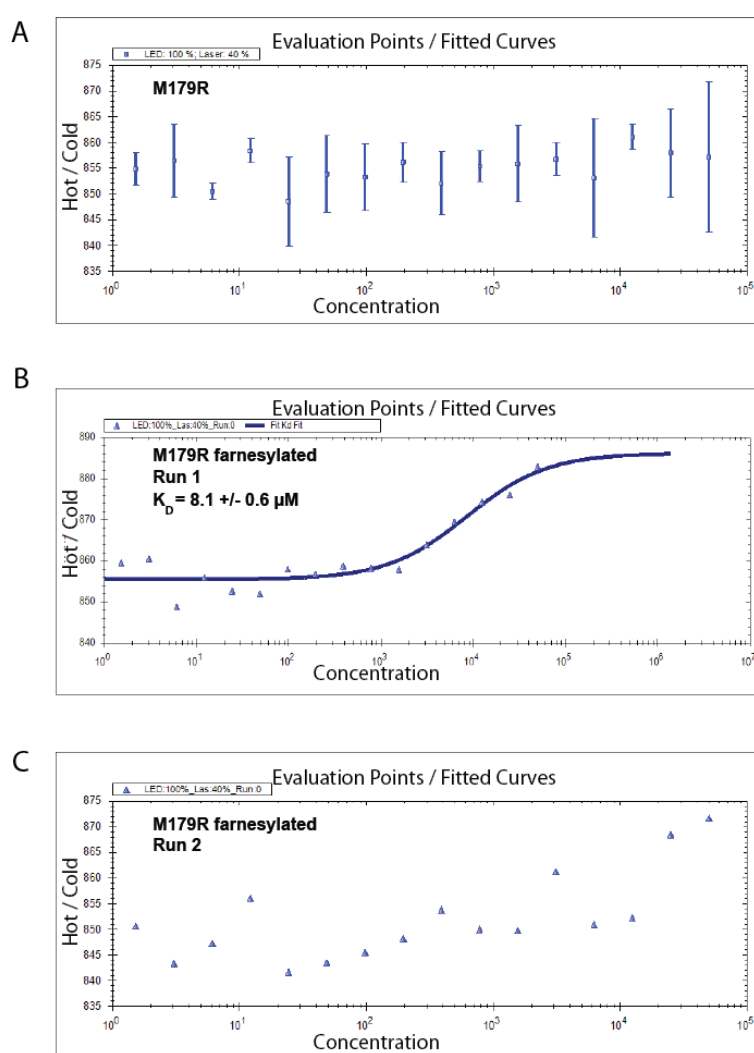


Figure 3.29 Microscale thermophoresis measurements of PEX19 CTD M179R. Thermophoresis was measured on a FITC-labeled peptide from PEX11 with a serial dilution of PEX19 CTD M179R. (A) Average values for M179R without farnesylation do not indicate binding to the peptide. The two experiments performed with farnesylated PEX19 CTD M179R show large deviations. (B) The first measurement shows a K_D of $8.1 \mu\text{M} \pm 0.58$. (C) No reliable fit can be obtained from the second dataset.

PEX19 CTD I195K retains a K_D of $20.9 \mu\text{M} \pm 1.98$ (fit quality 0.96) for the non-farnesylated and $5.43 \mu\text{M} \pm 0.76$ (fit quality 0.63) $8.1 \mu\text{M} \pm 0.58$ (Fig. 3.30) for the farnesylated protein. No binding activity both with and without farnesylation was detected for PEX19 CTD M255R (Fig. 3.31).

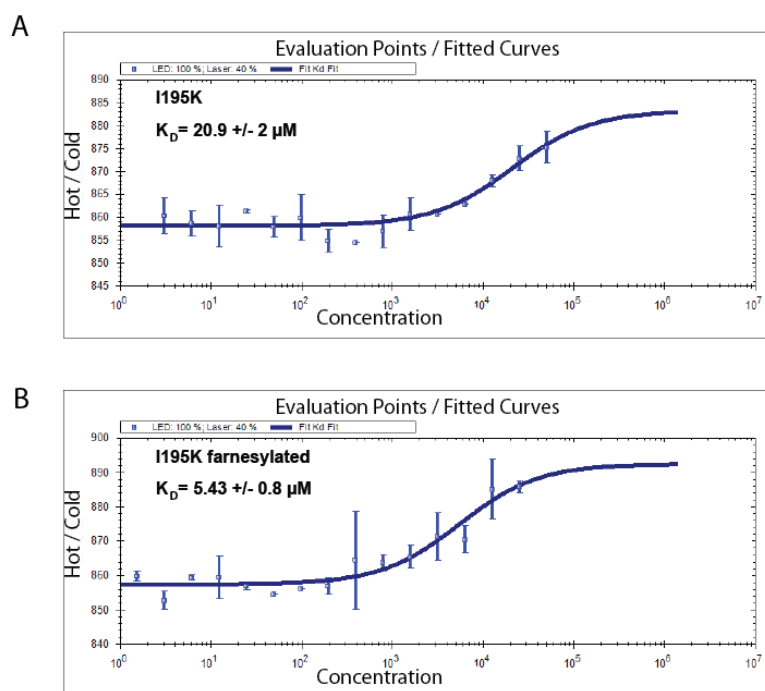


Figure 3.30 Microscale thermophoresis measurements of PEX19 CTD I195K. Thermophoresis was measured on a 100 nM FITC-labeled peptide from PEX11 with a serial dilution of PEX19 CTD I195K. The results show affinities of $20.9 \mu\text{M} \pm 1.98$ for the non-farnesylated (A) and $5.43 \mu\text{M} \pm 0.76$ for the farnesylated (B) protein

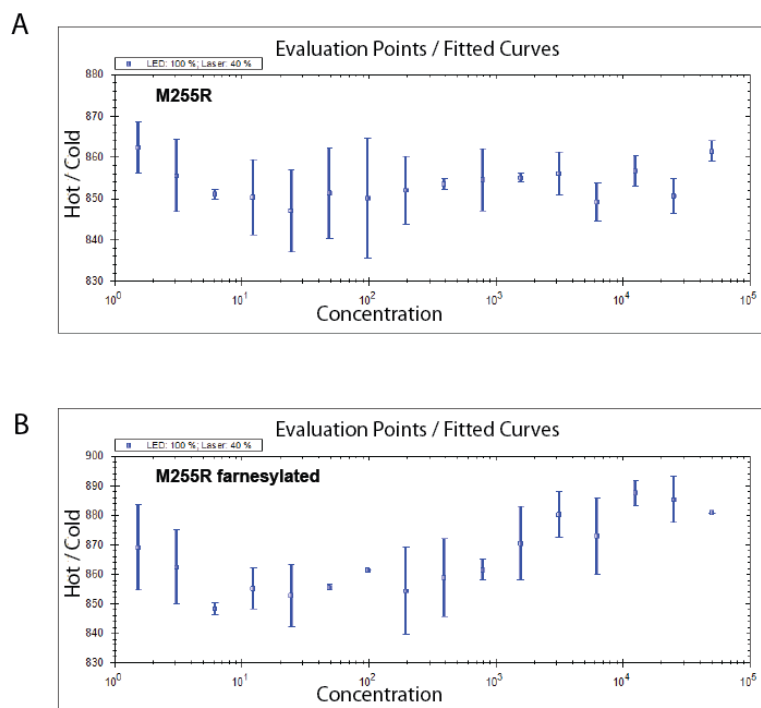


Figure 3.31 Microscale thermophoresis measurements of PEX19 CTD M255R. Thermophoresis was measured on a 100 nM FITC-labeled peptide from PEX11 with a serial dilution of PEX19 CTD. No binding was detected for the non-farnesylated (A) and farnesylated (B) protein.

3.3.4 Functional studies of PEX19 wildtype and mutants in a cell-based assay

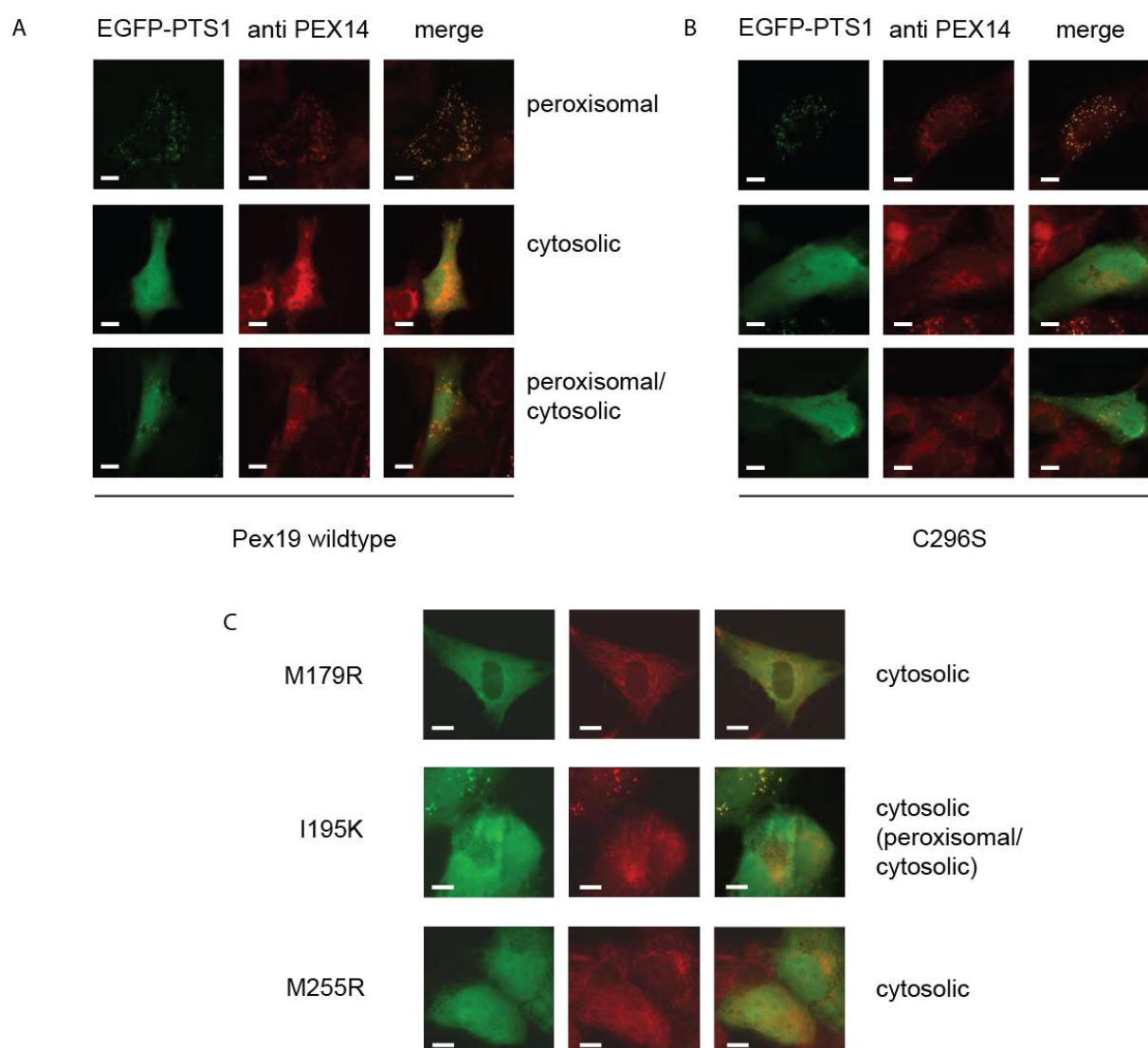


Figure 3.32 Functionality of PEX19 variants with farnesylation-related mutations in human fibroblasts. Cell-based assays were performed by E. Becker, Ruhr-Universität Bochum. Functional peroxisomal protein import is shown by a co-localization of EGFP-PTS1 with PEX14 in a punctate staining pattern. EGFP-PTS1 was monitored via fluorescence microscopy (left column). Endogenous PEX14 as a peroxisomal marker protein was detected using immunofluorescence microscopy (middle column). A punctate staining pattern and co-localization of EGFP-PTS1 and PEX14 indicate functional peroxisomal protein transport (merge, right column). Peroxisomal protein transport is partially restored upon introduction of wildtype PEX19 (A) and to a lesser extent for PEX19 C296S (B). Mutations in the farnesyl recognition site impair peroxisomal protein transport (C) EGFP-PTS1 is completely localized in the cytosol in the M179 mutant (upper panel). The I195K mutant maintains a reduced functionality (middle panel). PEX19 M255R does not complement the $\Delta pex19$ phenotype (lower panel).

In collaboration with Dr. W. Schliebs (Ruhr-Universität Bochum) the functionality of PEX19 with the described mutations was examined in a complementation assay of full-length PEX19 wildtype and mutants in human $\Delta pex19$ fibroblasts. A punctuate staining pattern of EGFP-PTS1 co-localized with PEX14 indicates functional peroxisomal transport (Fig. 3.32). Wildtype PEX19 restores peroxisomal protein transport to 60%. Functional complementation was reduced to 46% in PEX19 C296S which cannot be farnesylated as the farnesylation site is mutated. For PEX19 I195K complementation is further decreased to 23%. In the M179R and M255R mutants, no peroxisomal protein transport is detected (Fig. 3.33A). As shown by Western Blot analysis all PEX19 variants are expressed in significant amounts and, with the exception of C296S, are farnesylated in the cell (Fig. 3.33B). Mutational analysis shows defects in peroxisomal protein import in absence of farnesylation but more severe effects for mutations targeting residues involved in farnesyl recognition.

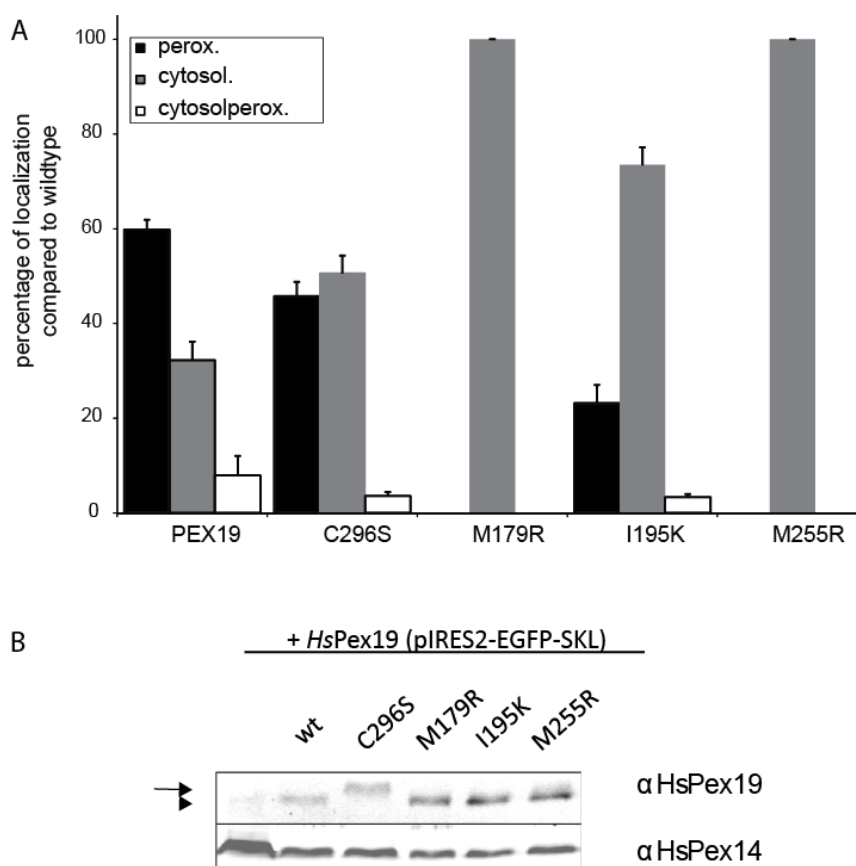


Figure 3.33 Quantitative evaluation of $\Delta pex19$ -phenotype complementation by the individual PEX19 variants and analysis of *in vivo* farnesylation. Experiments were performed by Elisabeth Becker and Dr. R. Rucktäschel, Ruhr-Universität Bochum. (A) Percentage of complementation by PEX19 variants calculated from three independent transfection experiments. (B) Western Blot analysis of the farnesylation mutants shows that all variants are expressed in significant amounts and, except from C296S, are farnesylated *in vivo*.

3.3.5 Discussion: Effects of mutations in the farnesyl recognition site

The conservation and importance for peroxisomal protein transport of PEX19 farnesylation suggests further roles in PEX19 functions, e. g. in membrane attachment. This question was addressed with structure-based mutational analysis. The tight interactions reflected by 203 protein-farnesyl NOEs and large number of residues participating in farnesyl binding complicate the design of point mutations which disrupt isoprenoid binding without destroying the overall protein fold. With the substitutions M179R, I195K and M255R aliphatic amino acids coordinating the farnesyl were exchanged against large charged residues to interrupt farnesyl recognition and cause a mislocalization of the farnesyl group.

Although expressed and farnesylated in fibroblasts PEX19 M179R cannot rescue the *Δpex19* phenotype. However, the M179R mutation hardly affects the structure of PEX19 CTD as chemical shift perturbations of this variant are limited to residues adjacent to the mutation site for the farnesylated and non-farnesylated proteins (s. 3.3.1). The farnesylation-induced increase in hydrophobicity measured by hydrophobic interaction chromatography is also similar to the wildtype protein (s. 3.3.2). Results of microscale thermophoresis measurements of PEX19 CTD M179R do not show interactions with the PEX11 peptide and did not allow for a reliable determination of a binding affinity for farnesylated PEX19 CTD M179R (s. 3.3.3). It is therefore likely that the M179R substitution in helix α 1 directly distorts this interface which explains the non-functional phenotype.

The I195K mutation within the farnesyl binding cavity has defects in peroxisomal protein import compared to wildtype PEX19 but can partially complement *Δpex19* cells. Binding affinities to the PEX11 peptides determined by microscale thermophoresis measurements are comparable to the wildtype for farnesylated and non-farnesylated PEX19 CTD (s. 3.3.3). Chemical shift perturbations in ^1H , ^{15}N HSQC spectra of PEX19 CTD I195K are mainly local in the non-farnesylated protein. However, a subset of signals that are shifted in wildtype PEX19 CTD upon farnesylation do not overlay with those in farnesylated PEX19 CTD I195K (s. 3.3.1). As hydrophobic interaction chromatography additionally shows a higher increase in hydrophobicity compared to wildtype PEX19 CTD and PEX19 CTD M179R the I195K mutation could weaken farnesyl binding (s. 3.3.2). Contacts between I195 and the farnesyl are restricted to the terminal farnesyl atoms, thus, the structural and functional effects of this mutation are limited.

Mutation M255R completely abolishes PEX19 function *in vivo*. The substitution in the hydrophobic core induces chemical shift perturbations in different regions of the protein (s. 3.3.1). Furthermore, no binding to the PEX11 peptide was observed in MST measurements (s. 3.3.3). However, a weaker binding might not have been detected in the chosen experimental setup as the protein concentrations were lower than for the wildtype protein due to the increased instability of the M255R mutant (s. 2.2.5). Expression and farnesylation in the cell as well as $\{^1\text{H}\}\text{-}^{15}\text{N}$ heteronuclear NOE data of M255R both with and without farnesylation underline the structural integrity of this variant (s. 3.3.1 and 3.3.4). The higher backbone flexibility in the C-terminal residues shown by lower $\{^1\text{H}\}\text{-}^{15}\text{N}$ heteronuclear NOE values and the remarkable 2.4 fold increase in farnesylation-induced hydrophobicity compared to wildtype PEX19 CTD indicate an impaired isoprenoid binding and could point to a mislocalization of the farnesyl group outside the protein. The exposed lipid could either compete with the PMP cargo for the hydrophobic binding site thus interfering with PMP binding or, if the farnesyl is involved in membrane attachment, lead to a premature association with the docking protein or the membrane skipping the cargo binding step.

3.4 NMR studies of the ubiquitin-conjugating enzyme Pex4p and its co-activator Pex22p (Collaboration with Dr. C. Williams and Dr. M. Wilmanns, EMBL Hamburg)

Biochemical studies demonstrate complex formation and ubiquitin-conjugating activity for a soluble fragment of ScPex22p including residues 54 - 180 lacking the transmembrane segment with a ScPex4p construct with the boundaries 15 - 183. The crystal structure of the complex shows that the large interface between Pex4p and Pex22p consists of α -helices α 3 and α 4 of Pex4p and helix α 4, α 5 and β -strand β 3 of Pex22p ((Williams et al., 2012). However, crystallization attempts of Pex4p or Pex22p alone were not successful. A possible reason could be additional flexibility of the individual protein, e. g. formation of a secondary structure element in one of the binding partners upon binding of the other. Therefore, the individual proteins were investigated by NMR.

Signals in the ^1H ^{15}N HSQC spectrum of the 127 residue and 14.2 kDa Pex22p are well dispersed reflecting the high β -sheet content within Pex22p (Fig. 3.34). The number of resonances in the ^1H ^{15}N HSQC spectrum of Pex4p is lower than expected from the amino acid sequence of the 171 residue and 19.5 kDa protein (Fig. 3.34B). A sequential assignment of backbone resonances in Pex4p was not possible due to the missing amide proton signals and poor signal-to-noise ratio in the 3D experiments. NMR titration experiments of ^{15}N labeled Pex4p with unlabeled Pex22p show chemical shift perturbations in Pex4p and additional signals in presence of Pex22p (Fig. 3.34C). From the chemical shifts of the additional signals in the ^1H ^{15}N HSQC spectrum the corresponding residues are expected to be part of folded protein regions. It is therefore possible that Pex22p binding induces folding of parts Pex4p. However, backbone assignments for Pex4p in the free and bound state would be required to support this hypothesis.

As a suggestion for future investigations, backbone assignments for Pex4p could be obtained from triple resonance experiments on Pex4p in complex with Pex22p and transferred to free Pex4p to allow conclusions about a structural influence of Pex22p on Pex4p to elucidate the mechanism of activation.

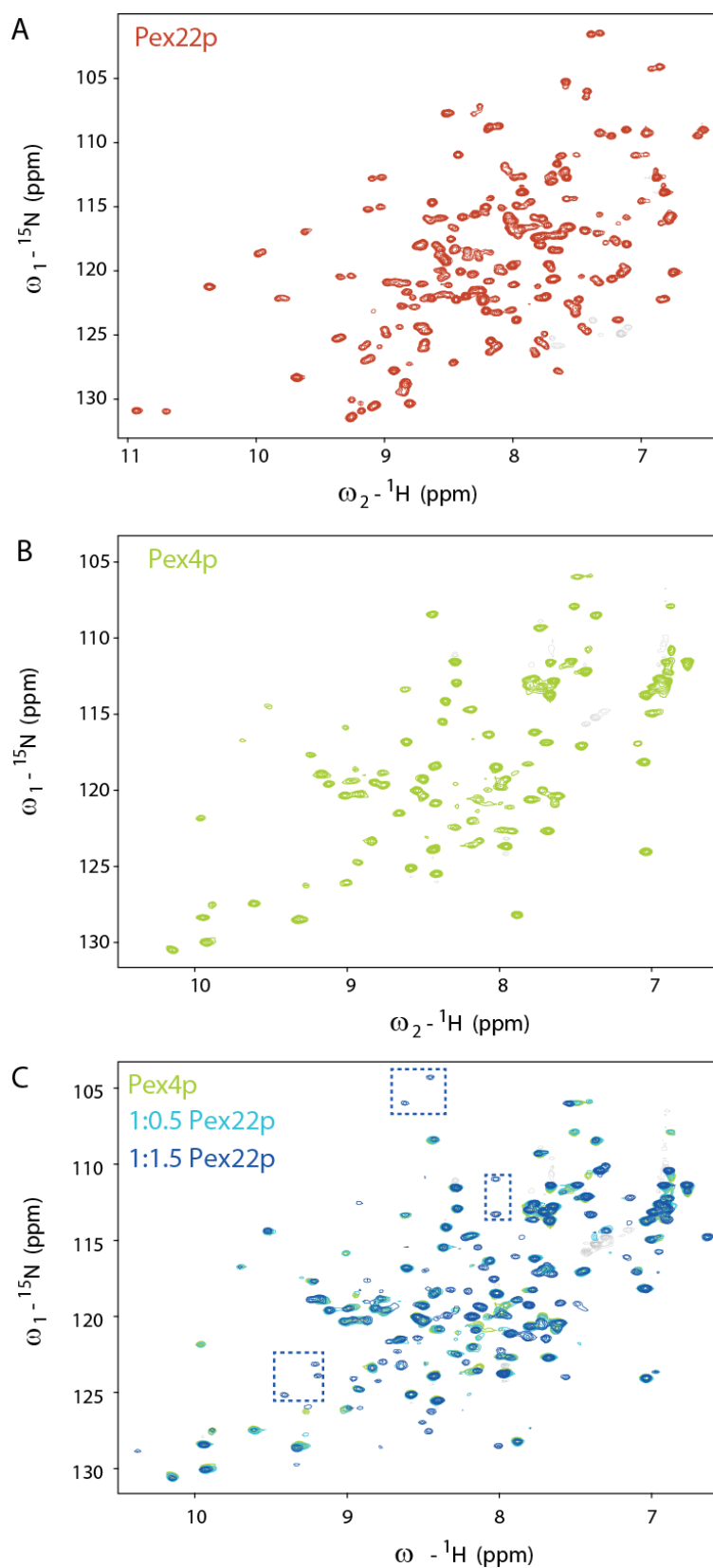


Figure 3.34 NMR spectra of Pex4p and Pex22p. ^1H , ^{15}N HSQC spectra of (A) Pex22p (54-180) and (B) Pex4p (15-183). The number of detected signals in the pex4p spectrum is lower than expected from the amino acid sequence of the construct. (C) Addition of increasing concentrations of unlabeled Pex22p to ^{15}N labeled Pex4p gives rise to additional signals from Pex4p (highlighted with dashed boxes).

3.5 Solvent paramagnetic relaxation enhancement studies of FKBP38 (Collaboration with Dr. Ye Hong and Prof. Dr. Ho Sup Yoon, School of Biological Sciences, Nanyang Technological University, Singapore)

FKBP stands for FK506-binding protein and describes the family of proteins which are able to bind the immunosuppressive drug FK506 and possess a peptidyl-prolyl *cis/trans* isomerase activity. Human FKBP proteins share a composition of one to three FKBDs (FK506-binding domain) and TPR domains (Solassol et al., 2011). Among those, FKBP38 is an important drug target as it inhibits mTOR, a serine/threonine kinase involved in the regulation of cell growth (Yang and Guan, 2007), and interacts with the anti-apoptotic protein Bcl2 (Edlich and Lucke, 2011). FKBP38 is an exception within the FKBP family as it is only enzymatically active in complex with calcium-saturated calmodulin which binds to two different binding sites in the C-terminus and the N-terminus of FKBP38 (Maestre-Martinez et al., 2010).

The catalytic FKBP domain between residue 33 and 149 is preceded by a stretch of 32 unstructured amino acids which has an autoinhibitory effect on the isomerase domain (Dr. Ye Hong, personal communication). Addition of this N-terminal region induces chemical shift perturbations in the catalytic domain as shown by differences in ^1H ^{15}N HSQC spectra of FKBD (residues 31-149) compared to NTD (residues 1-151). However, no NOEs between the N-terminus and the catalytic domain were observed (Dr. Ye Hong, personal communication) and thus solvent PRE measurements were performed to detect transient interactions.

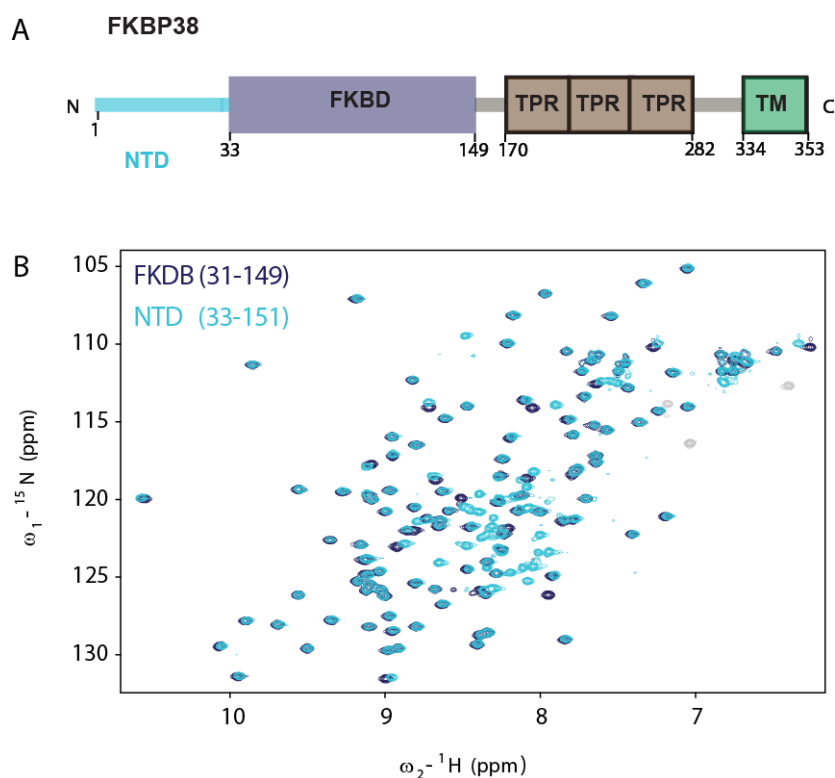


Figure 3.35 Domain composition and NMR spectra of FKBP38. (A) Schematic overview of the domains in FKBP38. (B) Overlay of ^1H ^{15}N HSQC spectra of FKBD (residues 31-149, dark blue) and NTD (residues 1-151, cyan). Signals for residues 1-30 cluster in the center of the spectrum.

The additional signals from the 32 N-terminal amino acids in the NTD construct are found in the center of the spectrum as expected for an unfolded region (Fig. 3.35). Chemical shift perturbations between FKBD and NTD affect two different sections of the catalytic FKBD domain, first from residue 60 to 65 and second from residue 85 to 95 (Fig. 3.36A). Solvent PRE rates for the N-terminal stretch in NTD are high compared to the structured catalytic domain between residue 30 and 149 and thus indicate a flexible and solvent-accessible part. Amide protons from small amino acids like G13, A14 and A30 are not shielded by extended amino acid side chains and therefore experience very intense relaxation enhancements. As the pattern for FKBD and NTD is highly similar these experiments do not allow conclusions about specific contacts of the N-terminus to the core domain. Interactions between the catalytic domain and the N-terminal stretch could be detected by measuring PRE effects of spin labels attached to various positions in the core domain.

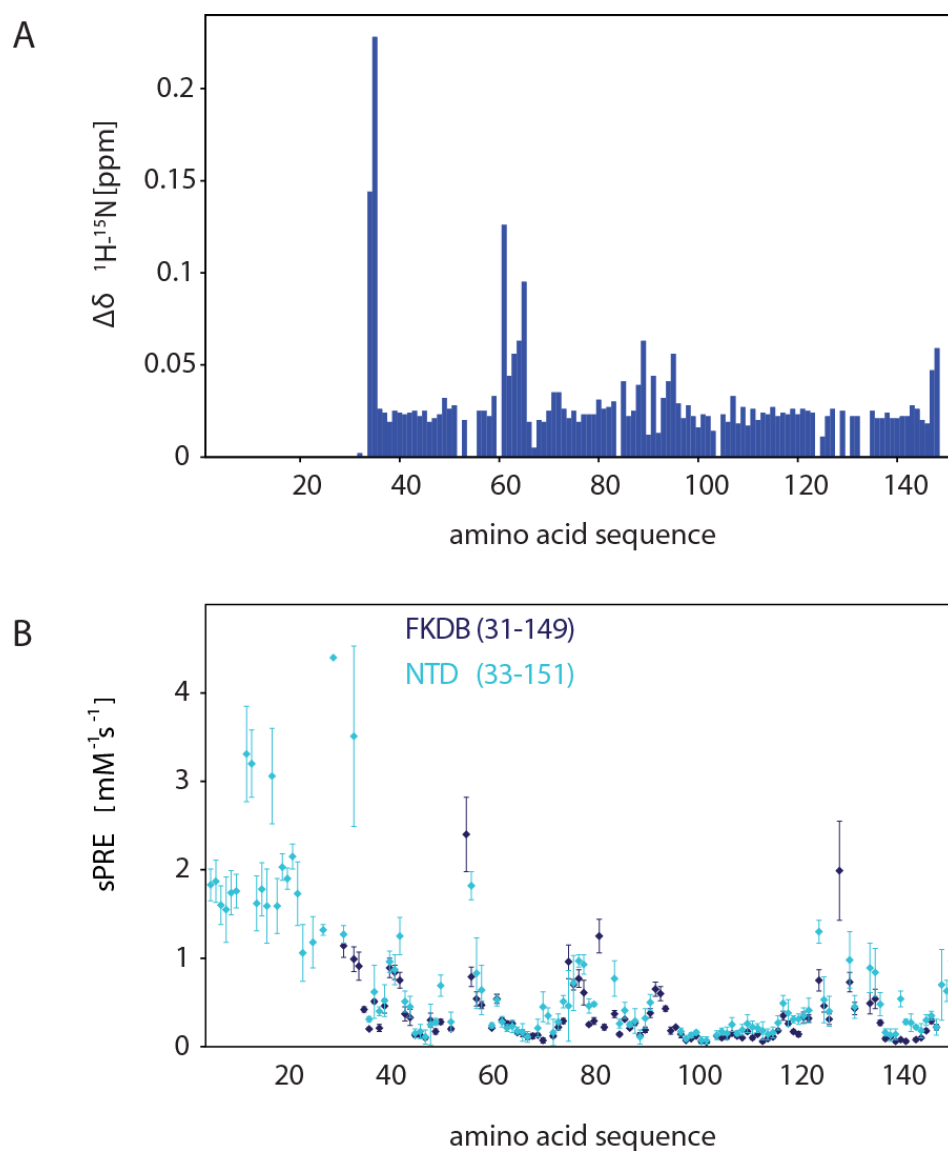


Figure 3.36 Comparison of chemical shift perturbations and solvent PRE rates in FKBD (residues 31-149) and NTD (residues 1-151). (A) Amide proton chemical shift differences plotted against the amino acid sequence. (B) Solvent PRE rates for amide protons of FKBD (dark blue) and NTD (cyan).

4. Discussion

4.1 A model for the role of farnesylation in peroxisomal membrane protein transport

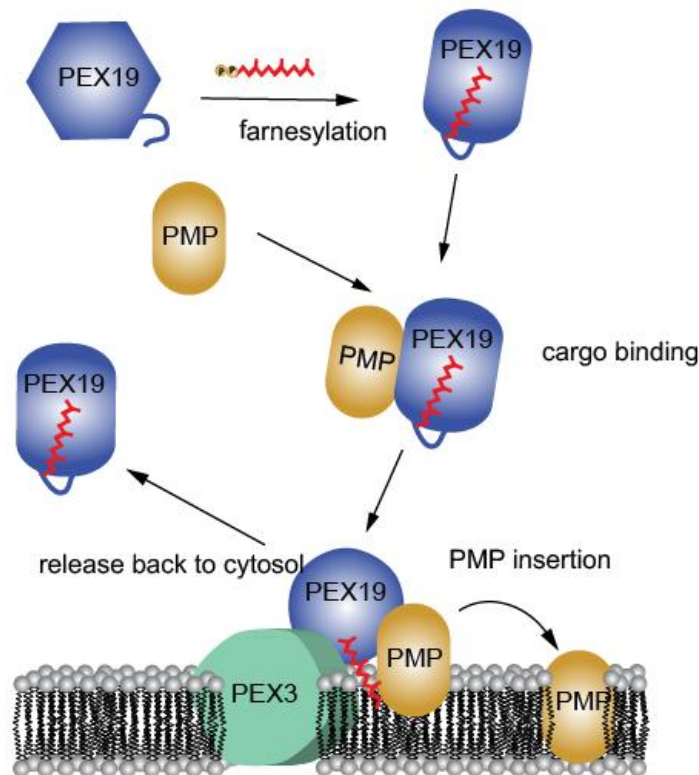


Figure 4.1 Model for a functional role for PEX19 farnesylation in PMP transport. Additional to the enhancement of the PMP binding affinity the farnesyl could be involved in membrane targeting. Cargo binding might induce a conformational change which also alters the position of the farnesyl group. An exposed farnesyl would favor the association with the peroxisomal membrane and the docking protein PEX3. After release of the PMP cargo PEX19 might readopt a more soluble state and return to the cytosol to enter a new round of cargo shuttling.

Experimental data obtained in this study together with previous findings can be combined to a model for the role of farnesylation in peroxisomal membrane protein transport with a mechanism similar to the one that has been suggested for prenylated RabGTPases involved in intracellular vesicle trafficking (Wu et al., 2007). The Rab escort protein (REP) mediates digeranylgeranylation by RabGGTase and the geranylgeranyl units anchor RabGTPase to the membrane (Goody et al., 2005). To release RABGTPase from the membrane the GDP dissociation factor (GDI) binds to RABGTPase, complex formation opens a prenyl binding

pocket within GDI to accommodate the geranyl moieties and thus extracts RabGTPase from the membrane (Itzen and Goody, 2011). As shown by Wu et al the thermodynamic driving force is provided by the 1000fold higher affinity of GDI for prenylated Rab7GTPase in comparison to the non-modified protein (Wu et al., 2007). In this system prenylation serves as a switch to regulate membrane bound or soluble intracellular localization.

As a shuttling receptor for peroxisomal membrane proteins PEX19 reversibly associates with the peroxisomal membrane. This step could be facilitated by farnesyl-membrane interactions. However, in the solution structure of farnesylated PEX19 CTD the isoprenoid is buried and solvent-protected inside the protein. Transfer of the Rab concept to the PMP transport system leads to the following model: First, binding of PMP cargo might induce a change of the position of the farnesyl group so that it is released from the cavity and available for membrane contacts. As shown by Silvius et al.(Silvius and l'Heureux, 1994) farnesylcysteinepeptides bind to lipid bilayers with a K_D of approximately 114 μM contributing about 9-12 kcal mol^{-1} which corresponds to a relatively weak interaction. Second, the PEX19-cargo complex has to reach the peroxisomal membrane. As described in 3.2 presence of PMP peptides enhance the hydrophobicity (3.2.1) and could favour membrane attachment by direct contacts to the membrane (3.2.3). Electrostatic interactions from PEX19 with the negatively charged membrane (3.2.5) and binding to the integral membrane protein PEX3 via the PEX19 N-terminus could energetically add up to a sufficient affinity for specifically targeting PEX19 with bound cargo to the peroxisomal membrane. Third, the PMP is inserted into the peroxisomal membrane by a so far unknown mechanism. The molecular details of the latter steps are unknown. PMP insertion is thought to require ATP whereas receptor release does not (Pinto et al., 2006). A posttranslational modification additional to farnesylation has been proposed for PEX19 (Rucktaschel et al., 2009). A global phosphoproteome analysis has identified several phosphopeptides in PEX19 and postulated a number of phosphorylated serine residues. Within the boundaries of PEX19 CTD S177 and S184 are suggested as phosphorylation targets (Molina et al., 2007). These residues are part of the highly conserved region around helix $\alpha 1$ in PEX19 CTD with S184 being invariant. A phosphorylation could interrupt the PEX19-PMP interface and thus facilitate cargo release into the membrane. The cargo-free PEX19 would decrease its hydrophobicity and, as step four of the PMP transport cycle, could be discharged from the organelle to re-enter the cytosol.

4.2 Conclusions and outlook

This study has addressed open questions on molecular details of processes in peroxisomal protein transport with a focus on human PEX19 and the role of PEX19 farnesylation. NMR investigations of PEX19 in presence and absence of farnesylation have elucidated how the farnesyl is accommodated in the protein and how farnesylation modulates structure and dynamics of PEX19. Biochemical approaches have provided new findings on PEX19-PMP and membrane interactions. Structure-based mutations targeting the farnesyl binding site were characterized *in vitro* and *in vivo*.

While there is evidence that helix $\alpha 1$ is essential for interactions with PMP cargo (Schueller et al., 2010) the exact binding site in PEX19 remains unknown. The results of this study have shown the difficulties to address this question using small peptides from PMPs. Future experiments should therefore aim on studies of complexes with complete domains or even full-length PMPs to reveal possible structural changes in PEX19 upon PMP binding. Including PEX3 as the docking protein would provide further insights into the structural and energetical interplay at the peroxisomal membrane. In the past years, several publications have underlined the importance of the endoplasmic reticulum for the transport of some PMPs (Halbach et al., 2009; Ma et al., 2011). Two recent publications even claim constitutive traveling via the ER for all PMPs and accordingly a different role for PEX19 (van der Zand et al., 2010; van der Zand et al., 2012). Together with PEX3 it is suggested to function as a budding factor for the preperoxisomal compartment in the ER. *In vivo* studies together with structural investigations of the key players will be required to complete our understanding of peroxisomal protein transport.

5. References

- Ahearn, I.M., Haigis, K., Bar-Sagi, D., and Philips, M.R. (2012). Regulating the regulator: post-translational modification of RAS. *Nat Rev Mol Cell Biol* *13*, 39-51.
- Ames, J.B., Tanaka, T., Stryer, L., and Ikura, M. (1996). Portrait of a myristoyl switch protein. *Curr Opin Struct Biol* *6*, 432-438.
- Ashkenazy, H., Erez, E., Martz, E., Pupko, T., and Ben-Tal, N. (2010). ConSurf 2010: calculating evolutionary conservation in sequence and structure of proteins and nucleic acids. *Nucleic Acids Res* *38*, W529-533.
- Banerjee, S.K., Kessler, P.S., Saveria, T., and Parsons, M. (2005). Identification of trypanosomatid PEX19: functional characterization reveals impact on cell growth and glycosome size and number. *Mol Biochem Parasitol* *142*, 47-55.
- Bertini, I., Luchinat, C., Parigi, G., and Pierattelli, R. (2005). NMR spectroscopy of paramagnetic metalloproteins. *Chembiochem* *6*, 1536-1549.
- Bracha-Drori, K., Shichrur, K., Lubetzky, T.C., and Yalovsky, S. (2008). Functional analysis of Arabidopsis postprenylation CaaX processing enzymes and their function in subcellular protein targeting. *Plant Physiol* *148*, 119-131.
- Brunsveld, L., Waldmann, H., and Huster, D. (2009). Membrane binding of lipidated Ras peptides and proteins--the structural point of view. *Biochim Biophys Acta* *1788*, 273-288.
- Caplan, A.J., Tsai, J., Casey, P.J., and Douglas, M.G. (1992). Farnesylation of YDJ1p is required for function at elevated growth temperatures in *Saccharomyces cerevisiae*. *J Biol Chem* *267*, 18890-18895.
- Clore, G.M., and Iwahara, J. (2009). Theory, practice, and applications of paramagnetic relaxation enhancement for the characterization of transient low-population States of biological macromolecules and their complexes. *Chem Rev* *109*, 4108-4139.
- Clore, G.M., Robien, M.A., and Gronenborn, A.M. (1993). Exploring the limits of precision and accuracy of protein structures determined by nuclear magnetic resonance spectroscopy. *J Mol Biol* *231*, 82-102.
- Cordier, F., Dingley, A.J., and Grzesiek, S. (1999). A doublet-separated sensitivity-enhanced HSQC for the determination of scalar and dipolar one-bond J-couplings. *J Biomol NMR* *13*, 175-180.
- Crowell, D.N. (2000). Functional implications of protein isoprenylation in plants. *Prog Lipid Res* *39*, 393-408.
- de Duve, D. (1969). The peroxisome: a new cytoplasmic organelle. *Proc R Soc Lond B Biol Sci* *173*, 71-83.

- Delaglio, F., Grzesiek, S., Vuister, G.W., Zhu, G., Pfeifer, J., and Bax, A. (1995). NMRPIPE - A MULTIDIMENSIONAL SPECTRAL PROCESSING SYSTEM BASED ON UNIX PIPES. *Journal of Biomolecular Nmr* *6*, 277-293.
- Doreleijers, J.F., Vranken, W.F., Schulte, C., Markley, J.L., Ulrich, E.L., Vriend, G., and Vuister, G.W. (2012). NRG-CING: integrated validation reports of remediated experimental biomolecular NMR data and coordinates in wwPDB. *Nucleic Acids Res* *40*, D519-524.
- Dosset, P., Hus, J.C., Marion, D., and Blackledge, M. (2001). A novel interactive tool for rigid-body modeling of multi-domain macromolecules using residual dipolar couplings. *J Biomol NMR* *20*, 223-231.
- Edlich, F., and Lucke, C. (2011). From cell death to viral replication: the diverse functions of the membrane-associated FKBP38. *Curr Opin Pharmacol* *11*, 348-353.
- Eisenberg, S., and Henis, Y.I. (2008). Interactions of Ras proteins with the plasma membrane and their roles in signaling. *Cell Signal* *20*, 31-39.
- Erdmann, R., and Schliebs, W. (2005). Peroxisomal matrix protein import: the transient pore model. *Nat Rev Mol Cell Biol* *6*, 738-742.
- Fang, Y., Morrell, J.C., Jones, J.M., and Gould, S.J. (2004). PEX3 functions as a PEX19 docking factor in the import of class I peroxisomal membrane proteins. *J Cell Biol* *164*, 863-875.
- Farrow, N.A., Muhandiram, R., Singer, A.U., Pascal, S.M., Kay, C.M., Gish, G., Shoelson, S.E., Pawson, T., Forman-Kay, J.D., and Kay, L.E. (1994). Backbone dynamics of a free and phosphopeptide-complexed Src homology 2 domain studied by ¹⁵N NMR relaxation. *Biochemistry* *33*, 5984-6003.
- Fransen, M., Vastiau, I., Brees, C., Brys, V., Mannaerts, G.P., and Van Veldhoven, P.P. (2004). Potential role for Pex19p in assembly of PTS-receptor docking complexes. *J Biol Chem* *279*, 12615-12624.
- Gans, P., Hamelin, O., Sounier, R., Ayala, I., Dura, M.A., Amero, C.D., Noirclerc-Savoye, M., Franzetti, B., Plevin, M.J., and Boisbouvier, J. (2010). Stereospecific isotopic labeling of methyl groups for NMR spectroscopic studies of high-molecular-weight proteins. *Angew Chem Int Ed Engl* *49*, 1958-1962.
- Girzalsky, W., Saffian, D., and Erdmann, R. (2010). Peroxisomal protein translocation. *Biochim Biophys Acta* *1803*, 724-731.
- Goddard, T., and Kneller, D. Sparky 3.
- Goody, R.S., Rak, A., and Alexandrov, K. (2005). The structural and mechanistic basis for recycling of Rab proteins between membrane compartments. *Cell Mol Life Sci* *62*, 1657-1670.
- Gootjes, J., Mooijer, P.A., Dekker, C., Barth, P.G., Poll-The, B.T., Waterham, H.R., and Wanders, R.J. (2002). Biochemical markers predicting survival in peroxisome biogenesis disorders. *Neurology* *59*, 1746-1749.

- Gotte, K., Girzalsky, W., Linkert, M., Baumgart, E., Kammerer, S., Kunau, W.H., and Erdmann, R. (1998). Pex19p, a farnesylated protein essential for peroxisome biogenesis. *Mol Cell Biol* *18*, 616-628.
- Gouet, P., Courcelle, E., Stuart, D.I., and Metz, F. (1999). ESPript: analysis of multiple sequence alignments in PostScript. *Bioinformatics* *15*, 305-308.
- Guntert, P. (2009). Automated structure determination from NMR spectra. *Eur Biophys J* *38*, 129-143.
- Halbach, A., Lorenzen, S., Landgraf, C., Volkmer-Engert, R., Erdmann, R., and Rottensteiner, H. (2005). Function of the PEX19-binding site of human adrenoleukodystrophy protein as targeting motif in man and yeast. PMP targeting is evolutionarily conserved. *J Biol Chem* *280*, 21176-21182.
- Halbach, A., Rucktaschel, R., Rottensteiner, H., and Erdmann, R. (2009). The N-domain of Pex22p can functionally replace the Pex3p N-domain in targeting and peroxisome formation. *J Biol Chem* *284*, 3906-3916.
- Hall, T.M., Porter, J.A., Young, K.E., Koonin, E.V., Beachy, P.A., and Leahy, D.J. (1997). Crystal structure of a Hedgehog autoprocessing domain: homology between Hedgehog and self-splicing proteins. *Cell* *91*, 85-97.
- Heiland, I., and Erdmann, R. (2005). Biogenesis of peroxisomes. Topogenesis of the peroxisomal membrane and matrix proteins. *FEBS J* *272*, 2362-2372.
- Honsho, M., Hiroshige, T., and Fujiki, Y. (2002). The membrane biogenesis peroxin Pex16p. Topogenesis and functional roles in peroxisomal membrane assembly. *J Biol Chem* *277*, 44513-44524.
- Huybrechts, S.J., Van Veldhoven, P.P., Hoffman, I., Zeevaert, R., de Vos, R., Demaerel, P., Brams, M., Jaeken, J., Franssen, M., and Cassiman, D. (2009). Identification of a novel PEX14 mutation in Zellweger syndrome. *BMJ Case Rep* *2009*.
- Ismail, S.A., Chen, Y.X., Rusinova, A., Chandra, A., Bierbaum, M., Gremer, L., Triola, G., Waldmann, H., Bastiaens, P.I., and Wittinghofer, A. (2011). Arl2-GTP and Arl3-GTP regulate a GDI-like transport system for farnesylated cargo. *Nat Chem Biol* *7*, 942-949.
- Itzen, A., and Goody, R.S. (2011). GTPases involved in vesicular trafficking: structures and mechanisms. *Semin Cell Dev Biol* *22*, 48-56.
- James, G.L., Goldstein, J.L., Pathak, R.K., Anderson, R.G., and Brown, M.S. (1994). PxF, a prenylated protein of peroxisomes. *J Biol Chem* *269*, 14182-14190.
- Jedd, G., and Chua, N.H. (2000). A new self-assembled peroxisomal vesicle required for efficient resealing of the plasma membrane. *Nat Cell Biol* *2*, 226-231.
- Jerabek-Willemsen, M., Wienken, C.J., Braun, D., Baaske, P., and Duhr, S. (2011). Molecular interaction studies using microscale thermophoresis. *Assay Drug Dev Technol* *9*, 342-353.
- John, M., and Otting, G. (2007). Strategies for measurements of pseudocontact shifts in protein NMR spectroscopy. *Chemphyschem* *8*, 2309-2313.

- Johnson, B.A., and Blevins, R.A. (1994). NMRView: A computer program for the visualization and analysis of NMR data. *J Biomol NMR* **4**, 603-614.
- Jones, J.M., Morrell, J.C., and Gould, S.J. (2004). PEX19 is a predominantly cytosolic chaperone and import receptor for class 1 peroxisomal membrane proteins. *J Cell Biol* **164**, 57-67.
- Jung, Y.S., and Zweckstetter, M. (2004). Mars -- robust automatic backbone assignment of proteins. *J Biomol NMR* **30**, 11-23.
- Kammerer, S., Arnold, N., Gutensohn, W., Mewes, H.W., Kunau, W.H., Hofler, G., Roscher, A.A., and Braun, A. (1997). Genomic organization and molecular characterization of a gene encoding HsPXF, a human peroxisomal farnesylated protein. *Genomics* **45**, 200-210.
- Keeler, J., ed. (2005). *Understanding NMR Spectroscopy*, 1 edn (John Wiley & Sons).
- Keller, G.A., Krisans, S., Gould, S.J., Sommer, J.M., Wang, C.C., Schliebs, W., Kunau, W., Brody, S., and Subramani, S. (1991). Evolutionary conservation of a microbody targeting signal that targets proteins to peroxisomes, glyoxysomes, and glycosomes. *J Cell Biol* **114**, 893-904.
- Kemp, S., and Wanders, R.J. (2007). X-linked adrenoleukodystrophy: very long-chain fatty acid metabolism, ABC half-transporters and the complicated route to treatment. *Mol Genet Metab* **90**, 268-276.
- Lane, K.T., and Beese, L.S. (2006). Thematic review series: lipid posttranslational modifications. Structural biology of protein farnesyltransferase and geranylgeranyltransferase type I. *J Lipid Res* **47**, 681-699.
- Linge, J.P., Williams, M.A., Spronk, C.A., Bonvin, A.M., and Nilges, M. (2003). Refinement of protein structures in explicit solvent. *Proteins* **50**, 496-506.
- Loew, A., Ho, Y.K., Blundell, T., and Bax, B. (1998). Phosducin induces a structural change in transducin beta gamma. *Structure* **6**, 1007-1019.
- Ma, C., Agrawal, G., and Subramani, S. (2011). Peroxisome assembly: matrix and membrane protein biogenesis. *J Cell Biol* **193**, 7-16.
- Madl, T., Bermel, W., and Zangger, K. (2009). Use of relaxation enhancements in a paramagnetic environment for the structure determination of proteins using NMR spectroscopy. *Angew Chem Int Ed Engl* **48**, 8259-8262.
- Maestre-Martinez, M., Haupt, K., Edlich, F., Jahreis, G., Jarczowski, F., Erdmann, F., Fischer, G., and Lucke, C. (2010). New structural aspects of FKBP38 activation. *Biol Chem* **391**, 1157-1167.
- Magee, T., and Seabra, M.C. (2005). Fatty acylation and prenylation of proteins: what's hot in fat. *Curr Opin Cell Biol* **17**, 190-196.
- Mann, R.K., and Beachy, P.A. (2000). Cholesterol modification of proteins. *Biochim Biophys Acta* **1529**, 188-202.

- Martin, D.D., Beauchamp, E., and Berthiaume, L.G. (2011). Post-translational myristoylation: Fat matters in cellular life and death. *Biochimie* 93, 18-31.
- Massi, F., Johnson, E., Wang, C., Rance, M., and Palmer, A.G., 3rd (2004). NMR R1 rho rotating-frame relaxation with weak radio frequency fields. *J Am Chem Soc* 126, 2247-2256.
- Matsuzono, Y., and Fujiki, Y. (2006). In vitro transport of membrane proteins to peroxisomes by shuttling receptor Pex19p. *J Biol Chem* 281, 36-42.
- McAndrew, R.P., Peralta-Yahya, P.P., DeGiovanni, A., Pereira, J.H., Hadi, M.Z., Keasling, J.D., and Adams, P.D. (2011). Structure of a three-domain sesquiterpene synthase: a prospective target for advanced biofuels production. *Structure* 19, 1876-1884.
- McNew, J.A., and Goodman, J.M. (1994). An oligomeric protein is imported into peroxisomes in vivo. *J Cell Biol* 127, 1245-1257.
- Meinecke, M., Cizmowski, C., Schliebs, W., Kruger, V., Beck, S., Wagner, R., and Erdmann, R. (2010). The peroxisomal importomer constitutes a large and highly dynamic pore. *Nat Cell Biol* 12, 273-277.
- Molina, H., Horn, D.M., Tang, N., Mathivanan, S., and Pandey, A. (2007). Global proteomic profiling of phosphopeptides using electron transfer dissociation tandem mass spectrometry. *Proc Natl Acad Sci U S A* 104, 2199-2204.
- Neri, D., Szyperski, T., Otting, G., Senn, H., and Wuthrich, K. (1989). Stereospecific nuclear magnetic resonance assignments of the methyl groups of valine and leucine in the DNA-binding domain of the 434 repressor by biosynthetically directed fractional ¹³C labeling. *Biochemistry* 28, 7510-7516.
- Neufeld, C., Filipp, F.V., Simon, B., Neuhaus, A., Schuller, N., David, C., Kooshapur, H., Madl, T., Erdmann, R., Schliebs, W., *et al.* (2009). Structural basis for competitive interactions of Pex14 with the import receptors Pex5 and Pex19. *EMBO J* 28, 745-754.
- Nilges, M., Macias, M.J., O'Donoghue, S.I., and Oschkinat, H. (1997). Automated NOESY interpretation with ambiguous distance restraints: the refined NMR solution structure of the pleckstrin homology domain from beta-spectrin. *J Mol Biol* 269, 408-422.
- Opperdoes, F.R., and Borst, P. (1977). Localization of nine glycolytic enzymes in a microbody-like organelle in *Trypanosoma brucei*: the glycosome. *FEBS Lett* 80, 360-364.
- Otting, G. (2008). Prospects for lanthanides in structural biology by NMR. *J Biomol NMR* 42, 1-9.
- Pinto, M.P., Grou, C.P., Alencastre, I.S., Oliveira, M.E., Sa-Miranda, C., Fransen, M., and Azevedo, J.E. (2006). The import competence of a peroxisomal membrane protein is determined by Pex19p before the docking step. *J Biol Chem* 281, 34492-34502.
- Platta, H.W., Grunau, S., Rosenkranz, K., Girzalsky, W., and Erdmann, R. (2005). Functional role of the AAA peroxins in dislocation of the cycling PTS1 receptor back to the cytosol. *Nat Cell Biol* 7, 817-822.

- Prestegard, J.H., Bougault, C.M., and Kishore, A.I. (2004). Residual dipolar couplings in structure determination of biomolecules. *Chem Rev* *104*, 3519-3540.
- Reumann, S., Quan, S., Aung, K., Yang, P., Manandhar-Shrestha, K., Holbrook, D., Linka, N., Switzenberg, R., Wilkerson, C.G., Weber, A.P., *et al.* (2009). In-depth proteome analysis of Arabidopsis leaf peroxisomes combined with in vivo subcellular targeting verification indicates novel metabolic and regulatory functions of peroxisomes. *Plant Physiol* *150*, 125-143.
- Rottensteiner, H., Kramer, A., Lorenzen, S., Stein, K., Landgraf, C., Volkmer-Engert, R., and Erdmann, R. (2004). Peroxisomal membrane proteins contain common Pex19p-binding sites that are an integral part of their targeting signals. *Mol Biol Cell* *15*, 3406-3417.
- Rucktaschel, R., Thoms, S., Sidorovitch, V., Halbach, A., Pechlivanis, M., Volkmer, R., Alexandrov, K., Kuhlmann, J., Rottensteiner, H., and Erdmann, R. (2009). Farnesylation of pex19p is required for its structural integrity and function in peroxisome biogenesis. *J Biol Chem* *284*, 20885-20896.
- Sacksteder, K.A., Jones, J.M., South, S.T., Li, X., Liu, Y., and Gould, S.J. (2000). PEX19 binds multiple peroxisomal membrane proteins, is predominantly cytoplasmic, and is required for peroxisome membrane synthesis. *J Cell Biol* *148*, 931-944.
- Salaun, C., Greaves, J., and Chamberlain, L.H. (2010). The intracellular dynamic of protein palmitoylation. *J Cell Biol* *191*, 1229-1238.
- Sato, Y., Shibata, H., Nakatsu, T., Nakano, H., Kashiwayama, Y., Imanaka, T., and Kato, H. (2010). Structural basis for docking of peroxisomal membrane protein carrier Pex19p onto its receptor Pex3p. *EMBO J* *29*, 4083-4093.
- Sattler, M., and Fesik, S.W. (1997). Resolving resonance overlap in the NMR spectra of proteins from different lanthanide-induced shifts. *J Am Chem Soc* *119*, 7885-7886.
- Sattler, M., Schleucher, J., and Griesinger, C. (1999). Heteronuclear multidimensional NMR experiments for the structure determination of proteins in solution employing pulsed field gradients. *Prog NMR Spectrosc* *34*, 93-158.
- Saveria, T., Halbach, A., Erdmann, R., Volkmer-Engert, R., Landgraf, C., Rottensteiner, H., and Parsons, M. (2007). Conservation of PEX19-binding motifs required for protein targeting to mammalian peroxisomal and trypanosome glycosomal membranes. *Eukaryot Cell* *6*, 1439-1449.
- Schmidt, F., Treiber, N., Zocher, G., Bjelic, S., Steinmetz, M.O., Kalbacher, H., Stehle, T., and Dodt, G. (2010). Insights into peroxisome function from the structure of PEX3 in complex with a soluble fragment of PEX19. *J Biol Chem* *285*, 25410-25417.
- Schmucki, R., Yokoyama, S., and Guntert, P. (2009). Automated assignment of NMR chemical shifts using peak-particle dynamics simulation with the DYNASSIGN algorithm. *J Biomol NMR* *43*, 97-109.
- Schrader, M., and Fahimi, H.D. (2008). The peroxisome: still a mysterious organelle. *Histochem Cell Biol* *129*, 421-440.

- Schueler, N., Holton, S.J., Fodor, K., Milewski, M., Konarev, P., Stanley, W.A., Wolf, J., Erdmann, R., Schliebs, W., Song, Y.H., *et al.* (2010). The peroxisomal receptor Pex19p forms a helical mPTS recognition domain. *EMBO J* 29, 2491-2500.
- Seykora, J.T., Myat, M.M., Allen, L.A., Ravetch, J.V., and Aderem, A. (1996). Molecular determinants of the myristoyl-electrostatic switch of MARCKS. *J Biol Chem* 271, 18797-18802.
- Shen, Y., Delaglio, F., Cornilescu, G., and Bax, A. (2009). TALOS+: a hybrid method for predicting protein backbone torsion angles from NMR chemical shifts. *J Biomol NMR* 44, 213-223.
- Shibata, H., Kashiwayama, Y., Imanaka, T., and Kato, H. (2004). Domain architecture and activity of human Pex19p, a chaperone-like protein for intracellular trafficking of peroxisomal membrane proteins. *J Biol Chem* 279, 38486-38494.
- Sies, H. (1974). Biochemistry of the peroxisome in the liver cell. *Angew Chem Int Ed Engl* 13, 706-718.
- Sievers, F., Wilm, A., Dineen, D., Gibson, T.J., Karplus, K., Li, W., Lopez, R., McWilliam, H., Remmert, M., Soding, J., *et al.* (2011). Fast, scalable generation of high-quality protein multiple sequence alignments using Clustal Omega. *Mol Syst Biol* 7, 539.
- Silvius, J.R., and l'Heureux, F. (1994). Fluorimetric evaluation of the affinities of isoprenylated peptides for lipid bilayers. *Biochemistry* 33, 3014-3022.
- Simon, B., Madl, T., Mackereth, C.D., Nilges, M., and Sattler, M. (2010). An efficient protocol for NMR-spectroscopy-based structure determination of protein complexes in solution. *Angew Chem Int Ed Engl* 49, 1967-1970.
- Solassol, J., Mange, A., and Maudelonde, T. (2011). FKBP family proteins as promising new biomarkers for cancer. *Curr Opin Pharmacol* 11, 320-325.
- Stanley, W.A., Filipp, F.V., Kursula, P., Schuller, N., Erdmann, R., Schliebs, W., Sattler, M., and Wilmanns, M. (2006). Recognition of a functional peroxisome type 1 target by the dynamic import receptor pex5p. *Mol Cell* 24, 653-663.
- Stanley, W.A., and Wilmanns, M. (2006). Dynamic architecture of the peroxisomal import receptor Pex5p. *Biochim Biophys Acta* 1763, 1592-1598.
- Steinberg, S.J., Dodt, G., Raymond, G.V., Braverman, N.E., Moser, A.B., and Moser, H.W. (2006). Peroxisome biogenesis disorders. *Biochim Biophys Acta* 1763, 1733-1748.
- Su, X.C., and Otting, G. (2010). Paramagnetic labelling of proteins and oligonucleotides for NMR. *J Biomol NMR* 46, 101-112.
- Swinkels, B.W., Gould, S.J., Bodnar, A.G., Rachubinski, R.A., and Subramani, S. (1991). A novel, cleavable peroxisomal targeting signal at the amino-terminus of the rat 3-ketoacyl-CoA thiolase. *EMBO J* 10, 3255-3262.

- Tolbert, N.E., and Essner, E. (1981). Microbodies: peroxisomes and glyoxysomes. *J Cell Biol* *91*, 271s-283s.
- van der Zand, A., Braakman, I., and Tabak, H.F. (2010). Peroxisomal membrane proteins insert into the endoplasmic reticulum. *Mol Biol Cell* *21*, 2057-2065.
- van der Zand, A., Gent, J., Braakman, I., and Tabak, H.F. (2012). Biochemically distinct vesicles from the endoplasmic reticulum fuse to form peroxisomes. *Cell* *149*, 397-409.
- Walton, P.A., Hill, P.E., and Subramani, S. (1995). Import of stably folded proteins into peroxisomes. *Mol Biol Cell* *6*, 675-683.
- Wanders, R.J., and Waterham, H.R. (2006). Peroxisomal disorders: the single peroxisomal enzyme deficiencies. *Biochim Biophys Acta* *1763*, 1707-1720.
- Weiner, L.M. (1986). Magnetic resonance study of the structure and functions of cytochrome P450. *CRC Crit Rev Biochem* *20*, 139-200.
- Weissman, A.M., Shabek, N., and Ciechanover, A. (2011). The predator becomes the prey: regulating the ubiquitin system by ubiquitylation and degradation. *Nat Rev Mol Cell Biol* *12*, 605-620.
- Will, G.K., Soukupova, M., Hong, X., Erdmann, K.S., Kiel, J.A., Dodt, G., Kunau, W.H., and Erdmann, R. (1999). Identification and characterization of the human orthologue of yeast Pex14p. *Mol Cell Biol* *19*, 2265-2277.
- Williams, C., van den Berg, M., Panjikar, S., Stanley, W.A., Distel, B., and Wilmanns, M. (2012). Insights into ubiquitin-conjugating enzyme/ co-activator interactions from the structure of the Pex4p:Pex22p complex. *EMBO J* *31*, 391-402.
- Williams, C., van den Berg, M., Sprenger, R.R., and Distel, B. (2007). A conserved cysteine is essential for Pex4p-dependent ubiquitination of the peroxisomal import receptor Pex5p. *J Biol Chem* *282*, 22534-22543.
- Wishart, D.S., and Sykes, B.D. (1994). The ¹³C chemical-shift index: a simple method for the identification of protein secondary structure using ¹³C chemical-shift data. *J Biomol NMR* *4*, 171-180.
- Wolf, J., Schliebs, W., and Erdmann, R. (2010). Peroxisomes as dynamic organelles: peroxisomal matrix protein import. *FEBS J* *277*, 3268-3278.
- Wu, Y.W., Tan, K.T., Waldmann, H., Goody, R.S., and Alexandrov, K. (2007). Interaction analysis of prenylated Rab GTPase with Rab escort protein and GDP dissociation inhibitor explains the need for both regulators. *Proc Natl Acad Sci U S A* *104*, 12294-12299.
- Yang, D., Venters, R.A., Mueller, G.A., Choy, W.Y., and Kay, L.E. (1999). TROSY-based HNCO pulse sequences for the measurement of ¹HN-¹⁵N, ¹⁵N-¹³CO, ¹HN-¹³CO, ¹³CO-¹³Cα and ¹HN-¹³Cα dipolar couplings in ¹⁵N, ¹³C, ²H-labeled proteins. *J Biomol NMR* *14*, 333-343.
- Yang, Q., and Guan, K.L. (2007). Expanding mTOR signaling. *Cell Res* *17*, 666-681.

Zha, J., Weiler, S., Oh, K.J., Wei, M.C., and Korsmeyer, S.J. (2000). Posttranslational N-myristoylation of BID as a molecular switch for targeting mitochondria and apoptosis. *Science* 290, 1761-1765.

6. List of Figures

Figure 1.1	Peroxisome proliferation in <i>H. polymorpha</i> (Erdmann and Schliebs, 2005).	2
Figure 1.2	Concepts in peroxisomal protein transport.	4
Figure 1.3	Model for peroxisomal matrix protein import.	5
Figure 1.4	The ubiquitin-conjugating enzyme Pex4p and its activator Pex22p.	7
Figure 1.5	Model for transport of class I peroxisomal membrane proteins.	9
Figure 1.6	Domain composition and structures of PEX5 and PEX19.	10
Figure 1.7	Glycine lipidation.	12
Figure 1.8	Cystein lipidation.	13
Figure 1.9	Energy levels for spin $\frac{1}{2}$ nuclei in presence of an external magnetic field.	17
Figure 1.10	The vector model.	18
Figure 1.11	Typical protein NMR spectra.	20
Figure 1.12	Paramagnetic relaxation enhancement.	24
Figure 3.1	Domain structure of PEX19.	45
Figure 3.2	Overlay of the ^1H ^{15}N HSQC spectra of full-length PEX19 (1-299; light green) with PEX19 (115-299, cyan) and the PEX19 C-terminus (161-299; blue).	46
Figure 3.3	<i>In vitro</i> farnesylation of PEX19.	47
Figure 3.4	Chemical shift perturbations upon farnesylation of PEX19 CTD.	48
Figure 3.5	Secondary chemical shift analysis and ^{15}N relaxation studies of PEX19 CTD without and with farnesylation plotted against the amino acid sequence.	49
Figure 3.6	Overlay of the ^1H ^{15}N HSQC spectra of PEX19 CTD and PEX19 CTD with a spin label at position 205.	51
Figure 3.7	Paramagnetic relaxation enhancement of PEX19 CTD with and without farnesylation	52
Figure 3.8	Solvent PRE rates of backbone amide protons of farnesylated and non-farnesylated PEX19 CTD.	53
Figure 3.9	Farnesyl protons.	54
Figure 3.10	Natural abundance ^1H , ^{13}C HSQC spectra of farnesyl pyrophosphate (cyan) and farnesylated PEX19 CTD labeled with U- ^{2}H , U- ^{13}C glucose (black).	55
Figure 3.11	Proton and carbon resonances of the farnesyl group.	56
Figure 3.12	Selective labeling of aliphatic amino acids in PEX19 CTD.	57
Figure 3.13	Reverse labeling of phenylalanine in farnesylated PEX19 CTD.	58

Figure 3.14	Protein-farnesyl NOESY cross peaks between specifically labeled farnesylated PEX19CTD. Representative farnesyl NOESY cross peaks are labeled in strips of ¹³ C edited HSQC NOESY spectra of the differently labeled samples.	59
Figure 3.15	Farnesyl recognition in PEX19 CTD.	61
Figure 3.16	Comparison of the NMR solution structure of farnesylated PEX19 CTD with the crystal structure of PEX19 (171-283).	62
Figure 3.17	Isoprenoid conformations.	64
Figure 3.18	NMR titration experiments of PEX19 with a PEX13 peptide.	66
Figure 3.19	NMR titration experiments of farnesylated PEX19 CTD with PMP peptides.	67
Figure 3.20	¹ H ¹⁵ N HSQC spectra of PEX11 peptide-PEX19 CTD.	68
Figure 3.21	Flotation assays of PEX19.	69
Figure 3.22	Microscale thermophoresis measurements of PEX19 CTD.	70
Figure 3.23	Comparison of back-calculated with experimental solvent PRE rates.	72
Figure 3.24	Surface charge and sequence conservation in PEX19 CTD.	74
Figure 3.25	Structural basis for the design of point mutations in the farnesyl recognition site	75
Figure 3.26	NMR spectra of wild type and mutant PEX19 CTD.	76
Figure 3.27	{ ¹ H}- ¹⁵ N heteronuclear NOE values of PEX19 CTD and PEX19 CTD M255R.	77
Figure 3.28	Hydrophobic interaction chromatography.	78
Figure 3.29	Microscale thermophoresis measurements of PEX19 CTD M179R.	80
Figure 3.30	Microscale thermophoresis measurements of PEX19 CTD I195K.	81
Figure 3.31	Microscale thermophoresis measurements of PEX19 CTD M255R.	82
Figure 3.32	Functionality of PEX19 variants with farnesylation-related mutations in human fibroblasts.	83
Figure 3.33	Quantitative evaluation of $\Delta pex19$ -phenotype complementation by the individual PEX19 variants and analysis of <i>in vivo</i> farnesylation.	84
Figure 3.34	NMR spectra of Pex4p and Pex22p. ¹ H, ¹⁵ N HSQC spectra of (A) Pex22p (54-180) and (B) Pex4p (15-183).	88
Figure 3.35	Domain composition and NMR spectra of FKBP38.	90
Figure 3.36	Comparison of chemical shift perturbations and solvent PRE rates in FKBD (residues 31-149) and NTD (residues1-151).	91
Figure 4.1	Model for a functional role for PEX19 farnesylation in PMP transport.	92

III. Appendix

III.I Primers for site-directed mutagenesis

Primer	Sequence (5' – 3')
C226A fw	GCACAGCGTCATGTGCAAAATAGCTGAGCAGTTTGAGGC
C226A rev	GCCTCAAACCTGCTCAGCTATTTTGACATGACGCTGTGC
C226A/C229A fw	GCAGCACAGCGTCATGGCCAAAATAGCTGAGCAGTTTGAGGC
C226A/C229A rev	GCCTCAAACCTGCTCAGCTATTTTGGCCATGACGCTGTGCTGC
S205C fw	ATCCAGAATGGTTGCAGTGTGCATCGGGAATCTCTA
S205C rev	TAGAGATTCCCGATGACACTGCAACCATTCTGGAT
S286C fw	CTGGATGCCCTCAATCTTTGCGGCCACCAG
S286C rev	CTGGTGGGCCGCAAAGATTGAGGGCATCCAG
C296S fw	GTGCAAGTGGTGAACAGAGTCTGATCATGTGATAA
C296S rev	TTATCACATGATCAGACTCTGTTCACTTGCAC
M179R fw	CCTCCCATCATGCAGAGTATTAGGCAGAACCTACT
M179R rev	AGTAGGTTCTGCCTAATACTCTGCATGATGGGGAGG
I195K fw	TGTGCTGTACCCATCACTGAAGGAGAAGACAGAAAAGTATCC
I195K rev	GGATACTTTTCTGTCTTCTCCTTCAGTGATGGGTACAGCACA
M225R fw	TTTTGAGATGGTGTGGATCTTAGGCAGCAGCTACA
M255R rev	TGTAGCTGCTGCCTAAGATCCAGCACCATCTCAAAA

III.II Resonance assignments of PEX19 CTD

res	atom	nucl	shift	res	atom	nucl	shift	res	atom	nucl	shift
G161	H	1H	8.383	D166	N	15N	120.308	I171	CA	13C	61.144
G161	HA3	1H	3.912	D166	QB	1H	2.608	I171	CB	13C	38.744
G161	N	15N	109.972	G167	CA	13C	45.494	I171	CD1	13C	13.055
M162	CA	13C	55.449	G167	H	1H	8.351	I171	CG1	13C	27.346
M162	CB	13C	33.032	G167	N	15N	109.214	I171	CG2	13C	17.667
M162	CG	13C	32.947	G167	QA	1H	3.878	I171	H	1H	8.048
M162	H	1H	8.115	E168	CA	13C	56.86	I171	HA	1H	4.086
M162	HA	1H	4.412	E168	CB	13C	30.268	I171	HB	1H	1.768
M162	N	15N	119.678	E168	H	1H	8.282	I171	HG12	1H	1.345
M162	QB	1H	1.894	E168	HA	1H	4.189	I171	HG13	1H	1.079
M162	QG	1H	2.008	E168	HB2	1H	1.99	I171	MD1	1H	0.745
D163	CA	13C	54.507	E168	HB3	1H	1.849	I171	MG2	1H	0.784
D163	CB	13C	41.291	E168	N	15N	120.46	I171	N	15N	120.722
D163	H	1H	8.389	E168	QG	1H	2.151	L172	CA	13C	54.168
D163	HA	1H	4.509	G169	CA	13C	45.514	L172	CB	13C	41.548
D163	HB2	1H	2.518	G169	H	1H	8.386	L172	CD1	13C	25.141
D163	HB3	1H	2.626	G169	N	15N	109.333	L172	CD2	13C	23.615
D163	N	15N	121.328	G169	QA	1H	3.841	L172	CG	13C	27.207
E164	H	1H	8.359	N170	CA	13C	53.259	L172	H	1H	8.273
E164	HA	1H	4.186	N170	CB	13C	39.068	L172	HA	1H	4.457
E164	N	15N	121.308	N170	H	1H	8.2	L172	HB2	1H	1.541
G165	H	1H	8.377	N170	HA	1H	4.633	L172	HB3	1H	1.474
G165	N	15N	109.513	N170	HB2	1H	2.689	L172	HG	1H	1.569
G165	QA	1H	3.881	N170	HB3	1H	2.626	L172	MD1	1H	0.826
D166	CA	13C	54.449	N170	HD21	1H	6.825	L172	MD2	1H	0.793
D166	CB	13C	41.373	N170	HD22	1H	7.541	L172	N	15N	127.154
D166	H	1H	8.204	N170	N	15N	118.572	P173	CA	13C	63.748
D166	HA	1H	4.548	N170	ND	15N	112.914	P173	CB	13C	31.935
res	atom	nucl	shift	res	atom	nucl	shift	res	atom	nucl	shift
P173	CD	13C	50.583	M175	HG2	1H	2.522	I178	HA	1H	3.879
P173	CG	13C	27.66	M175	HG3	1H	2.433	I178	HB	1H	1.85
P173	HA	1H	4.322	M175	ME	1H	1.95	I178	HG12	1H	1.547
P173	HB2	1H	1.808	M175	N	15N	121.987	I178	HG13	1H	1.068
P173	HB3	1H	2.208	M175	QB	1H	1.978	I178	MD1	1H	0.757
P173	HD2	1H	3.746	Q176	CA	13C	57.95	I178	MG2	1H	0.786
P173	HD3	1H	3.537	Q176	CB	13C	29.086	I178	N	15N	122.073
P173	HG2	1H	1.942	Q176	H	1H	8.187	M179	CA	13C	57.98
P173	HG3	1H	1.917	Q176	HA	1H	4.048	M179	CB	13C	32.395
I174	CA	13C	62.365	Q176	HE21	1H	7.382	M179	CE	13C	17.159
I174	CB	13C	38.413	Q176	HE22	1H	6.723	M179	CG	13C	32.513
I174	CD1	13C	13.252	Q176	N	15N	119.901	M179	H	1H	8.189
I174	CG1	13C	28.053	Q176	NE2	15N	111.396	M179	HA	1H	4.145
I174	CG2	13C	17.676	Q176	QB	1H	1.968	M179	HB2	1H	2.071
I174	H	1H	7.993	Q176	QG	1H	2.249	M179	HB3	1H	2.424
I174	HA	1H	3.969	S177	CA	13C	60.076	M179	ME	1H	1.899
I174	HB	1H	1.8	S177	CB	13C	63.511	M179	N	15N	119.317
I174	HG12	1H	1.427	S177	H	1H	8.05	M179	QG	1H	2.585
I174	HG13	1H	1.127	S177	HA	1H	4.227	Q180	CA	13C	58.485
I174	MD1	1H	0.781	S177	HB2	1H	3.893	Q180	CB	13C	28.603
I174	MG2	1H	0.815	S177	HB3	1H	3.815	Q180	CG	13C	34.192

I174	N	15N	120.052	S177	N	15N	115.589	Q180	H	1H	8.043
M175	CA	13C	56.331	I178	CA	13C	64.067	Q180	HA	1H	3.89
M175	CB	13C	32.276	I178	CB	13C	38.354	Q180	HE21	1H	7.252
M175	CE	13C	17.084	I178	CD1	13C	13.57	Q180	HE22	1H	6.623
M175	CG	13C	32.322	I178	CG1	13C	28.52	Q180	HG2	1H	2.144
M175	H	1H	8.256	I178	CG2	13C	17.56	Q180	HG3	1H	2.018
M175	HA	1H	4.269	I178	H	1H	8.008	Q180	N	15N	117.125

res	atom	nucl	shift	res	atom	nucl	shift	res	atom	nucl	shift
Q180	NE2	15N	111.257	L183	HA	1H	4.465	D186	H	1H	8.185
Q180	QB	1H	1.914	L183	HB2	1H	1.755	D186	HA	1H	4.264
N181	CA	13C	55.443	L183	HB3	1H	1.712	D186	HB2	1H	2.45
N181	CB	13C	39.221	L183	HG	1H	1.71	D186	HB3	1H	2.586
N181	H	1H	7.784	L183	MD1	1H	0.737	D186	N	15N	114.107
N181	HA	1H	4.502	L183	MD2	1H	0.711	V187	CA	13C	64.293
N181	HD21	1H	6.848	L183	N	15N	114.422	V187	CB	13C	33.331
N181	HD22	1H	7.518	S184	CA	13C	58.031	V187	CG1	13C	21.764
N181	N	15N	116.143	S184	CB	13C	65.06	V187	CG2	13C	21.894
N181	ND	15N	112.509	S184	H	1H	7.469	V187	H	1H	7.173
N181	QB	1H	2.755	S184	HA	1H	4.485	V187	HA	1H	3.907
L182	CA	13C	57.153	S184	HB2	1H	4.079	V187	HB	1H	2.005
L182	CB	13C	42.697	S184	HB3	1H	4.015	V187	MG1	1H	0.864
L182	CD1	13C	25.559	S184	N	15N	113.448	V187	MG2	1H	0.831
L182	CG	13C	27.061	K185	CB	13C	32.764	V187	N	15N	116.28
L182	H	1H	8.046	K185	CD	13C	29.555	L188	CA	13C	57.331
L182	HA	1H	4.128	K185	CE	13C	42.166	L188	CB	13C	43.858
L182	HB2	1H	1.685	K185	CG	13C	25.436	L188	CD1	13C	24.249
L182	HB3	1H	1.504	K185	H	1H	8.96	L188	CD2	13C	25.32
L182	HG	1H	1.675	K185	HA	1H	4.067	L188	CG	13C	27.382
L182	MD1	1H	0.748	K185	HB2	1H	1.65	L188	H	1H	8.089
L182	N	15N	119.788	K185	HB3	1H	1.708	L188	HA	1H	4.19
L183	CA	13C	53.927	K185	HE2	1H	2.259	L188	HB2	1H	1.824
L183	CB	13C	40.858	K185	HE3	1H	2.571	L188	HB3	1H	1.55
L183	CD1	13C	26.022	K185	QD	1H	1.468	L188	HG	1H	1.59
L183	CD2	13C	24.058	K185	QG	1H	1.114	L188	MD1	1H	0.931
L183	CG	13C	27.348	D186	CA	13C	56.403	L188	MD2	1H	0.966
L183	H	1H	7.568	D186	CB	13C	40.852	L188	N	15N	119.946

res	atom	nucl	shift	res	atom	nucl	shift	res	atom	nucl	shift
Y189	CA	13C	63.118	L192	CA	13C	57.703	K193	N	15N	122.44
Y189	CB	13C	36.27	L192	CB	13C	42.588	E194	CA	13C	59.414
Y189	CQD	13C	133.192	L192	CD1	13C	25.697	E194	CB	13C	29.55
Y189	CQE	13C	117.684	L192	CD2	13C	25.113	E194	CG	13C	36.043
Y189	H	1H	7.817	L192	CG	13C	26.969	E194	H	1H	7.219
Y189	HA	1H	4.033	L192	H	1H	7.854	E194	HA	1H	3.951
Y189	HB2	1H	3.054	L192	HA	1H	3.954	E194	HB2	1H	2.018
Y189	HB3	1H	2.133	L192	HB2	1H	1.601	E194	HB3	1H	1.965
Y189	N	15N	115.279	L192	HB3	1H	1.395	E194	HG2	1H	2.125
Y189	QD	1H	6.936	L192	HG	1H	1.633	E194	HG3	1H	2.236
Y189	QE	1H	6.78	L192	MD1	1H	0.837	E194	N	15N	117.263
P190	CA	13C	66.714	L192	MD2	1H	0.824	I195	CA	13C	65.577
P190	CB	13C	30.623	L192	N	15N	121.616	I195	CB	13C	38.054
P190	CD	13C	49.429	K193	CA	13C	58.409	I195	CD1	13C	13.898

P190	CG	13C	28.861	K193	CB	13C	31.635	I195	CG1	13C	29.316
P190	HA	1H	3.77	K193	CD	13C	29.15	I195	CG2	13C	18.224
P190	HB2	1H	2.162	K193	CE	13C	42.429	I195	H	1H	7.521
P190	HB3	1H	1.744	K193	CG	13C	23.978	I195	HA	1H	3.594
P190	HD2	1H	3.901	K193	H	1H	9.004	I195	HB	1H	1.812
P190	HD3	1H	3.289	K193	HA	1H	3.894	I195	HG12	1H	1.656
P190	HG2	1H	2.057	K193	HB2	1H	1.458	I195	HG13	1H	0.875
P190	HG3	1H	1.888	K193	HB3	1H	0.954	I195	MD1	1H	0.603
S191	CA	13C	61.881	K193	HD2	1H	1.718	I195	MG2	1H	0.747
S191	CB	13C	63.294	K193	HD3	1H	1.313	I195	N	15N	117.309
S191	H	1H	7.385	K193	HE2	1H	2.867	T196	CA	13C	67.805
S191	HA	1H	4.167	K193	HE3	1H	2.766	T196	CB	13C	69.06
S191	N	15N	111.864	K193	HG2	1H	1.166	T196	CG2	13C	24.273
S191	QB	1H	3.743	K193	HG3	1H	1.102	T196	H	1H	8.459

res	atom	nucl	shift	res	atom	nucl	shift	res	atom	nucl	shift
T196	HA	1H	4.046	K198	N	15N	117.885	E201	HA	1H	4.052
T196	HB	1H	4.31	K198	QE	1H	2.85	E201	HG2	1H	2.284
T196	HG1	1H	4.866	Y199	CA	13C	62.06	E201	HG3	1H	2.254
T196	MG2	1H	1.31	Y199	CB	13C	37.813	E201	N	15N	117.747
T196	N	15N	114.065	Y199	CQD	13C	131.641	E201	QB	1H	2.038
E197	CA	13C	58.558	Y199	CQE	13C	117.41	W202	CA	13C	63.051
E197	CB	13C	29.846	Y199	H	1H	7.91	W202	CB	13C	30.267
E197	CG	13C	36.861	Y199	HA	1H	4.278	W202	CD1	13C	126.708
E197	H	1H	7.786	Y199	HB2	1H	3.179	W202	CE3	13C	119.171
E197	HA	1H	4.172	Y199	HB3	1H	2.534	W202	CH2	13C	124.463
E197	HB2	1H	2.13	Y199	N	15N	122.367	W202	CZ2	13C	114.55
E197	HB3	1H	2.056	Y199	QD	1H	7.068	W202	CZ3	13C	120.955
E197	HG2	1H	2.431	Y199	QE	1H	6.322	W202	H	1H	7.659
E197	HG3	1H	2.254	P200	CA	13C	67.735	W202	HA	1H	4.076
E197	N	15N	118.481	P200	CB	13C	31.18	W202	HB2	1H	3.448
K198	CA	13C	57.472	P200	CD	13C	50.63	W202	HB3	1H	3.129
K198	CB	13C	34.787	P200	CG	13C	28.871	W202	HD1	1H	7.052
K198	CD	13C	29.537	P200	HA	1H	4.003	W202	HE1	1H	9.719
K198	CE	13C	42.283	P200	HB2	1H	2.244	W202	HE3	1H	7.023
K198	CG	13C	25.714	P200	HB3	1H	1.863	W202	HH2	1H	6.661
K198	H	1H	7.498	P200	HD2	1H	3.607	W202	HZ2	1H	6.866
K198	HA	1H	4.32	P200	HD3	1H	3.465	W202	HZ3	1H	6.528
K198	HB2	1H	1.833	P200	HG2	1H	2.183	W202	N	15N	122.381
K198	HB3	1H	1.75	P200	HG3	1H	1.423	W202	NE1	15N	129.887
K198	HD2	1H	1.588	E201	CA	13C	59.375	L203	CA	13C	59.111
K198	HD3	1H	1.527	E201	CB	13C	29.533	L203	CB	13C	41.436
K198	HG2	1H	1.665	E201	CG	13C	36.587	L203	CD1	13C	25.585
K198	HG3	1H	1.435	E201	H	1H	8.3	L203	CD2	13C	23.524

res	atom	nucl	shift	res	atom	nucl	shift	res	atom	nucl	shift
L203	CG	13C	27.73	H206	CB	13C	27.858	E208	H	1H	8.331
L203	H	1H	9.464	H206	CD2	13C	118.933	E208	HA	1H	4.056
L203	HA	1H	3.99	H206	CE1	13C	135.294	E208	HB2	1H	1.967
L203	HB2	1H	2.052	H206	H	1H	7.511	E208	HB3	1H	1.775
L203	HB3	1H	1.633	H206	HA	1H	4.326	E208	N	15N	113.98
L203	HG	1H	1.958	H206	HB2	1H	2.821	E208	QG	1H	2.1
L203	MD1	1H	0.499	H206	HB3	1H	1.693	S209	CA	13C	58.226

L203	MD2	1H	0.733	H206	HD2	1H	6.769	S209	CB	13C	64.257
L203	N	15N	121.535	H206	HE1	1H	7.85	S209	H	1H	7.521
Q204	CA	13C	59.16	H206	N	15N	116.079	S209	HA	1H	4.481
Q204	CB	13C	28.362	R207	CA	13C	60.358	S209	HB2	1H	3.88
Q204	CG	13C	33.567	R207	CB	13C	30.28	S209	HB3	1H	3.734
Q204	H	1H	8.065	R207	CD	13C	43.436	S209	N	15N	111.718
Q204	HA	1H	4.028	R207	CG	13C	26.244	L210	CA	13C	52.322
Q204	HB2	1H	2.154	R207	H	1H	7.324	L210	CB	13C	44.729
Q204	HB3	1H	2.118	R207	HA	1H	3.442	L210	CD1	13C	27.666
Q204	HE21	1H	7.446	R207	HB2	1H	1.71	L210	CD2	13C	24.174
Q204	HE22	1H	6.789	R207	HB3	1H	1.553	L210	CG	13C	26.658
Q204	N	15N	117.007	R207	HD2	1H	2.845	L210	H	1H	7.211
Q204	NE2	15N	111.779	R207	HD3	1H	2.774	L210	HA	1H	4.904
Q204	QG	1H	2.413	R207	HE	1H	6.983	L210	HB2	1H	1.831
S205	CA	13C	59.96	R207	HG2	1H	0.481	L210	HB3	1H	1.436
S205	CB	13C	63.633	R207	HG3	1H	1.108	L210	HG	1H	1.991
S205	H	1H	7.879	R207	N	15N	122.268	L210	MD1	1H	1.21
S205	HA	1H	4.168	R207	NE	15N	84.546	L210	MD2	1H	1.227
S205	N	15N	111.632	E208	CA	13C	57.939	L210	N	15N	122.666
S205	QB	1H	3.688	E208	CB	13C	29.345	P211	CA	13C	61.553
H206	CA	13C	57.309	E208	CG	13C	36.73	P211	CB	13C	31.612

res	atom	nucl	shift	res	atom	nucl	shift	res	atom	nucl	shift
P211	CD	13C	50.87	Q214	CB	13C	29.48	E216	HA	1H	3.936
P211	CG	13C	28.381	Q214	CG	13C	34.116	E216	HG2	1H	2.442
P211	HA	1H	4.787	Q214	H	1H	7.267	E216	HG3	1H	2.321
P211	HB2	1H	2.543	Q214	HA	1H	3.977	E216	N	15N	115.651
P211	HB3	1H	1.872	Q214	HE21	1H	6.554	E216	QB	1H	2.014
P211	HD1	1H	3.6	Q214	HE22	1H	6.959	K217	CA	13C	59.522
P211	HD2	1H	4.048	Q214	HG2	1H	2.327	K217	CB	13C	31.972
P211	QG	1H	2.134	Q214	HG3	1H	2.19	K217	CD	13C	29.363
P212	CA	13C	66.022	Q214	N	15N	119.018	K217	CE	13C	42.031
P212	CB	13C	32.069	Q214	NE2	15N	112.205	K217	CG	13C	25.083
P212	CD	13C	50.88	Q214	QB	1H	2.084	K217	H	1H	7.04
P212	CG	13C	27.857	F215	CA	13C	63.207	K217	HA	1H	4.029
P212	HA	1H	4.247	F215	CB	13C	39.832	K217	HB2	1H	1.71
P212	HB2	1H	2.38	F215	CQD	13C	131.637	K217	HB3	1H	1.645
P212	HB3	1H	2	F215	CQE	13C	131.547	K217	HG2	1H	1.247
P212	HG2	1H	2.164	F215	CZ	13C	129.777	K217	HG3	1H	1.522
P212	HG3	1H	2.032	F215	H	1H	8.185	K217	N	15N	119.661
P212	QD	1H	3.852	F215	HA	1H	4.037	K217	QD	1H	1.57
E213	CA	13C	59.549	F215	HB2	1H	3.198	K217	QE	1H	2.776
E213	CB	13C	28.351	F215	HB3	1H	3.162	Y218	CA	13C	59.22
E213	CG	13C	36.255	F215	HZ	1H	7.2	Y218	CB	13C	37.768
E213	H	1H	9.561	F215	N	15N	120.223	Y218	CQD	13C	132.429
E213	HA	1H	4.119	F215	QD	1H	7.13	Y218	CQE	13C	117.617
E213	HG2	1H	2.315	F215	QE	1H	7.331	Y218	H	1H	7.682
E213	HG3	1H	2.236	E216	CA	13C	59.372	Y218	HA	1H	4.345
E213	N	15N	116.295	E216	CB	13C	29.532	Y218	HB2	1H	3.233
E213	QB	1H	1.971	E216	CG	13C	36.46	Y218	HB3	1H	2.848
Q214	CA	13C	57.676	E216	H	1H	8.387	Y218	N	15N	118.52

res	atom	nucl	shift	res	atom	nucl	shift	res	atom	nucl	shift
-----	------	------	-------	-----	------	------	-------	-----	------	------	-------

Y218	QD	1H	7.082	Q221	HB2	1H	2.548	V224	CG2	13C	23.764
Y218	QE	1H	6.902	Q221	HB3	1H	2.048	V224	H	1H	8.348
Q219	CA	13C	59.735	Q221	HE21	1H	6.31	V224	HA	1H	3.386
Q219	CB	13C	29.318	Q221	HE22	1H	5.85	V224	HB	1H	1.976
Q219	CG	13C	35.019	Q221	HG2	1H	2.361	V224	MG1	1H	0.843
Q219	H	1H	8.372	Q221	HG3	1H	2.76	V224	MG2	1H	0.917
Q219	HA	1H	3.695	Q221	N	15N	119.957	V224	N	15N	121.667
Q219	HB2	1H	1.878	Q221	NE2	15N	108.195	M225	CA	13C	61.271
Q219	HB3	1H	1.844	H222	CA	13C	60.141	M225	CB	13C	33.092
Q219	HE21	1H	7.289	H222	CB	13C	30.013	M225	CE	13C	18.556
Q219	HE22	1H	6.799	H222	CD2	13C	118.887	M225	CG	13C	35.441
Q219	N	15N	118.824	H222	CE1	13C	138.136	M225	H	1H	8.615
Q219	NE2	15N	111.757	H222	H	1H	7.741	M225	HA	1H	3.769
Q219	QG	1H	1.979	H222	HA	1H	3.854	M225	HB2	1H	2.183
E220	CA	13C	59.136	H222	HB2	1H	2.915	M225	HB3	1H	2.109
E220	CB	13C	28.871	H222	HB3	1H	2.167	M225	HG2	1H	2.971
E220	CG	13C	36.063	H222	HD2	1H	6.888	M225	HG3	1H	2.123
E220	H	1H	8.046	H222	HE1	1H	7.678	M225	ME	1H	1.948
E220	HA	1H	4.075	H222	N	15N	117.438	M225	N	15N	119.007
E220	HG2	1H	2.296	S223	CA	13C	61.922	C226	CA	13C	64.905
E220	HG3	1H	2.249	S223	CB	13C	62.879	C226	CB	13C	26.499
E220	N	15N	121.595	S223	H	1H	7.885	C226	H	1H	8.439
E220	QB	1H	2.112	S223	HA	1H	3.773	C226	HA	1H	3.958
Q221	CA	13C	59.681	S223	N	15N	114.545	C226	HB2	1H	2.924
Q221	CB	13C	28.827	S223	QB	1H	3.92	C226	HB3	1H	2.643
Q221	CG	13C	34.414	V224	CA	13C	67.301	C226	N	15N	117.772
Q221	H	1H	8.399	V224	CB	13C	31.815	K227	CA	13C	59.751
Q221	HA	1H	3.608	V224	CG1	13C	23.877	K227	CB	13C	32.914

res	atom	nucl	shift	res	atom	nucl	shift	res	atom	nucl	shift
K227	CD	13C	29.423	C229	HA	1H	4.186	F232	CA	13C	60.496
K227	CE	13C	42.156	C229	HB2	1H	3.298	F232	CB	13C	39.197
K227	CG	13C	26.053	C229	HB3	1H	2.962	F232	CQD	13C	130.954
K227	H	1H	7.658	C229	HG	1H	2.551	F232	CQE	13C	131.026
K227	HA	1H	3.948	C229	N	15N	117.516	F232	CZ	13C	130.078
K227	HB2	1H	2.062	E230	CA	13C	59.567	F232	H	1H	7.442
K227	HB3	1H	1.754	E230	CB	13C	29.755	F232	HA	1H	4.317
K227	HG2	1H	1.585	E230	CG	13C	36.592	F232	HB2	1H	2.818
K227	HG3	1H	1.335	E230	H	1H	8.239	F232	HB3	1H	2.414
K227	N	15N	120.54	E230	HA	1H	3.912	F232	HZ	1H	7.214
K227	QD	1H	1.449	E230	HB2	1H	1.956	F232	N	15N	115.975
K227	QE	1H	2.779	E230	HB3	1H	2.056	F232	QD	1H	7.282
I228	CA	13C	66.837	E230	HG2	1H	2.375	F232	QE	1H	7.188
I228	CB	13C	38.169	E230	HG3	1H	2.113	E233	CA	13C	58.075
I228	CD1	13C	14.259	E230	N	15N	117.823	E233	CB	13C	28.925
I228	CG1	13C	31.512	Q231	CA	13C	58.093	E233	CG	13C	36.415
I228	CG2	13C	19.564	Q231	CB	13C	27.623	E233	H	1H	8.38
I228	H	1H	8.163	Q231	CG	13C	33.205	E233	HA	1H	3.776
I228	HA	1H	3.248	Q231	H	1H	7.35	E233	N	15N	118.769
I228	HB	1H	1.959	Q231	HA	1H	3.8	E233	QB	1H	1.95
I228	HG12	1H	1.937	Q231	HB2	1H	1.828	E233	QG	1H	2.414
I228	HG13	1H	0.6	Q231	HB3	1H	1.688	A234	CA	13C	52.206
I228	MD1	1H	0.661	Q231	HE21	1H	7.707	A234	CB	13C	19.39

I228	MG2	1H	0.784	Q231	HE22	1H	6.743	A234	H	1H	7.171
I228	N	15N	120.916	Q231	HG2	1H	2.517	A234	HA	1H	4.196
C229	CA	13C	66.349	Q231	HG3	1H	1.765	A234	MB	1H	1.372
C229	CB	13C	26.746	Q231	N	15N	117.002	A234	N	15N	119.922
C229	H	1H	8.257	Q231	NE2	15N	114.994	E235	CA	13C	57.76

res	atom	nucl	shift	res	atom	nucl	shift	res	atom	nucl	shift
E235	CB	13C	30.449	T238	CA	13C	60.411	E241	HB3	1H	2.042
E235	CG	13C	36.293	T238	CB	13C	68.368	E241	HG2	1H	2.308
E235	H	1H	6.956	T238	CG2	13C	21.617	E241	HG3	1H	2.208
E235	HA	1H	4.147	T238	H	1H	7.375	E241	N	15N	121.809
E235	HB2	1H	1.934	T238	HA	1H	4.36	T242	CA	13C	66.224
E235	HB3	1H	1.891	T238	HB	1H	4.466	T242	CB	13C	68.534
E235	HG2	1H	2.401	T238	MG2	1H	1.05	T242	CG2	13C	22.052
E235	HG3	1H	2.035	T238	N	15N	105.029	T242	H	1H	7.987
E235	N	15N	119.209	D239	CA	13C	55.303	T242	HA	1H	3.887
T236	CA	13C	59.396	D239	CB	13C	41.511	T242	HB	1H	4.024
T236	CB	13C	70.624	D239	H	1H	7.212	T242	MG2	1H	1.184
T236	CG2	13C	21.323	D239	HA	1H	4.425	T242	N	15N	113.683
T236	H	1H	8.411	D239	HB2	1H	2.436	T243	CA	13C	66.604
T236	HA	1H	5.041	D239	HB3	1H	2.752	T243	CB	13C	68.524
T236	HB	1H	4.308	D239	N	15N	123.336	T243	CG2	13C	21.842
T236	MG2	1H	1.175	S240	CA	13C	57.228	T243	H	1H	7.81
T236	N	15N	116.669	S240	CB	13C	65.395	T243	HA	1H	3.847
P237	CA	13C	64.255	S240	H	1H	8.913	T243	HB	1H	4.22
P237	CB	13C	32.616	S240	HA	1H	4.386	T243	MG2	1H	1.107
P237	CD	13C	51.362	S240	HB2	1H	4.042	T243	N	15N	122.706
P237	CG	13C	27.622	S240	HB3	1H	4.345	Q244	CA	13C	59.536
P237	HA	1H	4.445	S240	N	15N	119.133	Q244	CG	13C	34.28
P237	HB2	1H	2.388	E241	CA	13C	60.095	Q244	H	1H	8.443
P237	HB3	1H	1.896	E241	CB	13C	29.438	Q244	HA	1H	3.977
P237	HD2	1H	3.831	E241	CG	13C	36.689	Q244	HE21	1H	7.117
P237	HD3	1H	3.793	E241	H	1H	9.136	Q244	HE22	1H	6.761
P237	HG2	1H	1.94	E241	HA	1H	3.995	Q244	HG2	1H	2.302
P237	HG3	1H	1.984	E241	HB2	1H	2.012	Q244	HG3	1H	2.38

res	atom	nucl	shift	res	atom	nucl	shift	res	atom	nucl	shift
Q244	N	15N	121.156	R247	HE	1H	7.01	E249	N	15N	116.649
Q244	NE2	15N	111.738	R247	HG2	1H	1.646	M250	CA	13C	58.333
Q244	QB	1H	2.064	R247	HG3	1H	1.391	M250	CB	13C	32.223
K245	CA	13C	59.767	R247	N	15N	119.866	M250	CE	13C	17.137
K245	CB	13C	32.588	R247	NE	15N	85.194	M250	CG	13C	32.077
K245	CD	13C	29.491	R247	QB	1H	1.793	M250	H	1H	7.83
K245	CE	13C	42.199	R247	QD	1H	3.126	M250	HA	1H	4.178
K245	CG	13C	25.228	F248	CA	13C	61.311	M250	HB2	1H	2.123
K245	H	1H	8.331	F248	CB	13C	38.89	M250	HB3	1H	1.955
K245	HA	1H	4.063	F248	CQD	13C	132.162	M250	HG2	1H	2.373
K245	HG2	1H	1.366	F248	CQE	13C	131.502	M250	HG3	1H	2.426
K245	HG3	1H	1.497	F248	CZ	13C	129.446	M250	ME	1H	1.943
K245	N	15N	121.322	F248	H	1H	8.108	M250	N	15N	119.623
K245	QB	1H	1.853	F248	HA	1H	4.098	V251	CA	13C	67.948
K245	QD	1H	1.64	F248	HZ	1H	7.085	V251	CB	13C	31.218
K245	QE	1H	2.892	F248	N	15N	119.754	V251	CG1	13C	21.999

A246	CA	13C	54.941	F248	QB	1H	3.214	V251	CG2	13C	23.59
A246	CB	13C	17.926	F248	QD	1H	7.191	V251	H	1H	8.545
A246	H	1H	7.819	F248	QE	1H	7.19	V251	HA	1H	3.236
A246	HA	1H	4.115	E249	CA	13C	59.729	V251	HB	1H	1.977
A246	MB	1H	1.409	E249	CB	13C	29.238	V251	MG1	1H	0.728
A246	N	15N	120.927	E249	CG	13C	37.064	V251	MG2	1H	0.568
R247	CA	13C	59.633	E249	H	1H	8.135	V251	N	15N	120.233
R247	CB	13C	29.448	E249	HA	1H	3.578	L252	CA	13C	58.683
R247	CD	13C	43.386	E249	HB2	1H	2.026	L252	CB	13C	41.334
R247	CG	13C	27.591	E249	HB3	1H	1.946	L252	CD1	13C	24.669
R247	H	1H	7.963	E249	HG2	1H	2.57	L252	CD2	13C	24.908
R247	HA	1H	3.946	E249	HG3	1H	2.22	L252	CG	13C	26.825

res	atom	nucl	shift	res	atom	nucl	shift	res	atom	nucl	shift
L252	H	1H	8.281	M255	CB	13C	30.977	Q257	HB2	1H	2.266
L252	HA	1H	3.658	M255	CE	13C	16.927	Q257	HB3	1H	2.052
L252	HB2	1H	1.403	M255	CG	13C	33.412	Q257	HE21	1H	7.189
L252	HB3	1H	1.133	M255	H	1H	8.834	Q257	HE22	1H	6.46
L252	HG	1H	1.27	M255	HA	1H	4.116	Q257	HG2	1H	2.542
L252	MD1	1H	0.646	M255	HB2	1H	2.178	Q257	HG3	1H	2.208
L252	MD2	1H	0.662	M255	HB3	1H	1.8	Q257	N	15N	119.506
L252	N	15N	120.676	M255	ME	1H	1.8	Q257	NE2	15N	111.734
D253	CA	13C	57.574	M255	N	15N	118.777	L258	CA	13C	57.892
D253	CB	13C	41.553	M255	QG	1H	2.411	L258	CB	13C	41.612
D253	H	1H	7.473	Q256	CA	13C	59.153	L258	CD1	13C	25.23
D253	HA	1H	4.236	Q256	CB	13C	28.202	L258	CD2	13C	25.949
D253	N	15N	119.044	Q256	CG	13C	34.566	L258	CG	13C	26.767
D253	QB	1H	2.699	Q256	H	1H	8.033	L258	H	1H	8.347
L254	CA	13C	58.142	Q256	HA	1H	3.888	L258	HA	1H	3.96
L254	CB	13C	42.373	Q256	HB2	1H	2.222	L258	HB2	1H	1.889
L254	CD1	13C	26.13	Q256	HB3	1H	2.153	L258	HB3	1H	1.669
L254	CD2	13C	23.189	Q256	HE21	1H	7.225	L258	HG	1H	1.673
L254	CG	13C	27.587	Q256	HE22	1H	6.735	L258	MD1	1H	0.874
L254	H	1H	8.203	Q256	HG2	1H	2.386	L258	MD2	1H	0.8
L254	HA	1H	3.828	Q256	HG3	1H	2.231	L258	N	15N	119.24
L254	HB2	1H	1.774	Q256	N	15N	120.346	Q259	CA	13C	59.089
L254	HB3	1H	1.134	Q256	NE2	15N	112.304	Q259	CB	13C	28.604
L254	HG	1H	1.807	Q257	CA	13C	59.286	Q259	CG	13C	34.253
L254	MD1	1H	0.592	Q257	CB	13C	28.634	Q259	H	1H	8.112
L254	MD2	1H	0.817	Q257	CG	13C	34.364	Q259	HA	1H	3.899
L254	N	15N	120	Q257	H	1H	7.883	Q259	HB2	1H	2.12
M255	CA	13C	57.671	Q257	HA	1H	3.996	Q259	HB3	1H	2.062

res	atom	nucl	shift	res	atom	nucl	shift	res	atom	nucl	shift
Q259	HE21	1H	7.271	G262	N	15N	106.485	P265	HB3	1H	1.351
Q259	HE22	1H	6.771	H263	CB	13C	29.122	P265	HD2	1H	3.194
Q259	N	15N	118.758	H263	CD2	13C	120.227	P265	HD3	1H	2.338
Q259	NE2	15N	110.216	H263	CE1	13C	137.562	P265	HG2	1H	-0.269
Q259	QG	1H	2.312	H263	H	1H	8.224	P265	HG3	1H	-0.358
D260	CA	13C	56.11	H263	HA	1H	4.654	K266	CA	13C	59.325
D260	CB	13C	41.003	H263	HB2	1H	3.123	K266	CB	13C	32.212
D260	H	1H	7.584	H263	HB3	1H	2.916	K266	CD	13C	29.3
D260	HA	1H	4.487	H263	HD2	1H	7.131	K266	CE	13C	42.177

D260	N	15N	118.245	H263	HE1	1H	8.16	K266	CG	13C	24.667
D260	QB	1H	2.652	H263	N	15N	116.465	K266	H	1H	8.6
L261	CA	13C	55.337	P264	CA	13C	61.679	K266	HA	1H	3.762
L261	CB	13C	43.26	P264	CB	13C	29.597	K266	HB2	1H	1.734
L261	CD1	13C	25.954	P264	CD	13C	50.34	K266	HB3	1H	1.649
L261	CD2	13C	22.876	P264	CG	13C	27.199	K266	N	15N	126.688
L261	CG	13C	26.77	P264	HA	1H	5.206	K266	QD	1H	1.563
L261	H	1H	7.493	P264	HB2	1H	1.994	K266	QE	1H	2.862
L261	HA	1H	4.222	P264	HB3	1H	1.295	K266	QG	1H	1.312
L261	HB2	1H	1.986	P264	HD2	1H	3.35	E267	CA	13C	58.824
L261	HB3	1H	1.579	P264	HD3	1H	3.705	E267	CB	13C	29.445
L261	HG	1H	1.804	P264	HG2	1H	1.685	E267	CG	13C	37.02
L261	MD1	1H	0.768	P264	HG3	1H	1.58	E267	H	1H	9.012
L261	MD2	1H	0.846	P265	CA	13C	62.633	E267	HA	1H	3.889
L261	N	15N	119.233	P265	CB	13C	31.453	E267	HB2	1H	1.916
G262	CA	13C	44.738	P265	CD	13C	49.978	E267	HB3	1H	1.797
G262	H	1H	7.421	P265	CG	13C	26.39	E267	N	15N	116.31
G262	HA1	1H	4.037	P265	HA	1H	3.954	E267	QG	1H	2.291
G262	HA2	1H	3.583	P265	HB2	1H	0.468	L268	CA	13C	54.914

res	atom	nucl	shift	res	atom	nucl	shift	res	atom	nucl	shift
L268	CB	13C	42.327	E271	HB2	1H	1.952	P274	CD	13C	50.535
L268	CD1	13C	24.341	E271	HB3	1H	1.714	P274	CG	13C	27.526
L268	CD2	13C	22.966	E271	HG2	1H	2.116	P274	HA	1H	4.229
L268	CG	13C	26.742	E271	HG3	1H	2.076	P274	HB2	1H	1.788
L268	H	1H	6.885	E271	N	15N	119.061	P274	HB3	1H	2.176
L268	HA	1H	3.989	M272	CA	13C	53.29	P274	HD2	1H	3.717
L268	HB2	1H	0.91	M272	CB	13C	32.478	P274	HD3	1H	3.537
L268	HB3	1H	0.763	M272	CE	13C	17.638	P274	QG	1H	1.919
L268	HG	1H	0.388	M272	CG	13C	32.572	G275	CA	13C	45.576
L268	MD1	1H	-0.412	M272	H	1H	8.038	G275	H	1H	8.418
L268	MD2	1H	0.191	M272	HA	1H	4.542	G275	HA2	1H	3.649
L268	N	15N	115.764	M272	HG2	1H	2.481	G275	HA3	1H	3.864
A269	CA	13C	52.99	M272	HG3	1H	2.384	G275	N	15N	108.08
A269	CB	13C	19.672	M272	ME	1H	1.848	L276	CA	13C	54.829
A269	H	1H	7.299	M272	N	15N	121.781	L276	CB	13C	42.367
A269	HA	1H	3.943	M272	QB	1H	1.815	L276	CD1	13C	25.514
A269	MB	1H	1.072	P273	CA	13C	61.548	L276	CD2	13C	24.22
A269	N	15N	119.808	P273	CB	13C	30.917	L276	CG	13C	27.196
G270	CA	13C	45.508	P273	CD	13C	51.379	L276	H	1H	7.544
G270	H	1H	7.973	P273	CG	13C	27.703	L276	HA	1H	4.212
G270	HA2	1H	3.824	P273	HA	1H	4.579	L276	HG	1H	1.405
G270	HA3	1H	3.716	P273	HB2	1H	2.244	L276	MD1	1H	0.744
G270	N	15N	106.301	P273	HB3	1H	1.722	L276	MD2	1H	0.729
E271	CA	13C	55.639	P273	HD2	1H	3.764	L276	N	15N	119.714
E271	CB	13C	30.361	P273	HD3	1H	3.416	L276	QB	1H	1.399
E271	CG	13C	36.084	P273	QG	1H	1.875	N277	CA	13C	53.01
E271	H	1H	7.904	P274	CA	13C	63.77	N277	CB	13C	39.097
E271	HA	1H	4.225	P274	CB	13C	31.939	N277	H	1H	7.963

res	atom	nucl	shift	res	atom	nucl	shift	res	atom	nucl	shift
N277	HA	1H	4.543	L280	CB	13C	41.917	L283	CG	13C	27.098
N277	HB2	1H	2.643	L280	CD1	13C	25.307	L283	H	1H	7.619

N277	HB3	1H	2.518	L280	CD2	13C	23.722	L283	HA	1H	4.127
N277	HD21	1H	6.732	L280	CG	13C	27.167	L283	HB2	1H	1.602
N277	HD22	1H	7.409	L280	H	1H	8.238	L283	HB3	1H	1.48
N277	N	15N	118.568	L280	HA	1H	3.977	L283	HG	1H	1.591
N277	ND2	15N	112.347	L280	HB2	1H	1.586	L283	MD1	1H	0.789
F278	CA	13C	57.629	L280	HB3	1H	1.466	L283	MD2	1H	0.735
F278	CB	13C	39.84	L280	HG	1H	1.585	L283	N	15N	117.714
F278	CQD	13C	131.979	L280	MD1	1H	0.791	N284	CA	13C	53.528
F278	CQE	13C	131.31	L280	MD2	1H	0.728	N284	CB	13C	38.482
F278	CZ	13C	129.316	L280	N	15N	123.354	N284	H	1H	8.029
F278	H	1H	7.942	D281	CA	13C	56.026	N284	HA	1H	4.569
F278	HA	1H	4.43	D281	CB	13C	40.762	N284	HB2	1H	2.826
F278	HB2	1H	2.972	D281	H	1H	8.21	N284	HB3	1H	2.627
F278	HB3	1H	2.766	D281	HA	1H	4.387	N284	HD21	1H	6.747
F278	HZ	1H	7.023	D281	N	15N	119.105	N284	HD22	1H	7.516
F278	N	15N	120.099	D281	QB	1H	2.594	N284	N	15N	117.503
F278	QD	1H	7.047	A282	CA	13C	53.29	N284	ND2	15N	112.377
F278	QE	1H	7.111	A282	CB	13C	19.015	L285	CA	13C	55.358
D279	CA	13C	53.688	A282	H	1H	7.757	L285	CB	13C	42.439
D279	CB	13C	41.096	A282	HA	1H	4.102	L285	CD1	13C	25.528
D279	H	1H	8.099	A282	MB	1H	1.306	L285	CD2	13C	23.383
D279	HA	1H	4.531	A282	N	15N	122.081	L285	CG	13C	26.91
D279	HB2	1H	2.668	L283	CA	13C	55.514	L285	H	1H	8.117
D279	HB3	1H	2.456	L283	CB	13C	42.367	L285	HA	1H	4.279
D279	N	15N	121.403	L283	CD1	13C	25.584	L285	HB2	1H	1.583
L280	CA	13C	56.731	L283	CD2	13C	23.761	L285	HB3	1H	1.507

res	atom	nucl	shift	res	atom	nucl	shift	res	atom	nucl	shift
L285	HG	1H	1.528	P289	CD	13C	50.553	G293	HA3	1H	3.829
L285	MD1	1H	0.788	P289	CG	13C	27.638	G293	N	15N	110.359
L285	MD2	1H	0.748	P289	HA	1H	4.31	E294	CA	13C	56.969
L285	N	15N	121.052	P289	HB2	1H	2.16	E294	CB	13C	30.216
S286	CA	13C	58.439	P289	HB3	1H	1.818	E294	CG	13C	36.341
S286	CB	13C	64.095	P289	QD	1H	3.544	E294	H	1H	8.257
S286	H	1H	8.113	P289	QG	1H	1.956	E294	HA	1H	4.158
S286	HA	1H	4.391	G290	CA	13C	45.404	E294	HB2	1H	1.828
S286	HB2	1H	3.792	G290	H	1H	8.484	E294	HB3	1H	1.949
S286	HB3	1H	3.757	G290	HA2	1H	3.88	E294	HG2	1H	2.15
S286	N	15N	114.65	G290	HA3	1H	3.815	E294	HG3	1H	2.128
G287	CA	13C	44.615	G290	N	15N	109.625	E294	N	15N	120.263
G287	H	1H	7.938	A291	CA	13C	52.731	Q295	CA	13C	56.006
G287	HA2	1H	4.054	A291	CB	13C	19.402	Q295	CB	13C	29.926
G287	HA3	1H	3.914	A291	H	1H	8.011	Q295	CG	13C	34.091
G287	N	15N	110.132	A291	HA	1H	4.266	Q295	H	1H	8.252
P288	CA	13C	61.556	A291	MB	1H	1.294	Q295	HA	1H	4.27
P288	CB	13C	30.897	A291	N	15N	123.48	Q295	HB2	1H	1.893
P288	CD	13C	49.647	S292	CA	13C	58.652	Q295	HB3	1H	1.974
P288	CG	13C	27.407	S292	CB	13C	63.991	Q295	HE21	1H	7.446
P288	HA	1H	4.588	S292	H	1H	8.281	Q295	HE22	1H	6.766
P288	HB2	1H	1.816	S292	HA	1H	4.355	Q295	N	15N	119.637
P288	HB3	1H	2.209	S292	HB2	1H	3.804	Q295	NE2	15N	112.115
P288	HD2	1H	3.521	S292	HB3	1H	3.772	Q295	QG	1H	2.253
P288	HD3	1H	3.446	S292	N	15N	114.385	C296	CA	13C	56.711

P288	QG	1H	1.915	G293	CA	13C	45.644	C296	CB	13C	34.601
P289	CA	13C	63.65	G293	H	1H	8.284	C296	H	1H	8.267
P289	CB	13C	31.931	G293	HA2	1H	3.895	C296	H11	1H	2.991

res	atom	nucl	shift	res	atom	nucl	shift
C296	H12	1H	4.879	L297	MD2	1H	0.724
C296	H12A	1H	3.121	L297	N	15N	122.198
C296	H2	1H	5.001	I298	CA	13C	61.155
C296	H7	1H	4.883	I298	CB	13C	38.676
C296	HA	1H	4.294	I298	CD1	13C	13.349
C296	HB2	1H	2.777	I298	CG1	13C	27.374
C296	HB3	1H	2.694	I298	CG2	13C	17.885
C296	N	15N	120.509	I298	H	1H	7.846
C296	Q10	1H	1.377	I298	HA	1H	4.082
C296	Q11	1H	1.858	I298	HB	1H	1.764
C296	Q14	1H	1.376	I298	HG12	1H	1.31
C296	Q15	1H	1.451	I298	HG13	1H	0.981
C296	Q4	1H	1.48	I298	MD1	1H	0.693
C296	Q5	1H	1.812	I298	MG2	1H	0.757
C296	Q6	1H	1.887	I298	N	15N	119.846
C296	Q9	1H	1.761	M299	CA	13C	57.018
L297	CA	13C	55.086	M299	CB	13C	34.374
L297	CB	13C	42.824	M299	CE	13C	17.187
L297	CD1	13C	25.328	M299	CG	13C	32.42
L297	CD2	13C	23.94	M299	H	1H	7.7
L297	CG	13C	27.148	M299	HA	1H	4.165
L297	H	1H	8.077	M299	HB2	1H	1.96
L297	HA	1H	4.315	M299	HB3	1H	1.812
L297	HB2	1H	1.52	M299	HG2	1H	2.357
L297	HB3	1H	1.455	M299	HG3	1H	2.33
L297	HG	1H	1.469	M299	ME	1H	1.928
L297	MD1	1H	0.766	M299	N	15N	128.202

III.III RDCs included in structure calculation

first atom			second atom			
187	VAL	N	187	VAL	H	4.008
193	LYS	N	193	LYS	H	-11.212
194	GLU	N	194	GLU	H	-6.646
203	LEU	N	203	LEU	H	-8.286
205	SER	N	205	SER	H	-11.615
207	ARG	N	207	ARG	H	-2.13
210	LEU	N	210	LEU	H	4.613
213	GLU	N	213	GLU	H	-4.164
214	GLN	N	214	GLN	H	-8.535
216	GLU	N	216	GLU	H	-9.159
217	LYS	N	217	LYS	H	-1.825
222	HIS	N	222	HIS	H	-12.244
223	SER	N	223	SER	H	-8.271
225	MET	N	225	MET	H	-7.174
226	CYS	N	226	CYS	H	-13.425
231	GLN	N	231	GLN	H	0.218
234	ALA	N	234	ALA	H	1.945
236	THR	N	236	THR	H	-0.38
238	THR	N	238	THR	H	-8.929
239	ASP	N	239	ASP	H	1.738
240	SER	N	240	SER	H	2.766
241	GLU	N	241	GLU	H	-6.007
242	THR	N	242	THR	H	2.758
255	MET	N	255	MET	H	-5.531
262	GLY	N	262	GLY	H	-9.616
266	LYS	N	266	LYS	H	-7.317
268	LEU	N	268	LEU	H	-5.271

first atom			second atom			
269	ALA	N	269	ALA	H	-2.115
179	MET	C	180	GLN	N	-0.88
185	LYS	C	186	ASP	N	-0.06
186	ASP	C	187	VAL	N	0.62
194	GLU	C	195	ILE	N	-0.47
198	LYS	C	199	TYR	N	0.14
202	TRP	C	203	LEU	N	0.8
203	LEU	C	204	GLN	N	0.23
204	GLN	C	205	SER	N	0.88
205	SER	C	206	HIS	N	-0.11
206	HIS	C	207	ARG	N	1.16
207	ARG	C	208	GLU	N	-0.48
208	GLU	C	209	SER	N	-0.54
212	PRO	C	213	GLU	N	0.4
213	GLU	C	214	GLN	N	1.02
214	GLN	C	215	PHE	N	-0.2
215	PHE	C	216	GLU	N	-0.14
216	GLU	C	217	LYS	N	0.56
217	LYS	C	218	TYR	N	0.08
218	TYR	C	219	GLN	N	0.73
219	GLN	C	220	GLU	N	-0.07
221	GLN	C	222	HIS	N	-0.39
222	HIS	C	223	SER	N	0.02
223	SER	C	224	VAL	N	0.77
224	VAL	C	225	MET	N	0.72
225	MET	C	226	CYS	N	0
226	CYS	C	227	LYS	N	-0.15

first atom			second atom			
228	ILE	C	229	CYS	N	-0.01
231	GLN	C	232	PHE	N	1.59
233	GLU	C	234	ALA	N	0.07
234	ALA	C	235	GLU	N	0.51
235	GLU	C	236	THR	N	-0.63
237	PRO	C	238	THR	N	0.69
239	ASP	C	240	SER	N	0.46
242	THR	C	243	THR	N	-0.28
243	THR	C	244	GLN	N	-0.79
245	LYS	C	246	ALA	N	1.53
246	ALA	C	247	ARG	N	-0.2
249	GLU	C	250	MET	N	0.64
250	MET	C	251	VAL	N	-0.03
253	ASP	C	254	LEU	N	0.09
254	LEU	C	255	MET	N	-0.3
255	MET	C	256	GLN	N	0.19
256	GLN	C	257	GLN	N	0.6
259	GLN	C	260	ASP	N	0.77
260	ASP	C	261	LEU	N	-0.12
261	LEU	C	262	GLY	N	0.35
262	GLY	C	263	HIS	N	1.87
265	PRO	C	266	LYS	N	1.87

270	GLY	C	271	GLU	N	0.12
277	ASN	C	278	PHE	N	0.03
280	LEU	C	281	ASP	N	0.58
281	ASP	C	282	ALA	N	0.32
282	ALA	C	283	LEU	N	0.93

first atom			second atom			
289	PRO	C	290	GLY	N	0.23
290	GLY	C	291	ALA	N	0.56
297	LEU	C	298	ILE	N	-0.81
298	ILE	C	299	MET	N	0.22
183	LEU	C	184	SER	H	1.56
194	GLU	C	195	ILE	H	1.09
198	LYS	C	199	TYR	H	1.06
201	GLU	C	202	TRP	H	3.59
203	LEU	C	204	GLN	H	1.74
204	GLN	C	205	SER	H	1.85
205	SER	C	206	HIS	H	1.14
206	HIS	C	207	ARG	H	-1.38
208	GLU	C	209	SER	H	1.44
213	GLU	C	214	GLN	H	0.16
215	PHE	C	216	GLU	H	1.44
216	GLU	C	217	LYS	H	-1.04
217	LYS	C	218	TYR	H	2.58
218	TYR	C	219	GLN	H	2.18
221	GLN	C	222	HIS	H	4.26
222	HIS	C	223	SER	H	0.47
223	SER	C	224	VAL	H	0.1
224	VAL	C	225	MET	H	-1.56
225	MET	C	226	CYS	H	1.97
226	CYS	C	227	LYS	H	0.77
228	ILE	C	229	CYS	H	2.85
230	GLU	C	231	GLN	H	-0.39
231	GLN	C	232	PHE	H	-2.74

first atom			second atom			
233	GLU	C	234	ALA	H	-0.08
234	ALA	C	235	GLU	H	-4.92
235	GLU	C	236	THR	H	-0.53
237	PRO	C	238	THR	H	-0.9
239	ASP	C	240	SER	H	-1.65
242	THR	C	243	THR	H	2.62
243	THR	C	244	GLN	H	3.35
244	GLN	C	245	LYS	H	-0.94
245	LYS	C	246	ALA	H	-2.61
246	ALA	C	247	ARG	H	1.6
249	GLU	C	250	MET	H	-1.64
252	LEU	C	253	ASP	H	-4.03
255	MET	C	256	GLN	H	-0.94
256	GLN	C	257	GLN	H	-3.76
258	LEU	C	259	GLN	H	3.23
260	ASP	C	261	LEU	H	1.18
261	LEU	C	262	GLY	H	3.41
262	GLY	C	263	HIS	H	-4.22
265	PRO	C	266	LYS	H	-2.13
266	LYS	C	267	GLU	H	3.45
275	GLY	C	276	LEU	H	0.8
276	LEU	C	277	ASN	H	-0.32

280	LEU	C	281	ASP	H	-0.85
282	ALA	C	283	LEU	H	1.69
289	PRO	C	290	GLY	H	-0.72
290	GLY	C	291	ALA	H	-0.31
297	LEU	C	298	ILE	H	1.72
298	ILE	C	299	MET	H	-1.12

Abbreviations

1D, 2D, 3D	one-, two-, three-dimensional	NMR	nuclear magnetic resonance
aa	amino acid	NMT	N-myristoyl transferase
AAA	ATPase associated with various cellular functions	PBD	peroxisomal biogenesis diseases
ARF	adp ribosylation factor	PCR	polymerase chain reaction
CSP	chemical shift perturbation	PCS	pseudo contact shift
DHAP	dihydroxyacetone phosphate	PD	peroxisomal disease
DHAPAT	dihydroxyacetone phosphate acyltransferase	PED	peroxisomal enzyme deficiency
DBP	D-bifunctional protein	peroxin	peroxisomal protein
DTT	dithiothreitol	pex	peroxisomal protein
Dy(DTPA)	dysprosium diethylenetriaminepentaacetate	PH1	primary hyperoxaluria type 1
ER	endoplasmic reticulum	PMP	peroxisomal membrane protein
farn	farnesylated	ppm	parts per million
FID	free induction decay	PRE	paramagnetic relaxation enhancement
FKBP	FK506-binding protein	PTM	posttranslational modification
fl	full-length	PTS	peroxisomal targeting signal
FPP	farnesyl pyrophosphate	Rab	Ras-related in brain
FTase	farnesyl transferase	Ras	rat sarcoma
Gd(DTPA-BMA)	diethylenetriaminepentaacetate bismethylamide	RCDP	rhizomelic chondrodysplasia punctate
GDI	GDP dissociation factor	RDC	residual dipolar coupling
GGTase	geranylgeranyl transferase	rmsd	root mean square deviation
HSQC	heteronuclear single quantum correlation	SDS-PAGE	sodium dodecyl sulfate polyacrylamide gel electrophoresis
LB	lysogeny broth	TEV	tobacco etch virus
mPTS	membrane targeting signal	TMS	tetramethylsilane
MST	microscale thermophoresis	TOCSY	total correlation spectroscopy
mTOR	mammalian target of rapamycin	TPR	tetratricopeptide repeats
MWCO	molecular weight cut-off	TROSY	transverse relaxation optimized spectroscopy
NOE	nuclear Overhauser effect	VLCFA	very long chain fatty acid
NOESY	nuclear Overhauser effect spectroscopy		

Acknowledgements

I would like to thank Michael Sattler as my supervisor for my time in his lab. He gave me the opportunity, freedom and support to pursue own ideas and will always impress me with his never ending work enthusiasm and passion for science.

I feel deeply committed to my colleagues Helge Meyer and Tobias Madl. To work with Tobias was a challenging, informative and extremely fun experience and I'm happy to know him as an outstanding scientist as well as a reliable and kind person. Helge has guided my first steps into the fabulous world of NMR and always remained my advisor for every aspect of our scientific life. Although we did not always agree and our discussions were sometimes exhausting I appreciate his sharp and indefatigable mind and his honest character as a true and loyal friend.

Thomas and Gülden are my sunshines inside and outside the lab. Their support at work made life easier and much more fun. The same holds true for Rainer, without him we would all be lost. Thanks for superfast competent support and for thousands of cappuccini. Nicole was my most diligent and reliable apprentice ever, we quickly became a very good team and she was a great support. Right from his start in the Sattler group, Lee has been a friendly and helpful colleague. Konstantinos Tripsianes contributed a lot to the structure determination. Thanks to all of my former and present colleagues in the Sattler group for interesting four years.

I would like to thank all of my colleagues from the Elitenetzwerk Bayern graduate school Protein dynamics in health and disease for the exceptional organization, commitment and spirit in the group, fun retreats and good collaborations and Anders, Alex and Leo for being part of it.

My Thesis Advisory Committee with Prof. Elena Conti and Prof. Jerzy Adamski has dedicated much time and thought to me and my project. Their advice was very valuable for the development of my project and has encouraged me a lot during my PhD work.

Robert, Janina and Wolfgang from Prof. Erdmann's group at the Ruhr-Universität Bochum were extremely competent as collaboration partners and at least as much fun when meeting on conferences. Wolfgang even made me feel some respect for Schalke 04. Prof. Wilmanns at the EMBL Hamburg provided the initial starting material for the project, and Chris, Krizstian and Jana from his group were always helpful in Pex discussions.

I owe my deepest gratitude to my family, to my parents and grandparents who have given me the courage and freedom to go for this challenging path and incessantly supported me all along the way, to my smart and compassionate sister who always believes in me and to Stefan who is more to me than I can say here. Thanks to all of my friends, life is nothing without you. And now I'm back...

Curriculum Vitae

Ulrike Schütz
 Dipl. Biol.
 * 15.12.1981 in Ulm

Education

May 2008 to present Doctoral student, Technische Universität München
 2002 - 2007 Diploma studies in Biology Ludwig-Maximilian-Universität München
 1993 - 2001 Lessing-Gymnasium, Neu-Ulm

Research

May 2008 to present Doctoral Thesis Research at the Chair of Biomolecular NMR Spectroscopy in the Department of Chemistry, Technische Universität München, and Institute of Structural Biology, Helmholtz Zentrum München
 Title: Studies of protein-protein interactions linked to peroxisomal membrane protein biogenesis
 Supervisor: Prof. Dr. M. Sattler
 Oct 2006 - Jul 2007 Diploma Thesis in the Department of Microbiology, Ludwig-Maximilian-Universität, München
 Title: Posttranslational Modifications of the Universal Stress Protein UspG in *Escherichia coli*
 Supervisor: Prof. Dr. K. Jung

Internships

Feb 2006 - May 2006 Internship at the School of Medical Sciences, University of Aberdeen, Great Britain
 Title: Mutational Analysis of the *Escherichia coli* potassium channel KefC
 Aug 2007 - Dec 2007 Internship at SloningBioTechnology, Puchheim, Germany

Oral Presentations at International Conferences

Sept 2011 The EMBO Meeting, Wien, Austria
 Oct 2010 Open Peroxisome Meeting, Lunteren, Netherlands
 Oct 2009 Herbsttreffen Schloss Hochhausen, Biochemie-Zentrum Universität Heidelberg

Poster Presentations at International Conferences

Sept 2011 The EMBO Meeting, Wien, Austria
 Oct 2010 Open Peroxisome Meeting, Lunteren, Netherlands
 Aug 2010 International Conference on Magnetic Resonance in Biological Systems, Cairns, Australia
 Sept 2009 EMBO Meeting, Amsterdam, Netherlands

Scientific Awards and Scholarships

Aug 2010 Student Poster Prize at the International Conference on Magnetic Resonance in Biological Systems in Cairns, Australia
 Jan 2009 to present Member of the International Graduate Programme "Protein Dynamics in Health and Disease" of Elitenetzwerk Bayern www.protein-dynamics.de